UNIVERSITY OF BIRMINGHAM

SYNTHESIS AND CHARACTERISATION OF GRAPHENE OXIDE AND ITS IMPACT ON SOIL BACTERIA

By

Hussam Fallatah

A thesis submitted to

The University of Birmingham for the degree of

DOCTOR OF PHILOSOPHY

School of Chemical Engineering
College of Physical and Engineering Sciences
University of Birmingham
October 2020

Acknowledgments

I wholeheartedly thank my mighty God for being able to complete this dissertation. I dedicate my dissertation to my family and many friends. I am highly indebted to my Dad and Mom for their support, encouragement, and love were undeniably the bedrock on my life. I know I could not finish the study without their faithful prayers. My siblings, Areej, Mohannad, Eyad and Morooj were always by my side.

I dedicate this work to my daughter Aram and my son Amro. Their smiles always give me the energy to achieve my study. And a special thanks to my lovely wife Hanadi who support me for better or worse. I would also like to thank my friends Mohammad Al-Hunaid, Hong Li, Boki, Hani El Kadri, Mohd Fauzi and Putu Virgina Devanthi for your friendship all these years.

I would like to gratefully and sincerely thank Dr. Kostas Gkatzionis for his direction, understanding and patience throughout my graduate study at University of Birmingham. He encouraged me to not only develop my research skills but also to become an independent scientist and I feel honoured to have the opportunity to work with him. I would like to thank my supervisors, Dr. Tim Overton and Dr. Hanene Ali-Boucetta for their constructive criticisms and guidance. I really appreciate their encouragement and help to successfully get through this PhD.

Many thanks go to Elaine Mitchell and David French, the technical staff that helped me throughout the PhD. Their supports gratefully acknowledged.

Finally, many thanks to my sponsor KACST for the generous funding.

Summary

Carbon based materials such as graphene have recently been widely studied. Graphene oxide (GO) is a member of the graphene family with functional groups which make it hydrophobic, thus making it useful for many applications such as an antibacterial agent. However, there is controversy in the literature about the effect of GO on bacteria. Therefore, it was important to prepare a highly purified GO using Hummers' method and characterise it before studying the biological test. The final product shows that GO had 1-2 layers with oxygen group on the GO sheets.

Bacteria are often found in nature in a form called biofilms. Bacterial cells are embedded in an extracellular matrix composed of polymers. This protects bacteria from harmful factors such as antibacterial agents more than planktonic (free) cells.

In this study, the objective was to study the effect of GO on soil bacteria. GO was prepared and characterised using optical and surface techniques. Then GO was applied to two species of bacteria found in soil, *Pseudomonas putida* and *Acinetobacter* sp., in biofilm and planktonic forms. It was found that biofilms showed more susceptibility to GO than planktonic cells. Moreover, the antibacterial effects of GO on biofilms depended on the maturity stage of the biofilm.

The impact of GO and environmental stresses (temperature, pH and NaCl) on *P. putida* was examined. It was found that environmental conditions changed the susceptibility of biofilm to GO. Moreover, it was found that the removal of EPS from biofilms increases the susceptibility to GO. Finally, it was found that GO changed the chemical compounds of the cell wall.

Publications and conferences

1- Journals

Fallatah, H., Elhaneid, M., Ali-Boucetta, H., Overton, T., El Kadri, H., and Gkatzionis, K. (2019) Antibacterial effect of graphene oxide (GO) nano-particles against *Pseudomonas putida* biofilm of variable age. *Environmental Science and Pollution Research*, 1-14. doi.org/10.1007/s11356-019-05688-9

2- Conferences

H. Fallatah, M. I. Fauzi, J. Mattock, H. Ali-Boucetta, T. Wi. Overton, K. Gkatzionis, Graphene Oxide Interaction with *Pseudomonas putida*: Effects on Biofilms and Planktonic cells. EPS conference, Birmingham, 2014

H. Fallatah, H. Ali-Boucetta, T. W. Overton, K. Gkatzionis, Graphene oxide Interaction with *Pseudomonas putida*: effect on biofilms and planktonic cells, S*f*AM summer conference, Dublin, 2015.

Acknowledgments

Summary

Publications and conferences

Table of Contents

List of figures

List of tables

Chapter 1. Introduction

1.1. Brief Introduction

Graphene-based nanomaterial have gained prominence in future application such as biomedical application due to their physiochemical and biological properties (Goenka et al., 2014). Although the application of graphene-family products has economic importance, large-scale manufacture of these compounds could increase their release to the environment. Moreover, due to their physical and chemical properties, graphene products might interact with living organisms and harm the environment (Hu and Zhou, 2013).

The antimicrobial properties of graphene have been well documented (Zou et al., 2016) and microorganisms that are widespread in the environment can be affected by graphene that may leach into the environment. The existence of these compounds may impact the activity and structure of microorganisms, and possibility influence the balance of the whole ecosystem (Ahmed and Rodrigues, 2013; Combarros et al., 2016).

To date, several studies have demonstrated the antimicrobial properties of Graphene Oxide (GO) compounds. For instance, Liu et al., (2011) showed a decrease in viability of *Escherichia coli* (*E. coli*) of 89% or 74.9% when adding 40 μg/mL GO or reduced graphene oxide (rGO) after a 4 h incubation period, respectively. Akhavan and Ghaderi (2010) showed that GO possesses antimicrobial properties against *E. coli* and *Staphylococcus aureus* (*S. aureus*). However, there is inconsistency and contradiction with regard to the antimicrobial effects of GO since some studies show that GO does not possess antimicrobial properties against bacteria. For instance, Chen et al. investigated the impact of GO on gut microorganisms. They found that GO sheets can

act as a scaffold to increase microbial growth (Chen et al., 2014b). Ruiz et al. also obtained similar results when they found that the growth of bacterial cells was enhanced by the presence of GO (Ruiz et al., 2011b). It was suggested that the contradiction in the literature was due to the differences in composition of the media that were used when testing the antimicrobial effects of GO against bacteria (Hui et al., 2014). It was shown that nutrients in rich media can mask the antimicrobial activity of GO making it inactive against bacteria (Hui et al., 2014).

The above findings developed our understanding of the interaction between GO and bacteria. However, the effect of GO on bacteria in the environment is not well understood. In natural environments, most bacteria tend to colonize biotic and abiotic surfaces in groups forming biofilms (Davey and O'toole, 2000). Bacterial biofilms are composed of a group of planktonic cells (free swimming bacteria) where the cells are attached to the surface and adhere together by a gel-like structure (Davey and O'toole, 2000; Shim et al., 2002).

These cells are wrapped in secreted molecules called Extracellular Polymeric Substances (EPS). The components of EPS include extracellular DNA (e-DNA), proteins, and polysaccharides, phospholipids and lipids depending upon the organism and the biofilm-forming environmental conditions. Biofilms often stick on biotic or abiotic surfaces and they are widespread in nature aquatic or potable water systems, medical devices, living tissues, and in industry. Moreover, the formation of biofilms can cause harm to humans, animals, and plants as well as huge economic losses. It has been demonstrated that bacterial cells in biofilms are more resistant to external stress such as environmental stresses and antibacterial drugs than planktonic cells (Antoniou and Frank, 2005). Previous studies showed the efficacy of different drugs against biofilms at different stages of its formation may vary (Krishnakumar et al.,

2015; Rodrigues and Elimelech, 2010). Although most of the recent studies that investigated the toxicity of GO were performed on planktonic cells only since they grow faster, few studies investigated the toxicity of GO on biofilms (Ruiz et al., 2011a; Mejías Carpio et al., 2012; Kumar et al., 2015). Moreover, there is contradiction in the literature regarding the impact of GO on biofilms. In one study, GO made biofilm more dense which means there was no toxicity effect (Ruiz et al., 2011a). In another study, it was shown that GO can inhibit the formation of biofilm (Mejías Carpio et al., 2012). Therefore, more investigation is required to establish the antimicrobial effects of GO on microbial biofilms.

In the environment, GO might interact with bacteria in different ways. GO might come in contact with planktonic cells and influence their growth and adherence and thus biofilm formation. However, GO might not have any influence on planktonic cells. GO might impact biofilms that have been adhered on surfaces and as result of that, the biofilm maturation stage could be affected. The evidence presented in literature supports the idea that graphene family molecules affected biofilm distinctively in two ways. For example, Rodrigues and Elimelech (2010) demonstrated that in the early stage of biofilm formation, when single walled carbon nanotubes (SWCNTs) attached to the bacterial cells, SWCNTs inhibit the biofilm development. However, the results suggest that mature biofilms are less sensitive (Rodrigues and Elimelech, 2010).

Many studies investigated the antibacterial activity of graphene family molecules in saline or minimal medium. However, the behaviour and toxicity of GO in rich media are not well understood yet. Since media can influence the graphene family molecules and their toxicity to bacteria, it is therefore important to study the effects of GO against bacteria with various types of media.

In this study, the effect of GO on biofilm formation (initial attachment of cells) development (maturation and growth of biofilm) by *Pseudomonas putida* and *Acinetobacter* sp. was studied. The specific objectives of the proposed research are:

1- To understand the physicochemical properties (lateral size, thickness, chemical properties, functional group, absorbance, elemental content and surface charge) of GO;
2- To determine the impact of GO on bacterial planktonic cell and biofilm formation;
3- To measure the effects of GO on developed biofilms;
4- To measure the effect of GO on biofilm under additional environmental stresses (temperature, pH and osmotic stress); and
5- To study the effect of EPS on the susceptibility of bacteria to GO.

1.2. Carbon based nanomaterials

Recent developments in nanomaterials have increased their use and applications in different fields. Carbon based nanomaterials are one of these novel materials; they are composed mainly of carbon atoms and have sp, sp^2 and sp^3 hybridized orbitals. The anisotropic sp^2 in molecular carbon atoms could cause anisotropy in some crystals of those materials (Yan et al., 2016). Therefore, a big diversity is found in carbon materials. They can be found in different forms such diamond, fullerenes, car bon nanotube, graphite, graphene and graphene oxide (**Figure 1**).

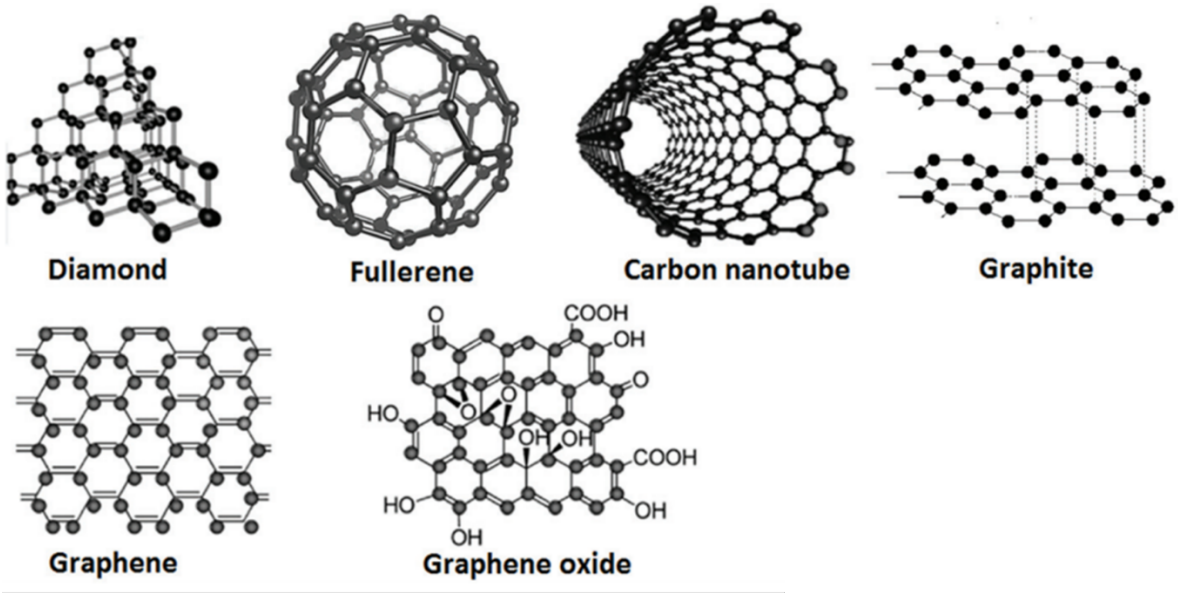

Figure 1.1 Different forms of carbon nanomaterial (Yan et al., 2016)

Graphene was discovered by Novoselov et al. (2004) and it is a single atom thick sheet of sp^2 bonded carbon atoms with 2 dimensional properties (Jastrzębska et al., 2012). The lateral dimension varies from a few nanometres to micrometres. The unique structure and physicochemical properties, make it suitable for different applications (Seabra et al., 2014). The extensive researches of graphene-related materials led to novel developments including biomedical technologies (Zhang et al., 2010; Bitounis et al., 2013), battery electrodes (Su et al., 2010), structural composites (Stankovich et

al., 2007), transport barriers (Bunch et al., 2008). It was also used in environmental application to absorb hazardous materials (Kemp et al., 2013).

Another form of carbon-based material is carbon nanotubes (CNTs), which were first discovered by Ijima in 1991 using the arc-discharge method. They are composed of single-, double- or multi-walled seamless sheets with sp^2 bond, forming hollow cylinders of carbon atoms (Ganesh, 2013; Bussy et al., 2013). Moreover, carbon nanotubes come in three different shapes: chiral, zigzag and armchair. Although the diameter of the CNTs is extremely thin at approximately 2-20 nm (fifty thousand times thinner than human hair), the strength of CNTs is greater than the steel per unit weight (Ganesh, 2013).

The potent toxicity of these nanomaterials has encouraged researchers to use novel approaches to minimize the toxicity. Studies have indicated that nanomaterials have an antimicrobial activity and can effectively inhibit the growth of the microorganisms. Therefore, there are many ongoing studies to develop new nanomaterial-based antimicrobial drugs. **Table 1.1** summarises the effect of graphene family molecules on bacteria cells.

Table 1. 1 Summarize the effect of graphene based nanomaterials on bacterial cells

Graphene family	GO characterization	Methodology	Concentration (µg/mL)	Bacteria Species	Medium	Conclusions	Comments	References
GO	Th: 0.794 nm Si: not provided	Modified Hummers methods	10-500 µg/mL	*Pseudomonas syringae and Xanthomonas campestris pv. undulosa*	Luria-Bertani (LB)	Inhibited the bacterial viability and growth By optical density (OD) and CFU	GO damages cell membrane	(Chen et al., 2014a)
GO GO-Ag	Th: 0.7 and 1.2 nm Si: 300-800 nm	Modified Hummers methods	0.1 – 5.0 µg/mL	8 different species were used	Brain Heart Infusion (BHI)	GO: no effect on bacteria growth GO-Ag: MIC 2.5 µg/mL with *Pseudomonas aeruginosa* By CFU	GO-Ag damages cell membrane but not GO	(de Faria et al., 2014)
Cotton GO	Th: 1.1 nm Si: not provided	Not provided	2000 µg/mL	*Escherichia coli* *Bacillus subtilis*	Grown in LB then added to the cotton	Inactivate 98% of bacteria By CFU	Damage cell membrane	(Zhao et al., 2013)
GO	Th: 1 nm Si: (0.010-0.753) μm^2	Modified Hummers methods	40 µg/mL 80 µg/mL	*E. coli*	Deionized water (DI)	Loss viability: big GO (38.7-99.3)% ; small GO (18.5-56.2)% using CFU Loss% = (counts of control-counts of treated sample)/counts of control	Damaged cell membrane	(Liu et al., 2012a)

PVK-GO	Not provided	Modified Hummers methods	10-1000 µg/mL	*E. coli*, *Cupriavidus metallidurans, B. subtilis Rhodococcus opacus*	Tryptone soy broth (TSB)	PVK-GO: inhibited the bacterial growth 7-16% > GO but not *C. metallidurans.* By optical density (OD) and plate count	PVK-GO has higher antibacterial effect than GO	(Mejías Carpio et al., 2012)
GO	Not provided	Modified Hummers methods	300 µg/mL	*Shewanella oneidensis* *Shewanella* sp.	TSB	Has no effect on bacteria By (OD)	GO has no effects on the cell membrane and it reduced to graphene	(Wang et al., 2011)
GO	Not provided	Modified Hummers methods	25 and 75 µg/mL	*E. coli*	LB	Bacteria grew faster By OD	GO enhanced the bacterial growth	(Ruiz et al., 2011a)
Gr, GrO, GO & rGO	Th: 1 nm Si: 5.25, 4.42, 0.56 and 2.93 µm	Modified Hummers methods	40 µg/mL	*E. coli*	Isotonic saline solution	All graphene family has antibacterial effects GO>rGO>Gr> GrO BY CFU (loss viability)	The effects depend on time and concentration	(Liu et al., 2011)
GO rGO paper	Th: 1 -1.1 nm Si: 1.5 and 4.6 µm	Modified Hummers methods	20 and 85 µg/mL	*E. coli*	Saline solution (0.95%)	Both GO and rGO reduced the growth By CFU	Damaged cell membrane	(Hu et al., 2010)
GONWs RGONWs	Not provided	Modified Hummers methods	1000 µg/mL	*E. coli* *S. aureus*	LB	Antibacterial effect Using drop test method then CFU; and measurement of efflux of RNA by extracting RNA and measured by NanoDrop	*E. coli* resist more than *and S. aureus*	(Akhavan and Ghaderi, 2010)

GO rGO	Th: Not provided Si: 0.3 – 0.7 µm	Provided from company (Graphene Supermarket INC, USA	500 mg/L with different concentrations 0.1-0.08%	*B. subtilis* *P. aeruginosa*	LB	rGO has anti-bacterial activity for both bacteria GO was harmless for both Bacteria were grown on LB agar with GO and measured by colony area	The results showed the response of bacteria depends on the graphene type	(Mokkapati et al., 2018)
GO	Not provided	Modified Hummers methods	10 and 40 mg/L	*E. coli* *S. aureus*	Normal saline	Both species were affected Bacteria cell membrane integrity was evaluated using the BacLight kit by confocal	GO coat the cells which leads membrane to be damaged	(Gao et al., 2017)
GO	Th: 0.8 nm Si: 0.19 μm^2	Not provided	3.125-200 µg/mL	*Staphylococcus aureus* *E. coli*	ddH_2O, NaCl, PBS, $CaCl_2$ and LB	inhibited the bacterial growth Measured by CFU and AFM	The toxicity depends on the concentration and solution	(Palmieri et al., 2017)
GO	Th: 0.8 nm Si: not provided	Graphene Supermarket	200 µg/mL	*E. coli*	Saline solution	Has an antibacterial activity Bacteria were placed on GO film and the viability was determined by live/dead assay and CFU	the orientation-dependent interaction of GO plays a role for enhancing the toxicity	(Lu et al., 2017)

GO-H2O GO-PBS GO-MG	Th: one or two layer Si: 100 nm	Modified Hummers methods	2-200 µg/mL	*E. coli*	Water, PBS	Has an antibacterial activity only in high concentration The viability was measured by OD	GO-H2O and GO-PBS has no antibacterial effect while at higher concentration it decreased the growth rate	(Campos-Delgado et al., 2016)
GO	Not provided	Hummers methods	0.05-1.0 mg/mL	*Pseudomonas putida*	Rich/minimal medium	The growth was inhibited The growth was measured by OD and CFU	The main impact of GO on *P. putida* was the lost the membrane integrity due to the sharp edges of GO	(Combarros et al., 2016)

Abbreviations: GO: graphene oxide, rGO: reduced graphene oxide, PVK-GO: polyvinyl-N-carbazole graphene oxide, Gr: graphite, GrO, graphite oxide, GONWs, graphene oxide nanowalls, RGONWs: reduced graphene oxide nanowalls, GO-Ag: GO-Silver, GO-H2O: GO in water; GO-PBS: GO in phosphate-buffered saline (PBS), GO-MG: manually ground and dispersed in water, MIC: minimum inhibitory concentration, Si: size, Th: thickness

1.3. Graphene Oxide

Graphene oxide (GO) is a graphene sheet covered by oxygen functional group on the basal plane and edges. Due to the functional groups of GO, this can affect its properties, therefore make GO differ from pristine graphene (Gómez-Navarro et al., 2010). Structural defects exist in GO caused by the chemical oxidation process and this limits its use in applications such as a conductor in electronic devices since the presence of the oxygen functional groups reduces the electrical conductivity of GO sheets (Mkhoyan et al., 2009). The functional groups have an advantage in that they make GO hydrophilic and easily dispersed in many solvents (Dreyer et al., 2010) especially in water increasing its functionality and derivation (Park and Ruoff, 2009).

GO involves functional groups, which make it a useful material and could be used in many applications. GO is developed from graphite oxide and favourable methods to produce large-scale graphene platelets have been developed (Dreyer et al., 2010). However, the main disadvantage of graphene is its poor dispersibility in water which makes it aggregate. The aggregation of graphene platelets is a result of strong interaction through van der Waals and π–π stacking. Hence, this limits their applications (Chauke et al., 2015; Georgakilas et al., 2016).

By adding functional groups on grapheme sheets by chemical oxidation, GO is able to disperse well in water (Ali-Boucetta et al., 2013). Adding these functional groups to graphene can reduce the aggregation and form GO (Chauke et al., 2015). The hydrophilic functional groups increase the dispersibility of GO (Ali-Boucetta et al., 2013). Furthermore, different functionalities on the surface of this material make it

perfect for chemical modification, which might produce materials with good properties (Hashim et al., 2016).

1.4. Structure of Graphene oxide

It is important to understand the structure and properties of GO for determining its potential applications. GO has a unique structure which makes it different from pristine graphene sheets, which consist of sp^2 carbon atoms with a honeycomb lattice shape (Lui et al., 2009). GO includes both of sp^2 and sp^3 hybridized carbon atoms where oxygen functional groups are present (Lu et al., 2004).

However, there has been debate about the detail of the chemical structure of GO over decades, and there is not a confirmed model of GO. The main common evidence is the structural characteristics of GO, this includes the presence of oxygen groups on the surface of GO such as carboxyl, hydroxyl and epoxy groups (Zhang et al., 2014). Because of lacking details of analytical techniques to characterise the unstructured property of GO, and nonstoichiometric berthollide character of GO, finding an actual model of GO became problematic (Dreyer et al., 2010).

Many of the earliest studies such as Hofmann and Holst, Ruess, Scholz-Boehm and Nakajima-Matsuo proposed a structural model for GO based on a regular lattice composed of discrete repeated units (Dreyer et al, 2010). For example, Hofmann and Holst (1939) suggested epoxy groups among the basal planes of graphite. Ruess (1947) proposed hydroxyl groups into the basal plane with O atoms of epoxies connected with C atoms in the 1,3 site.Scholz and Boehm (1969) illustrated a model with no epoxied groups, replacing regular quinoidal species in a corrugated backbone. Another study by Nakajima and Mastsuo suggested a model based on lattice framework akin to poly (dicarbon monofluroride), which forms a stage 2 graphite

intercalation compound. Szabó and Dekeny's (2006) model is a compilation of Rues' and Scholz-Boehm's model (Szabó et al., 2006). These studies give a better understanding of the GO structure (Dreyer et al., 2010).

Recent studies rejected the lattice-based model and focused on a nonstoichiometric, amorphous alternative (Dreyer et al., 2010). One of the best known models is Lerf-Klinowski's model and it is used widely by researchers. They proposed the structure and hydration behaviour of GO as epoxy (1,2-ether) and hydroxyl as the main functional groups on the graphene layer, randomly distributed across the graphene layer. The carboxyl, lactones and carbonyls are common at the edge (Lerf et al., 1998).

In addition, Mkhoyan et al. (2009) measured the C and O k-edges to study the atomic and electronic structure of GO. They showed that GO has an average surface roughness of 0.6 nm and the structure is amorphous because of the distortions from sp^3 C-O bonds. They also reported, around 40% sp^3 bonding is coming from the ratio of O and C which is 1:5. A similar study was done by Erickson et al. (2010). They studied the GO structure and indicated that the graphitic region is about 8 nm^2 and the oxidized regions showed no order because the oxidation has minimal sp^2 bonding and makes a continuous network across the sheet. Moreover, hydroxyl and epoxy groups are widely spread (Erickson et al., 2010).

1.5. Synthesis of Graphene oxide

In 1840 was the first time to attempt the syntheses of graphite oxide and graphite intercalated compounds by Schafhacult, when he tried to exfoliate graphite to purify impure graphite (Eigler, 2011). After two decades, in 1859, graphite oxide was for the first time synthesised by Brodie (Brodie, 1859; Brodie and Chemical, 1860). The method used for the synthesis was done by the addition of potassium chlorate $KClO_3$

to graphite in fuming nitric acid (HNO_3) (Dreyer et al., 2010). The reaction showed an increase of the overall mass of the initial graphite flake and it was composed of hydrogen, oxygen and carbon. The product of this reaction was called graphitic acid (Brodie, 1859; Eigler, 2011). Forty years later, a new improved method was used by Staudenmaier, who proposed further steps. The method used was to treat graphite in sulphuric acid H_2SO_4 and fuming (HNO_3) with the additional of $KClO_3$ then washed by hydrochloric acid (HCl) to remove the sulphate ions (Poh et al., 2012). Hoffman used the same methods for graphite oxidation; however, the concentration of acids was higher than in Staudenmaier's (Staude's) method (Staudenmaier, 1898).

However, Staude's method has the most oxidised graphite oxide. This method takes several days to be completed (Tuantranont, 2013). $KClO_3$ and HNO_3 which have been used in previous methods, are toxic. HNO_3 cause release of gases such as NO_2 or N_2O_4 (Chua and Pumera, 2014) and it is an oxidising agent reacting with aromatic carbon such as graphite (Lakshminarayanan et al., 1983). While $KClO_3$ is an explosive compound thus it is important to take care while dealing with it (Yusoff et al., 2015).

Hummers and Offeman (1958) proposed a different method to improve and increase the oxidation (Nethravathi and Rajamathi, 2008). The method includes concentrated H_2SO_4, sodium nitrate ($NaNO_3$), and potassium permanganate ($KMnO_4$), followed by hydrogen peroxide (H_2O_2) to remove the residue of $KMnO_4$ and manganese dioxide (MnO_2) (Chen et al., 2013). It is interesting to note that this method was adapted from Charpy et al. in 1909 who used H_2SO_4 and $KMnO_4$ at 45°C during the oxidation and it took several days to accomplish (Charpy, 1909). However, Hummer's method takes only two hours for the whole process. Therefore, Hummer's method is the most efficient method to oxidise graphite (Shamaila et al., 2016). Moreover, the formation

of dimanganese heptoxide (Mn_2O_7) makes the process faster. This is due to the addition of $KMnO_4$, which has a robust ability to oxidise graphite (Wang et al., 2014).

1.6. Characterisation techniques for graphene oxide

To study the structure and properties of GO, several techniques are used such as X-ray photoelectron spectroscopy (XPS), Raman spectroscopy, Fourier Transform Infrared (FTIR), electron microscopy (Toh et al., 2014), atomic force microscopy (AFM) and UV-visible spectroscopy, or in combination with other techniques to reveal the structural evolution of the GO from the graphite.

1.6.1. X-ray photoelectron spectroscopy (XPS)

XPS is a technique to analyse the structure of atoms. It works by irradiating a sample with a high energy X-ray beam and then quantifying the kinetic energy and number of electrons that are rejected from the material. This technique is able to obtain the chemical composition of various materials and it reveals which chemical elements are present at the surface. This technique is one of the most commonly used techniques to detect the amount of carbon and functional groups in GO. It can also determine the ratio of oxygen to carbon atoms, and the results can be compared to elemental analysis (Marcano et al., 2010; Shao et al., 2012). In this technique, two peaks appear at 530 eV and 284 eV, which correspond to O1s and C1s spectra respectively (Zeng et al., 2011). Both spectra determine the oxygen functionalities in the graphene carbon sheets. In addition, the ratio between these peaks can be used to determine the oxygen content in the oxygenated graphene. The O1s spectrum can be deconvoluted (into several peaks, each peak indicates the presence of carbonyl groups at 530.4-530.8 eV, hydroxyl group and/or ether groups at 532.4-533.1 eV and chemisorbed oxygen and/or water at 534.8-535.6eV (Biniak et al., 1997). The C1s in GO spectrum

shows two main peaks approximately 2 eV apart while there is a single sharp peak in graphite. Both peaks represent the sp2 C=C bonds and the sp3 carbon with different C-O bonding configurations. The degree of oxidation determines the intensity of the peaks. The C1s spectrum can be deconvoluted into four peaks. However, it is difficult to determine the exact position (binding energy) of the peaks. In general, carbon to carbon or carbon to hydrogen bonds are located at 284.5 and 285 eV respectively, with a chemical shift of (+1.5 eV ± 2) for C-OH group, (+2.7 eV ± 3) for C=O group and (+4.2 eV ± 2) for O=C-OH group.

1.6.2. Raman spectroscopy

This technique study the vibrational characteristics of molecules. It is based on the scattering of light by molecules causing the molecule to vibrate. When monochromatic light interacts with a sample, the light scatter reveals information about molecular structure. This technique is useful to study the electronic properties of the GO. This technique has been used to study carbon-based materials such as graphene (Ferrari, 2007), carbon nanotubes (Dresselhaus et al., 2005), graphite (Tuinstra and Koenig, 1970) and GO (López-Díaz et al., 2017). Usually, the Raman spectrum of GO shows two main bands, D and G, and a weak 2D band. The D and 2D bands refer to a disorder in graphene structure while the G band refers to the graphitic lattice (sp^2 carbon structure (López-Díaz et al., 2017). The D, G and 2D bands are detected at 1350, 1580 and 2700 cm^{-1} respectively by using a laser at 514 nm for excitation (Ferrari et al., 2006).

The 2D band can be seen is all graphene family such as graphene, GO and graphite. The 2D band is linked with the second order of the zone boundary arising from double resonance Raman scattering with two-photon emission. The number of layers or sheets can be determined by the intensity and shape of the 2D band. Ferrari et al.

(2006) reported that the 2D band is sensitive to the number of layers, and they were able to distinguish a single sheet of GO from multi-sheets.

The G band in GO is extended and blue-shifted compared with graphene or graphite. Conversely, the D band of the GO is prominent, which means small size of in-plane sp^2 domains, due to the extensive oxidation.

1.6.3. Fourier Transform Infrared (FTIR) spectroscopy

FTIR uses infrared light to scan samples and observes chemical properties. The analysis of FITR measures the wavelengths reflected form sample. The FTIR is a standard method used along with Raman spectroscopy to identify the functional groups and bonding configuration in GO sheets. Several absorption signals appear in the IR spectrum of the GO, at about 3400 cm^{-1}, representing O-H stretching of carboxyl groups. There is a sharp peak at 1720-1740 cm^{-1}, attributed to C=O stretching of carbonyl or carboxyl groups, a weak peak at 1590-1620 cm^{-1} assigned to C=C of unoxidised graphite, and strong peak at 1100 cm^{-1}, corresponding to an alkoxy C-O stretching. Additionally, another absorbed peak assigned to epoxy C-O stretching has been described in a previous study (Doğan et al., 2013). This was in agreement with Lerf et al. (1998) in which epoxides reside in the basal plane of GO sheet. However, the absorption peak of the epoxy group is variable between studies (Lerf et al., 1998). León et al. (2017) detected the peak of epoxy group at 1242 cm^{-1}, while Rodríguez-González et al. (2012) reported the peak at 1228 cm^{-1}. The difference in peak positions could be due to the differences in the preparation of samples and in the working environment. In addition, some studies showed absorption peaks below 3000 cm^{-1}, attributed to C-H asymmetric and symmetric stretching variations of the $–CH_2$ groups.

1.6.4. Electron Microscopy

In addition to the previous techniques that are used to characterise GO, electron microscopy is a useful technique to study the topography and morphology of GO. Scanning electron microscopes (SEM) and transmission electron microscopes (TEM) are two of the most commonly used electron microscopes to study the morphology of GO.

The sample in the SEM is heated by an electron beam. The electron signals from the sample are reflected and used to generate the surface image of GO. TEM electron gun emits a high voltage electron beam. When the beam hits the sample, a fraction of electrons are scattered, hit the fluorescent sensor, and reveal the sample.

The GO sheets are observed with a wide range of lateral sizes (Kim et al., 2009). The lateral dimension of GO sheets depends on the size of graphite as starting material (Toh et al., 2014). The lateral dimensions of GO sheets vary from less than one hundred nanometres to several micrometres (Akhavan and Ghaderi, 2010; Ali-Boucetta et al., 2013; Hu et al., 2010). GO sheets under SEM are thin and have a wrinkled texture.

1.6.5. Atomic force microscopy (AFM)

This technique allows measurement of the thickness of GO sheets. It consists of a cantilever (probe), which scans the surface area of the GO. A laser beam around the cantilever emits electrons that are detected by a photodetector to decipher the distance between the surface and the cantilever, and thus measure the thickness of the GO and the roughness of the surface. Typically, the thickness of GO sheets varies between 0.9 and 2.3 nm (Shao et al., 2012). However, it is difficult to scan bulk graphene via this microscopy because of its large area. Paredes et al. (2009) have

reported the chemically reduced GO (rGO) with distinguished GO sheets via a simple technique called tapping-mode AFM. The thicknesses of rGO and GO were 0.6 and 1.0 nm, respectively (Paredes et al., 2009).

1.6.6. UV-visible spectroscopy

UV-visible spectroscopy is used determine the absorbance and spectra of GO dispersion. It consists of a source of light which goes through a monochromator and hits a prism, which is placed between two slits (Kurtz and Huffman, 1990; Verma and Mishra, 2018). When the light passes the first slit and contacts the prism, it is refracted into a range of different range colours. Only one colour targets the sample; this colour is then detected to measure the transmittance and absorbance of the sample (Verma and Mishra, 2018). An intense peak is exhibited at 230 nm which corresponds to π-π* transitions of the C=C bonds (Kashyap et al., 2014). **Table 1.2** shows the advances and disadvantages these techniques for analysis of GO.

Table 1. 2 Summary of the advantages and disadvantages of the techniques for analysis of GO

Technique	Advantages	Disadvantages
UV-Vis spectroscopy	Simple and inexpensive, quantitative (Beer's law)	Sensitive: mixture of molecules can overlap), spectra are not highly specific for particular molecules, needs calibration
AFM	Provide 3D images, don't require any special treatments which might change or damage the sample, high resolution	Slow scanning, can be affected by hysteresis of the piezoelectric material and crosstalk between *x*, *y* and *z* axes.
SEM	Fast scanning, 2D images to determine the GO sheets sizes.	Requires special training time consuming, cost, size, maintenance
FTIR	Fast, does not destroy the sample, can be used with solid or liquid sample, tiny amounts of samples required (few drops) for liquid	Cannot detect elements or diatomic molecules such as nitrogen or oxygen. The spectral regions usually overlap if there are many components
TEM	Powerful magnification, provides information on compound structure, high quality images, useful to provide shape, size and structure, easy to learn.	Requires special treatments for fixation
Raman spectroscopy	Can be used with solid or liquid samples, no preparation, not interfered by water, highly specific, quick, small volume.	Strong laser beam which might damage samples
XPS	Provides information about chemical state of surfaces, can differentiate between oxidation groups.	Expensive, solid sample is required, slow processing, high vacuum is required

1.7. Nanomaterials and biofilms

Microorganisms in nature usually form biofilms as one of the main strategies for their survival in the environment (Gjermansen et al., 2005; Bridier et al., 2011). Biofilms are groups of bacteria that colonize biotic or abiotic surfaces (Bridier et al., 2011). It is difficult to have a common description of biofilms. Rizzello et al. (2013) have five different descriptions for biofilms based on different parameters. For instance, from a chemical point of view, biofilms are a complex of extracellular polymeric substances (EPSs), such as polysaccharides, DNA and catalytic proteins produced by the bacteria on the cell surface after their adherence. Physically, biofilms are slime matrix with specific structure; this structure varies based on the environmental conditions and bacterial species. However, from an ecology point of view, bacterial biofilms are groups of bacterial cells stuck to each other and usually adhere to the surface. Biofilms have different profiles of gene expression and thus different protein expression compared to their planktonic form (Rizzello et al., 2013).

Biofilm development starts with attachment of free bacteria to the surface, formation of irreversibly attached monolayer and multilayers, excretion of extracellular compounds and finally the formation of a 3D architecture (Romeo, 2008). There are two approaches to study the antimicrobial effects on biofilms *(a priori*), before the formation of the biofilms, or *(a posteriori*), after the formation of the biofilms. Most of the previous studies focused on the first steps (the initiation of the biofilm), which can be applied in food industries and medical devices. In food industries, biofilms cause hygienic problems, disease and economic losses (Yang et al., 2011). The bacterium *Campylobacter jejuni* is one of the major causes of foodborne disease usually when contaminated meat or poultry products are consumed (Van Houdt and Michiels, 2010). In clinical environments, several studies have shown that the existence of biofilms on

indwelling devices such as central venous catheters resulted in significant morbidity and mortality and had a substantial impact on healthcare delivery (Yang et al., 2011).

Nanomaterials such as metals, silver, copper, gold, titanium and zinc have been used as antimicrobial agents (Seil and Webster, 2012; Hajipour et al., 2012; Azam et al., 2012). Silver and copper, however, are the most commonly used. They have been coated or incorporated into different materials such as poly (methyl methacrylate) and hydrogels (Allaker and Memarzadeh, 2014). Although the antimicrobial mechanism is not yet not fully understood, some studies suggest that nanoparticles physically damage the membrane of the biofilm cells, while other studies suggest that nanoparticles release ions, which are toxic to the biofilm (Seil and Webster, 2012). Studies have shown an inverse relationship between the antibacterial effect and the nanoparticles' sizes; the small sizes ranging from 1-10 nm are more toxic to bacteria than larger sizes (Allaker and Memarzadeh, 2014).

Silver (Ag) has been widely investigated and it is been used in biomedical applications because of the relatively less toxic effects to human cells. The antibacterial activity of Ag might come from the silver nanoparticles alone or could be even increases with other compounds. For instance, a surface coated with silver bromide (AgBr) prevents the biofilm formation by Gram-positive and Gram-negative bacteria (Sambhy et al., 2006). Although the exact mechanism is still under investigation, it is likely that Ag has more than one mechanism to kill the bacteria. The positive charges of the silver ions allow the electrostatic attraction between the ions and the bacterial cell membranes (the bacterial membrane is negatively charged) which then has antimicrobial activity (Abbaszadegan et al., 2015). Silver ions can also target cells at the molecular level. For example, they inhibit DNA replication and important enzymes for ATP production (Feng et al., 2000). It has been showed that these ions change the cell membrane

structure leading to cell death (Sondi and Salopek-Sondi, 2004). Results from different studies suggested that silver ions are likely to target sulphur-containing protein or elements such as DNA. The attachment of silver nanoparticles to the bacterial cell releases the silver ions, which penetrate the bacterial cell wall and inhibit enzymes responsible for respiration, and thus, generate free radicals at the cell membrane (Kim et al., 2007).

Similar to Ag, copper (Cu) also interacts with bacterial cells; however, the exact antibacterial mechanisms are still unclear. Agarwala et al. (2014) have shown that CuO possess antibacterial effects on *Staphylococcus aureus* biofilm. The bacteria died after four days of exposure to the CuO as a result of DNA and bacterial envelope damage. This finding suggested that subsequent to the specific binding of this metal to DNA, OH redox is generated, causing DNA damage (Agarwala et al., 2014). Silver and copper-based nanomaterials seem to be very effective tools as antimicrobials.

Rodrigues and Elimelech (2010) have investigated the impact of single walled carbon nanotubes (SWNTs) on biofilm formation of *E. coil* in three different stages (i) cell and biofilm formation (ii) mature biofilm (iii) biofilm formation on surface coated with these nanoparticles. Results showed that SWNTs inhibited the initial attachment of cells. The EPS in mature biofilm was found to play an important role in reducing the toxicity of SWNTs. They also exposed bacterial cells to SWNTs with or without EPS; biofilms without soluble EPS in the media were more sensitive to SWNTs, and had greater biomass loss compared to the group with soluble EPS in the media (Rodrigues and Elimelech, 2010). Several studies have suggested that EPS interacts with antimicrobials such as antibiotics and protects the cells by reducing their concentrations or by preventing their penetration to the biofilm (Sutherland, 2001). EPS can also protect biofilms from other antimicrobial agents such as heavy metals

by the binding of metals to various EPS functional groups (Starkey et al., 2004). EPS of many biofilms contains DNA, RNA and polysaccharides, these polysaccharides are relatively soluble and produce viscous aqueous solution (Sutherland, 2001). The viscous layer reduces the transportation of nanomaterials, and thus, reduces the contact of nanomaterials with the cells inside the biofilms. Therefore, this mechanism reduces the toxicity of nanomaterials to cells (Rodrigues and Elimelech, 2010).

The anti-adhesion and antibacterial activity of GO coated with silver nanoparticles was tested against *Pseudomonas aeruginosa* (de Faria et al., 2014). The GO-Ag nanoparticles were of 7.5 nm in diameter, the dispersion of GO alone showed no antibacterial effect on the bacterial cells at different concentrations (0.1-5.0 µg/ml). On the other hand, the combination of GO with silver showed high biocidal activity on planktonic cells when used at 2.5 µg/ml. The antibiofilm activity was also studied using stainless steel surfaces covered with GO-Ag. Results showed that biofilm formation was completely inhibited, because cells were not able to adhere to the surface. This was probably due to the Ag^{+} ions release. Ag+ ions penetrate the bacterial cells wall and interact with proteins containing sulphur. Moreover, silver nanoparticles produce reactive oxygen species (ROS) under oxidative conditions; leading to DNA damage. Therefore, the interaction of silver with sulphur and phosphorus may affect the metabolic pathway and the mechanism of cell division, which leads to the destruction of the bacterial cell (de Faria et al., 2014).

Combined materials with GO such as polyvinyl-*N*-carbazole (PVK)-graphene oxide (PVK-GO) have shown potent antibacterial activity both in two Gram-negative *Escherichia coli* and *Cupriavidus metallidurans*, and two Gram-positive bacteria, *Bacillus subtilis* and *Rhodococcus opacus* (Mejías Carpio et al., 2012). It was observed that PVK-GO has higher antimicrobial effects on biofilms compared to the

pristine GO (**Table 1.3**). When PVK-GO was applied to biofilm, metabolic activity was significantly reduced in the bacteria, resulting in bacterial death.

Table 1. 3 The loss of biofilms in percentage when exposed to PVK-GO and GO. Biofilms were grown on PVK-GO and GO surfaces with different concentrations of GO on agar plates. The measurements were taken by agar plate test (SPT) and OD (Mejías Carpio et al., 2012)**.**

	PVK-GO 30 µg/mL		GO 1000 µg/mL	
Exposure time	**1 h (SPT)**	**48 h (OD)**	**1 h (SPT)**	**48 h (OD)**
E. coli	42.1 ± 8.4	93.6 ± 4.5	19.6 ± 7.6	67.7 ± 7.9
C. metallidurans	—	95.3 ± 5.2	—	37.9 ± 4.8
B. subtilis	53.6 ± 5.1	97.0 ± 4.8	20.8 ± 5.9	60.9 ± 4.3
R. opacus	—	73.3 ± 4.1	—	42.8 ± 6.3

Hu et al. (2010) studied the antibacterial activity of GO and reduced GO (rGO) papers against *E. coli* biofilm (Hu et al., 2010). It has been demonstrated by the airborne bacteria test, which is when bacteria are placed on GO or rGO paper in a petri dish and air-dried before adding media, that after overnight incubation *E. coli* cells were not able to grow on GO paper, while very small number of cells grew on rGO. SEM studies showed that *E. coli* cells on the GO paper lost the integrity of membranes, resulting in cell death. The physiochemical characteristics of graphene sheets seem to play a crucial role on bacterial cell death. However, the results were questioned by Ruiz et al. (2011). Their study showed that GO did not inhibit bacterial cell growth; on the contrary, GO actually increased *E. coli* growth from 1.0×10^6 to 9.5×10^9 cells after 16 -18 h incubation. It was also observed that bacterial growth on GO filters grew two and three times faster compared with non-GO filters (Ruiz et al., 2011). These results indicate that GO had no bacteriostatic activity in this experimental system.

Palmieri et al. (2017) studied GO stability and its effects on two bacterial species, *S. aureus* and *E. coli*, in different solutions: H_2O, PBS, NaCl, $MgCl_2$ and $CaCl_2$. In water,

the killing efficacy increase when GO concentration increase. While in other solutions, GO does not affect bacterial growth, this is due to the aggregates that shield GO edges. When the GO cluster is greater than the bacterial size, GO wraps the bacterial cell and impedes the growth. Results also showed that lower concentrations of GO in water, had an antibacterial effect on both species by cutting their membranes. Conversely, at higher concentrations, GO formed complexes with both species and either enhanced or inhibited the growth. At higher concentrations, there are different scenarios. For instance, GO dissolves in water, which means that it has a greater ability to cut the cell membrane due to the increased number of GO particles coming into contact with the cell membrane.

Lu et al. (2017) used *E. coli* with GO in random and horizontal orientations and studied phospholipid vesicles as a model system and found that the lipid layer was physically disrupted by GO. Moreover, they studied glutathione, an antioxidant, paired with reactive oxygen and suggested that oxidation happened through direct electron transfer (Lu et al., 2017). These mechanisms enhanced the antibacterial activity with vertically aligned GO stems.

Mokkapati et al. (2018) used *B. subtilis* and *P. aeruginosa* to study the antibacterial effect of GO and rGO, which was applied to LB agar plates, by measuring the bacterial biofilm area of plate. Results showed that both species were inhibited by rGO but not GO which showed no any toxicity for both. However, there was a slight reduction in *P. aeruginosa* after day 2 and 5 but not at 24h. Previous study showed that *P. aeruginosa* can convert GO to rGO (Gurunathan et al., 2013). Therefore, the toxicity of GO could possibly be due to reduction of GO to rGO; however, because of the lower number of bacteria at 24 h, it could not convert GO to rGO but this thought has still not been proven.

The best understood scenarios of the GO antibacterial mechanisms are (i) damaging the cell membrane (ii) inducing oxidative stresses (iii) or wrapping the bacterial cells (Zou et al., 2016). But still the overall efficacy of GO is not fully understood as described in recent reviews (Zou et al., 2016; Smith and Rodrigues, 2015; Tegou et al., 2016). Moreover, several studies mentioned GO has no antibacterial impact or sometimes it even enhances the growth (de Faria et al., 2014; Ruiz et al., 2011).

Furthermore, Combarros et al. (2016) showed the toxicity effect of 0.05, 0.1, 0.25 and 1.0 mg/mL GO on *P. putida* in two media: rich and minimum media. The growth was measured over time by OD. The presence of GO had a negative impact on the cells at all concentrations.

Several studies conclude that GO affects the cell membrane of bacteria (Chen et al., 2014a; Zhao et al., 2013; Liu et al., 2012a). Gao et al. (2017) demonstrated that wrapping the bacterial cells with GO causes damage. The study also showed that the antibacterial effect depends on the species of bacteria and size of GO. *E. coli* is more resistant than *S. aureus*.

Campos-Delgado et al. (2016) tested the impact of GO on *E. coli*; their results showed that GO had no impact on bacterial cells with H_2O or PBS. Interestingly, Wang et al. (2011) showed that *Shewanella* cells can reduce GO to rGO in a normal aerobic setup.

1.8. Microorganisms of interest

Soil microorganisms are important for recycling mineral nutrients (Johnsen et al., 2005; Kim et al., 2007). Researchers also showed that microorganisms in soil are key determinants of soil properties including water holding, soil compaction and erosion (Gil-Sotres et al., 2005; Winding et al., 2005). Johansen et al. (2008) contend that if there is an impact of nanomaterial on the existence of microbial communities in the soil it will then indirectly have an impact on the delicate balance of the ecosystem. The dispersion of nanoparticles in the natural environment including the associated biotransformation and bioavailability is still not clear (Peulen and Wilkinson, 2011). However, there are evidences that bacterial biofilms play a critical role in the binding and concentration of nanoparticles (Ge et al., 2011). Therefore, bacterial biofilms can be considered as important elements as a barrier for nanoparticles, and can help to explain multiple factors including movement, transformation and the effect on the natural system. Hansen et al. (2007) contend that *Acinetobacter* sp. and *P. putida* are unrelated but commonly coexist together within the soil flora as a mixture when benzyl alcohol is present. *Acinetobacter* sp. produces benzoate as a by-product from benzyl alcohol which can be utilised by *P. putida* as the carbon source. *P. putida* and *Acinetobacter* sp. were used in this study as model terrestrial bacteria.

1.8.1. Pseudomonas putida

P. putida is an aerobic, Gram-negative, rod-shaped, motile and non-sporulating bacterium. It is a ubiquitous bacterium found in contaminated soil with hydrocarbons. This bacterium can degrade several aromatics compounds (Møller et al., 1998). This bacterium plays an important role in metabolic activities in the environment, including

element cycling and degradation of pollutants such as biogenic and xenobiotic pollutants. It has been used in biotechnology applications, particularly in bioremediation, biocatalysts and for bioplastics productions (Nelson et al., 2002).

Biofilm formation of this bacterium depends on the motility and adherence. Motility and chemotaxis play a major role in biofilm formation through MorA, (a membrane-localized regulator involved in movement and chemotaxis in *P. putida*). It was shown that species lacking this regulator were unable to form biofilm (Choy et al., 2004). In addition, adhesion is enhanced by the production of extracellular DNA through the TOL plasmid (D'Alvise et al., 2010).

The strain *P. putida* KT2440 (Hansen et al, 2007) is the best characterised strain that has the ability to survive in the environment. It was the first Gram-negative bacteria that lived in the soil to be certified as generally regarded as safe strain (GRAS). This bacterium is a preferred host for cloning (Nelson et al., 2002) and biofilm studies (Hansen et al., 2007; Arevalo-Ferro et al., 2005; Choy et al., 2004).

1.8.2. Acinetobacter sp.

Acinetobacter spp. are aerobic, Gram-negative, coccoid, non-motile bacteria. They are found in soil, water and on human skin (Juni, 1978). The first description of this organism was in 1911 when *Micrococcus calcoaceticus* was isolated from the soil. *Acinetobacter* means nonmotile, it was named by Brisou and Prevot in 1954. Scientists have become increasingly interested in these species due to their ecological and biotechnological applications. It has been found that some strains of *Acinetobacter* sp. are involved in the biodegradation of various pollutants such as toluene, phenol and benzyl alcohol in the environment (Abdel-el-haleem, 2003).

The pathway in which *Acinetobacter* sp. degrade benzyl alcohol involves the two enzymes benzyl alcohol dehydrogenase and benzaldehyde dehydrogenase II. The genes encoding these enzymes are *xylB* and *xylC* respectively on an operon which is very similar to the TOL plasmid pWW0 in *P. putida* (Gillooly et al., 1998). Benzyl alcohol transforms into benzaldehyde and finally to benzoic acid mediated by benzaldehyde dehydrogenase II.

Several mechanisms are involved in the biofilm formation in *Acinetobacter baumannii*. These mechanisms include the type IV fimbriae which is involved in the initial attachment (Eijkelkamp et al., 2011), the excretion of poly-β-1,6-N-acetylglucosamine, an exopolysaccharide functioning as an intercellular adhesin in biofilm (Choi et al., 2009) and the biofilm associated protein, which is important to build the 3D form within the mature biofilm (Brossard and Campagnari, 2012). In addition, it has been observed that strains containing the *blaPER-1* gene are more adherent and form thicker biofilms than those strains without this gene. Moreover, the expression of this gene was found to be correlated with the formation of the biofilm (Brossard and Campagnari, 2012).

1.9. Biofilm production methods

Biofilm model systems are important to understand the mechanisms involved in biofilm formation and resistance generally; the mechanism of biofilm formation can be studied *in vitro* and/or *in vivo*. The *in vitro* models will be discussed here, which can be achieved by closed or open systems.

Microtiter plate-based (MTP) systems such as 6, 12, 24 or 96-well plate are the most frequently used. In this system, biofilms grow on the bottom and on the walls of the

plate (Thuptimdang et al., 2015; Mejías Carpio et al., 2012). This is a closed system, which means that there is no continuous nutrient flow during the experiment. Instead, media is replaced intermittently. The main advantages of this system are: this system is relatively cheap, straightforward and requires small volumes of reagents. Furthermore, large number of tests could be done by using this system, which makes it suitable for quick screening studies (Niu and Gilbert, 2004). In addition, the examination of coating materials can be easily performed (Coenye and Nelis, 2010). The system is ideal for testing multiple parameters such as nutrient content (Marsden et al., 2017), temperatures, atmosphere and dynamic conditions (Stepanović et al., 2003).

In contrast to the closed systems, the open systems allow fresh media to continuously flow to biofilms. Several devices were used to study biofilms in open systems. These models try to mimic the biofilm behaviour, which allows testing of different conditions. In addition, they have been used to achieve a diversity of goals in laboratories such as modelling biofilm formation (Miller et al., 2013), study the biofilm in drinking water mains (Chang and Craik, 2012) or biofilm formation in the dairy industry (Willcock et al., 2000).

1.9.1. Annular Reactor

The annular reactor or Rototorque has been used for several decades to develop biofilms (Fang et al., 2010; Zhou et al., 2009; Chang and Craik, 2012). This reactor consists of two cylinders, external (static) and internal (rotating) cylinders (Fang et al., 2010). The inner cylinder holds coupons where biofilms grow, and the rotation of cylinder controls the shear stress (Figure 1.2).

Furthermore, this reactor was also used to study the impact of temperature on biofilm development. Pintar and Slawson (2003) have studied the impact of different temperatures and concentrations of chloramine residual on ammonia oxidizing bacteria biofilms. Results showed that biofilms were developed at all temperatures (6, 12, 22 C^o) but the chloraminatin inhibited biofilms at lower temperature during 5 weeks monitoring. Similar studies also showed that temperature and nutrient levels are important and should be considered (Ndiongue et al., 2005).

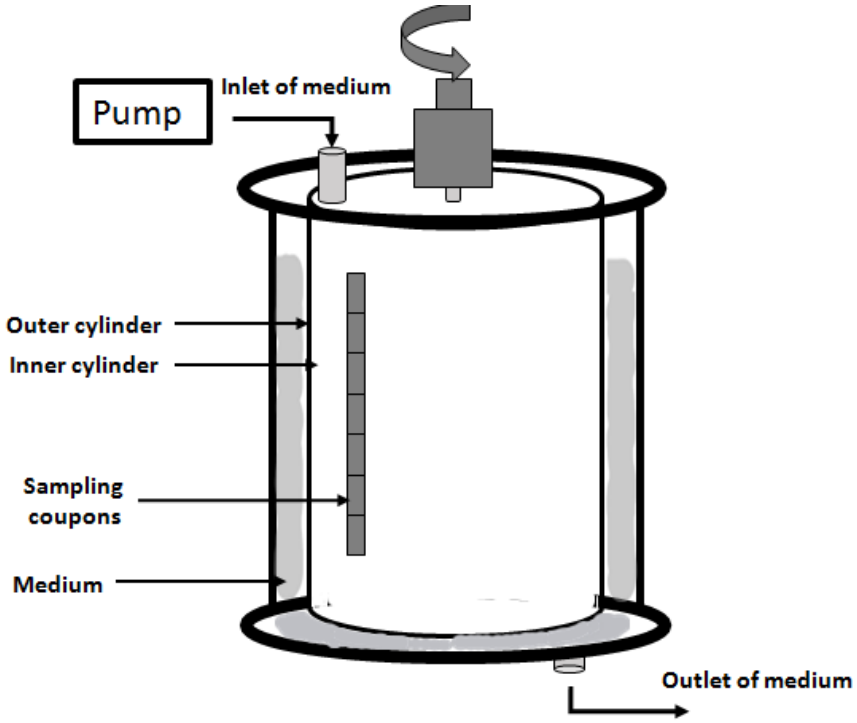

Figure 1.2 Diagram of the annular reactor

1.9.2. Concentric Cylinder Reactor (CCR)

This reactor was applied to study biofilm formation in dairy industries (Willcock et al., 2000). It consists of four rotating cylinder pipes and four stationary cylinder chambers (Figure 1.3). Different shear rates can be applied in this reactor in the same inoculating community (Willcock et al., 2000). Rickard et al. (2004) used the CCR to study drinking water biofilms and to describe the effects of different shear forces on biofilm formation

and its effects on microbial diversity. Different diameters were used at rotation speed of 43 rpm and provided different shear rates. The study showed that shear rates affected the biofilm diversity and the aggregating of bacteria.

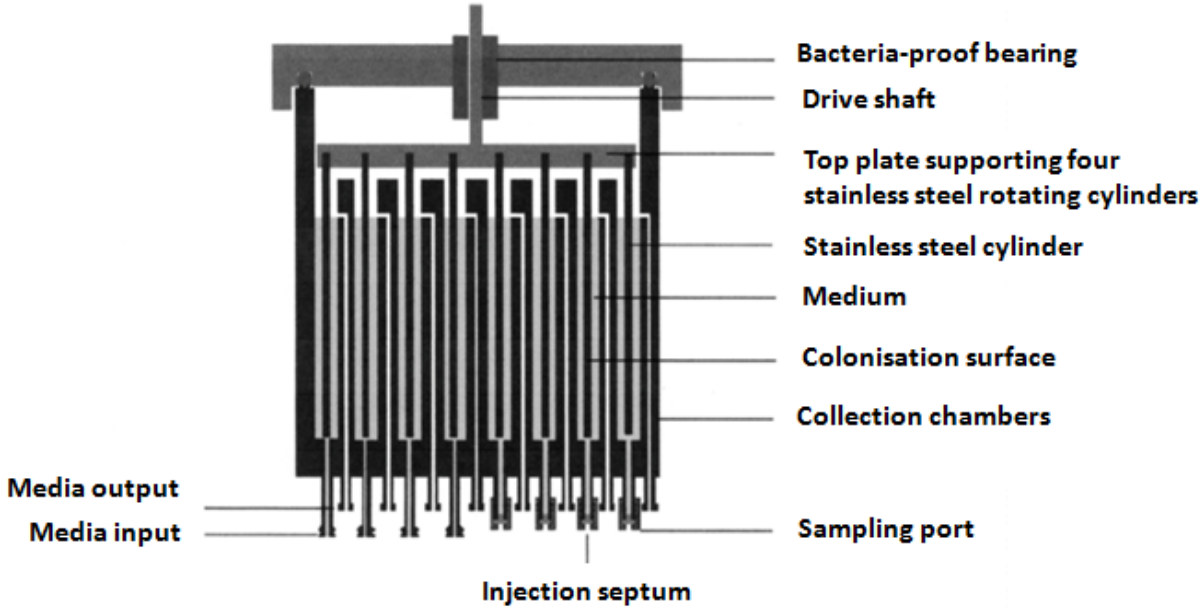

Figure 1.3 Cross sction of the CCR from Willcock et al., 2000

1.9.3. Propella Reactor

The propella reactor is commonly applied to study water biofilms (Dailloux et al., 2003; Gosselin et al., 2013; Lehtola et al., 2006). It is composed of two cylinders in which the propeller pushes the liquid down through the inner tube and then up through the annular section between both cylinders and the sampling coupons are placed on the outer cylinder facing the inner tube (Figure 1.4). The flow rate is controlled by the rotation speed of the propeller (Gomes et al., 2014). Pathogenic bacteria such as *E. coli*, *Legionella pneumophila* and *Mycobacterium avium* grown on polyvinyl chloride (PVC) coupons can survive under high shear turbulent flow conditions by using 2.3 L propella reactor with a flow rate of 183 ml/min (Lehtola et al., 2007).

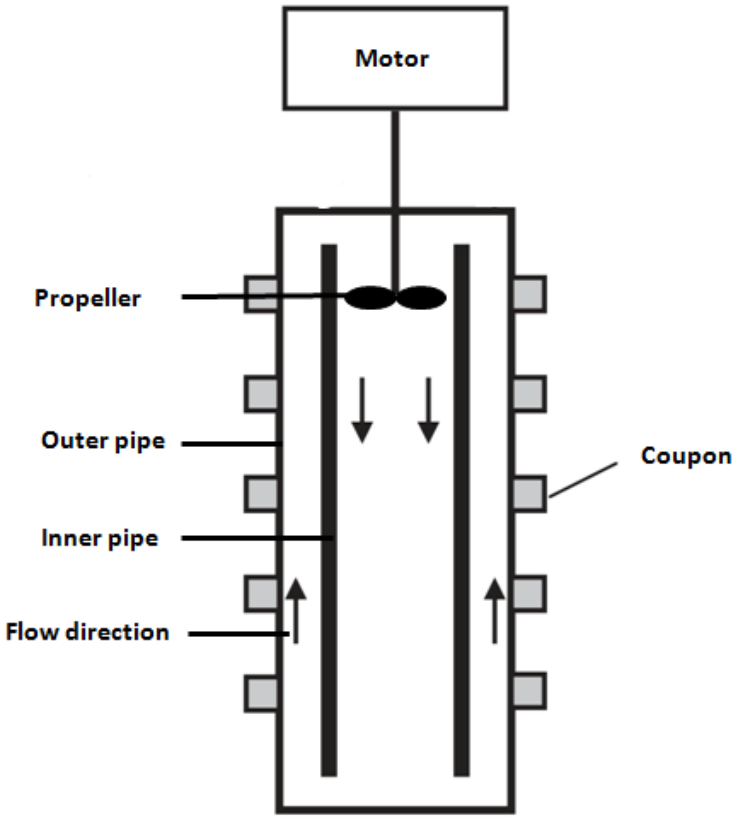

Figure 1.4 Cross section of the propella reactor

1.9.4. Flow Cell System

The flow cell system can be used for modelling biofilm formation in real-time non-destructive confocal laser scanning microscopy (CLSM).

The system operates under continuous flow conditions. Therefore, the medium is pumped from the medium supply though a bubble trap, where the air bubbles within the fluid rise up so that only air bubble-free medium is transported to the flow cell, using a peristaltic pump (Figure 1.5). The biofilm growing within the flow cell is provided with nutrients and oxygen continuously. Biofilm are developed after the attachment of the bacterial cells in a surface. To observe the evolution of biofilm, the surfaces that are used for this system are usually transparent and non-fluorescent coverslips. The microscopic analysis is carried out by the CLSM (Macià et al., 2014).

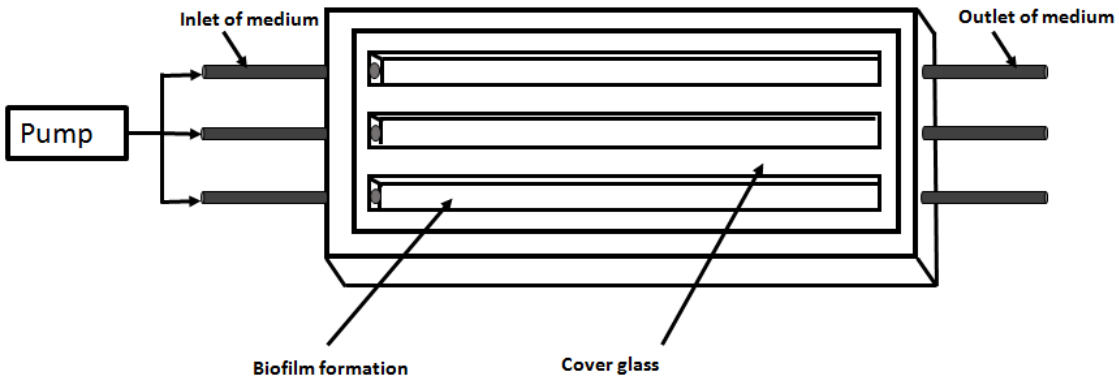

Figure 1.5 Diagram of the cell flow system

1.9.5. Rotating Disc Reactor (RDR)

The reactor is composed of a tank with a disc that rotates the fluid and holds several coupons (Figure 1.6). Similar to CCR, the shear forces depend on the location of coupons in the reactor and the rotation speed. However, the entire disc rotates in the fluid; each radial position has variable hydraulic shear stress, which enables simultaneous formation of biofilms under different hydrodynamic conditions (Gomes et al., 2014).

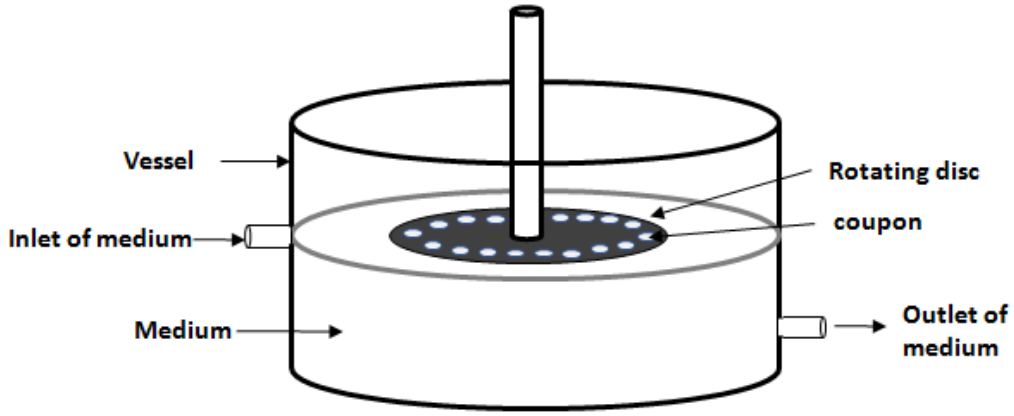

Figure 1.6 Diagram of the RDR

1.9.6. CDC Biofilm Reactor (CBR)

The Centre for Disease Control (CDC) reactor is composed of a one litre glass vessel with a polyethylene top holding eight removable polypropylene rods. These rods hold three removable coupons where biofilm is developed on a total of 24 coupons (Figure 1.7). These coupons can be composed from different materials such as polycarbonate, porcelain, mild steel, stainless steel, glass, etc. The mixing is provided by a baffled magnetic stir bar, which gives coupons a consistent shear. The shear force can be controlled by the rotation speed. The reactor operates a continuous flow system, which means that medium is continuously pumped into and flows out of the reactor at the same rate. The CBR is a reliable experimental tool to study biofilm development by various organisms (Goeres et al., 2005; Coenye and Nelis, 2010). CBR is suitable to grow *Pseudomonas aeruginosa* biofilm. The large volume used in the reactor (approximately 500ml) makes it less accurate to assess the effect of antimicrobial agents, because in this case, large volumes of reagents will be required to get the desired concentrations (Thuptimdang et al., 2015). CDC bioreactor was used in this thesis.

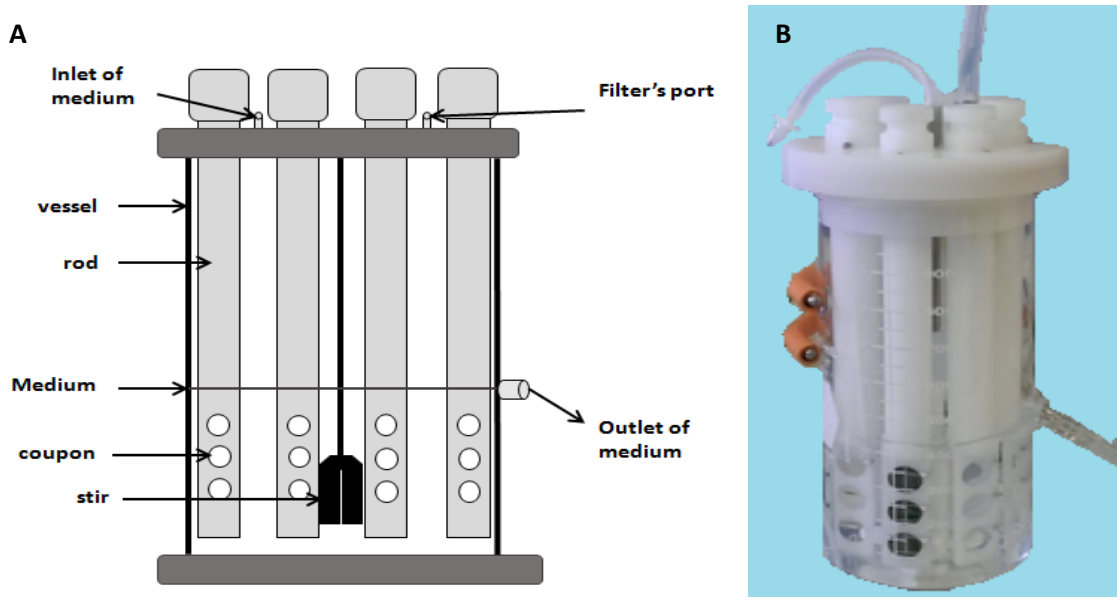

Figure 1. CDC bioreactor A) a cross view of the CDC B) a photo of the CDC

Chapter 2. Preparation and Characterization of Graphene Oxide

2.1. Abstract

Graphene oxide (GO) can be defined as few layers of graphene sheet with oxygen - groups attached to its surface. In this chapter, GO was synthesised from graphite flakes using the modified Hummers-Offeman method. The structural, optical and chemical properties of the GO were characterized by transmission electron microscopy (TEM), atomic force microscopy (AFM), Raman microscopy, Fourier transform infrared spectroscopy (FTIR), UV-Visible spectrometer (UV-Vis), X-ray photoelectron spectroscopy (XPS) and charge through zeta potential. The existing of GO was initially confirmed using Raman Spectroscopy by the presence of the characteristic G and D bands (1583 cm^{-1}, 1328 cm^{-1}, respectively). TEM and AFM then confirmed the thickness of the GO sheets to be between 1.6 and 2 nm suggesting 1-2 sheets. It was also confirmed that GO was negatively charged (– 36.4mV) and FTIR technique confirmed the presence of oxygen-containing functional groups (hydroxyl and carbonyl). The carbon to oxygen ratio was 2:1 as determined by XPS. Therefore, ultrapure GO was prepared and characterised using multiple techniques and will be discussed in this Chapter.

2.2. Introduction

Graphene consists of a thin flat monolayer of carbon atoms tightly packed into a two-dimensional (2D) honeycomb lattice (Geim and Novoselov, 2007; Jamialahmadi et al., 2018). Attention to graphene has been recently increased, due to its fascinating physical and mechanical properties including its unique electronic (Oh and Zhang, 2011) and biomedical applications (Bitounis et al., 2013). Moreover, graphene sheets are difficult to distribute homogeneously in water and display weak interaction with organic solvents (Johnson et al., 2015). As a result, genuine composites with desirable properties cannot be generated (Wu et al., 2018).

Unlike graphene, graphene oxide (GO) can be synthesized in a dry or wet medium (Pendolino and Armata, 2017). The dry synthetic methods consists of oxidation reaction of graphene through atomic oxygen in ultrahigh vacuum (Hossain et al., 2012). In the wet method, graphite is used as a graphene source because of the low-cost and its natural abundance (Pendolino and Armata, 2017). There are two main approaches to produce GO. The first method starts with a mechanical approach to synthesize graphene followed by further oxidation (Bosch-Navarro et al., 2013). The other method requires oxidation and exfoliation process with strong acids as found in Brodie (Brodie, 1859), Staudennmaier (Staudenmaier, 1898) and Hummers methods (Hummers and Offeman, 1958). All these approaches can synthesize GO, however, the structural properties of the GO produced by each method are different (Rodriguez-Pastor et al., 2015). The most commonly used method to produce GO is the Hummers' method and there are many modifications in this method to improve on the yield and purity of the produced GO (Ali-Boucetta et al., 2013; Huang et al., 2011).

Herein, pure GO was synthesized from graphite flakes through the modified Hummers' method (Ali-Boucetta et al., 2013). The synthesized GO was characterized in terms of its purity, chemical structure and morphology by various methods including: TEM, AFM, Raman, FTIR, UV-Vis, XPS and zeta potential.

2.3. Methodology

2.3.1. Synthesis of graphene oxide

GO was prepared by a modified Hummers-Offeman method (Hummers and Offeman, 1958) as described by (Ali-Boucetta et al., 2013) with small modification in incubation times. Simply, 0.2 g of natural graphite flakes from Sigma Aldrich was mixed with 0.1 g sodium nitrate ($NaNO_3$) and 4.6 mL of 96% sulphuric acid (H_2SO_4) slowly in a 125 mL conical flask and placed in an ice bath using a magnetic stirrer and stirred for 20 min with a speed of 150 rpm. A thermometer was used to monitor the temperature throughout the process and to keep it below 5 ˚C. 0.6 g of potassium permanganate ($KMnO_4$) was added gradually to the mixture as shown in **Figure 2.1**. The resultant reaction mixture was taken out from the ice bath and kept at room temperature while stirring for 30 min until the mixture started thickening and turn to dark green paste at a speed of 100 rpm. In the next step, 9.2 mL of deionized water was slowly added and the paste was stirred manually. Temperature rapidly raised to approximately 50˚C, using a hot plate to maintain temperature around 95˚C to 100˚C for 60 min followed by further dilution of with 28 mL warm water. 3 mL of 30% hydrogen peroxide (H_2O_2) was then added to the mixture to stop the oxidation process (Huang et al., 2010) and reduce the residual permanganate, manganese dioxide and manganese heptoxide to soluble manganese sulphate.

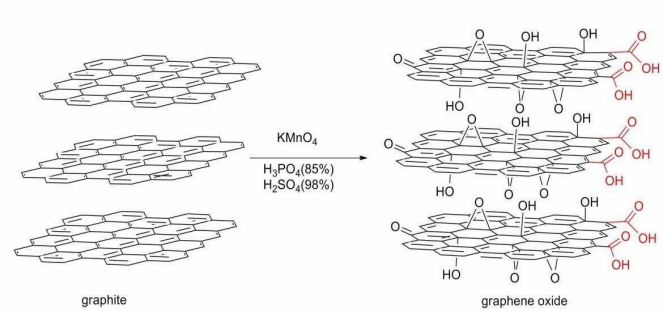

Figure 2.1 Schematic diagram shows the exfoliation of GO from graphite with Hummer's Method (Zuo et al, 2013).

The purification process was carried out with several centrifugation steps under sterile conditions. The mixture was transferred to a 50 mL falcon tubes and vortexed for a few seconds. Each tube was washed with 20 mL warm sterile water in a biological safety cabinet. Then each tube was vortexed and centrifuged at 6,650g for 25 min at 40 ˚C. After centrifugation, the pellet was separated from the supernatant by decantation. This process was carried out 2-3 times. The pH of the supernatant was checked using pH paper after each wash, as it gradually becomes less acidic and more colourless. When the pH value of the discarded supernatant is approximately 3-4, the washing step was repeated with cold water, and the centrifuge was set at 20˚C with the same speed. When pH > 6, GO appeared in the form of a brown/golden viscous layer on top of the rest of the oxidation by-products. The appearance of this layer when pH > 6 represented the final washing step.

To collect the GO from the pellet, warm water was added gently to the tube and it was then shaken manually to suspend the GO. This step was repeated several times. A cell strainer, a sterile nylon filter with micron pores of 40 μm, was also used to remove any impurities such as graphite particles from the GO dispersion. The mixture was then transferred into a sterile tube. To determine the concentration of the brown/golden

layer of GO, 1 mL was transferred into a glass vial and was dried at 40°C for 48 h. According to the weight of the dry product; the concentration of the original suspension was detected. The single layer sheet of GO is achieved by sonication using a water bath for 2 h.

2.3.2. Transmission Electron Microscopy (TEM)

The lateral size of GO sheets was measured using an electron transmission microscope (TEM). A volume of 5 µL of GO (10 µg/ml) was placed on a grid covered with support of Formvar/carbon film, air dried, and examined under a TEM (JEOL 2100EX model) to obtain higher resolution images with an operating voltage ranging from 40 to 120 keV using an LaB_6 filament. The lateral sizes distributions of more than 60 GO sheets were measured using ImageJ software.

2.3.3. Atomic Force Microscopy (AFM)

Atomic force microscopy (AFM) was used for characterizing the morphology and thickness of individual GO sheets. A volume of 10 µL of the sonicated GO dispersion was transferred onto a silicon surface (due to its smooth surface) and dried at 40 ^{o}C for 20 min and the surface morphology of GO was characterized using an AFM NanoWizard II AFM (JPK, UK) in contact mode at a 512 x 512 scanning resolution by JPK Nano-wizard 2 software, with a scan area of 20 µm x 20 µm.

2.3.4. Raman spectroscopy

Raman spectroscopy was used to identify the chemical properties of GO. The Raman spectra of GO was recorded after preparing the aqueous dispersions and dried on a microscope glass by evaporating the solvent in oven. Results were recorded by 100x objective and excitation was provided by a He-Ne 633 nm laser using Renishaw inVia

Raman spectrometer with WIRE 3.1 software and an average of 3 locations were measured.

2.3.5. Fourier-transform infrared (FT-IR) spectroscopy

Fourier-transform infrared (FT-IR) spectroscopy was employed to determine the functional group on the surface of the GO. For the transmittance readings, the GO samples were ground and mixed with KBr at a 1:9 ratio (w/w). This mixture (0.1 g) was then compressed into a thin KBr disc under a pressure of 0.4 bar for 3 min. The disc was placed for 10 min in the FT-IR spectroscopy before starting the analysis to reduce the interference of water molecule from the air. FT-IR spectra were obtained on a Nicolet 6700 spectrometer and the range of the spectrum was from 4000 to 500 cm^{-1} at a resolution of 4 cm^{-1}. After running the sample, data were collected by signals and each of the peaks are characteristics of different vibrational modes on molecules.

2.3.6. UV-Visible spectrophotometer (UV-Vis)

The absorbance and spectra of GO dispersion was determined using UV-Visible (UV-Vis) spectrophotometer. The UV-Vis absorption spectra were recorded on a Varian Cary 50 Bio spectrophotometer equipped with an integrating sphere accessory for diffuse reflectance spectra over a range of 200–900 nm. The collected data was then analysed using the Cary Win UV software.

2.3.7. X-ray photoelectron spectroscopy (XPS)

X-ray photoelectron spectroscopy (XPS) was used to determine the elemental contents and the C/O ratio of the GO. An aliquot of 100 µL of GO dispersion was added five times throughout a day onto a mould placed in an oven at 60 ^{o}C for three days to create a solid disk with dimensions of approximately 7 x 7 x 3 mm. Data were collected using an Omicron Multiprobe. The measurements were conducted in the main analysis

chamber using an XM1000 monchromatic Al Kα x-ray source (hv = 1486.6 eV) at room temperature. The photoelectrons were detected using Sphera electron analyser (Omicron Nanotechnology) using a step size of 0.5 eV and pass energies at 50 eV. Selected high resolution core level spectra recorded using a step size of 0.1 eV and pass energies of 10 eV (resolution approx. 0.47 eV). All binding energies were corrected with reference to the C-C/C-H bond at 284.6 eV during data analysis.

The data was analysed with CasaXPS package and Shirley background, and were fitted according to the mixed Gaussian–Lorentzian (Voigt) line-shapes components and asymmetry parameters where appropriate. Calibration of the binding energies was achieved using the Fermi-edge of polycrystalline Ag sample, measured immediately before starting the measurements. The transmission function of the spectrometer was calibrated using a variety of clean metal foils to ensure compositional accuracy. This work was done at the Warwick Photoemission Facility at University of Warwick with the help of Dr. Marc Walker.

2.3.8. Zeta Potential measurements

GO dispersion (60 μg/mL) was injected in a universal folded capillary cell (Model DTS 1070, Malvern Instruments Ltd, UK) equipped with platinum electrodes and a folded capillary, ensuring that air was removed. The electrophoretic mobility (EM) at 150V of the suspended GO particles was then measured at 25 ^{o}C using Malvern ZetaSizer Nano ZS (Malvern Instruments Ltd, UK), which uses the scattering of incident laser light to detect the GO particles at relative low magnification. The instrument was calibrated using the ζ-potential transfer standard (DTS1235) which has a ζ-potential of -42mV ±4.2mV. The mobility of the GO particles under the applied voltage was converted to the ζ-potential using the Henry equation and reported as the average and

standard deviation of measurements made on three freshly prepared samples, with each sample analysed in triplicate.

2.4. Results and discussion

2.4.1. Synthesis of graphene oxide

GO samples were synthesis from graphite flakes using the modified Hummers and Offeman's method as described by Ali-Boucetta et al (2013). This method differs than the original one in that it involves further purification and centrifugations steps in order to purify the GO from the other unreacted graphite contaminants and the poorly soluble oxidised by-products (Ali-Boucetta et al., 2013). The GO prepared by this method critically depends on the separation of a brownish/golden gel layer (GO) from a thick black sediment (impurities) (**Figure 2.2**). GO layer appeared when pH became neutralised after several washings. The GO was well dispersed in aqueous colloidal suspension and was stable for more than six months as shown in **Figure 2.2C and D** due to the hydrophilic functional groups on the GO surface such as epoxy, carboxyl and hydroxyl group (Liu et al., 2011).

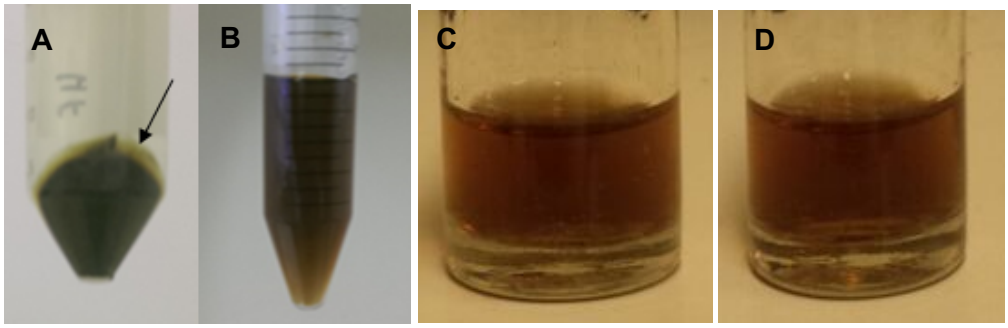

Figure 2.2 Graphene oxide purification steps (washings) before (A) and after (B) separating from graphite. The arrow in (A) represent the GO layer. (C) Image of fresh GO and (D) image of 6 months old GO

To accurately determine the concentration of GO from this method, the sample was dried at 40^{o}C for 48 h. The achieved yield was about 58.5% (vs graphite), which is

higher than the yield achieved by other studies which had 17.5% (Jasim et al., 2016) and 22.4% (Ali-Boucetta et al., 2013).

2.4.2. Structural properties

The morphology of GO was studied by transmission electron microscopy (TEM) and atomic force microscopy (AFM).

After the synthesis of GO, the purified GO was sonicated for 10 or 120 min to obtain two different sizes as shown in **Figure 2.3A** and **Figure 2.3B**. The sonicated GO sheets show average sizes between 400-600 nm (38.5%) or 100-200 nm (62%) of the total GO sheets count and sonicated for 10 or 120 min, respectively (**Figure 2.4**). The images also show flake like structures as sheets and it was really challenging to obtain their dimension. This is due to the irregular boundaries of the GO sheets. These structures exhibit wrinkled GO sheets as shown in **Figure 2.3C**.

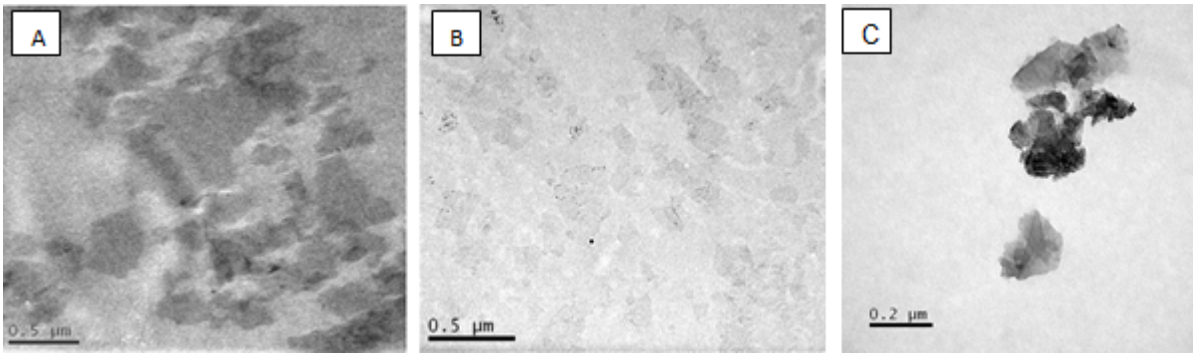

Figure 2.3 Structural characterization of GO using TEM. (A) TEM shows the GO sonicated for 10 min (GO10) and (B) GO sonicated for 120 min (GO120) (C) wrinkled GO sample.

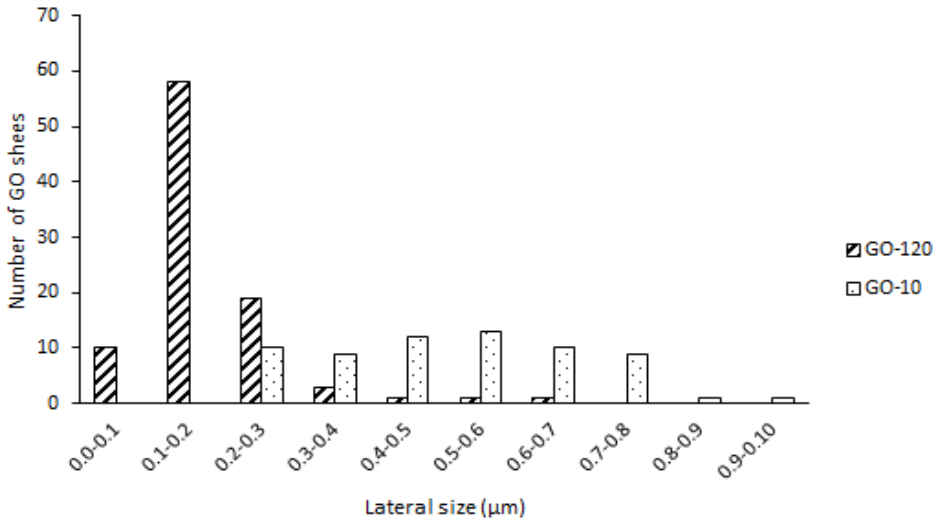

Figure 2.4 Size distribution of GO as determined by TEM and analysed using imageJ software. GO-120 were sonicated for 10 min. GO-120 were sonicated for 120 min. The Y axis represent the number of GO sheets counted and X axis shows the lateral dimensions (µm).

The morphology of GO was characterized using TEM. Graphite has a high degree of crystallinity and it contains multi-layers, around 10-20 layers according to the edge width and transparency under TEM (Rodriguez-Pastor et al., 2015). After the chemical oxidation of graphite, the number of layers reduces to few layers. Comparing this method with other methods such as Brodie and Staudenmaier, mono or bi-layer sheets could not be achieved and the sample were non-exfoliated. Rodriguez-Pastor et al. (2015) studied four methods to oxidize graphite; Hummers and Offeman (involving $KMnO_4/NaNO_3/H_2SO_4$), modified Hummers and Offeman (involving $KMnO_4/H_2SO_4$), Brodie (involving $KClO_3$ and HNO_3) and Staudenmaier (involving $KClO_3$, H_2SO_4 and HNO_3). They found that a high yield of monolayer was achieved when using $NaNO_3$ in the reaction. Huang et al. (2011) reported a large lateral dimension of GO reached up to 120 µm and an area of approximately 8000 μm^2. Based on their findings a possible reason for large GO sheets is a complete oxidation of graphite. Another possible explanation for the large GO sheets is that the reaction was carried out for three days

at room temperature compared with Hummer's method that took 2 h. It has been reported that high temperature reduced the size of GO within the oxidation step (Huang et al., 2011; Zhao et al., 2010).

The thickness of GO was then analysed by **AFM** (**Figure 2.5**). A two dimensional line profile recorded along the blue line of **Figure 2.5C** is demonstrated in **Figure 2.5D**. The height profile showed ~1-2 nm layer thickness which confirms the presence of single GO layers (**Figure 2.5D**). However, single and multiple GO sheets can also be differentiated form the optical contrast in the bar of the AFM images. The whitish colour in the top shows the thicker layers. **Figure 2.5B** shows the sharp edges of the GO.

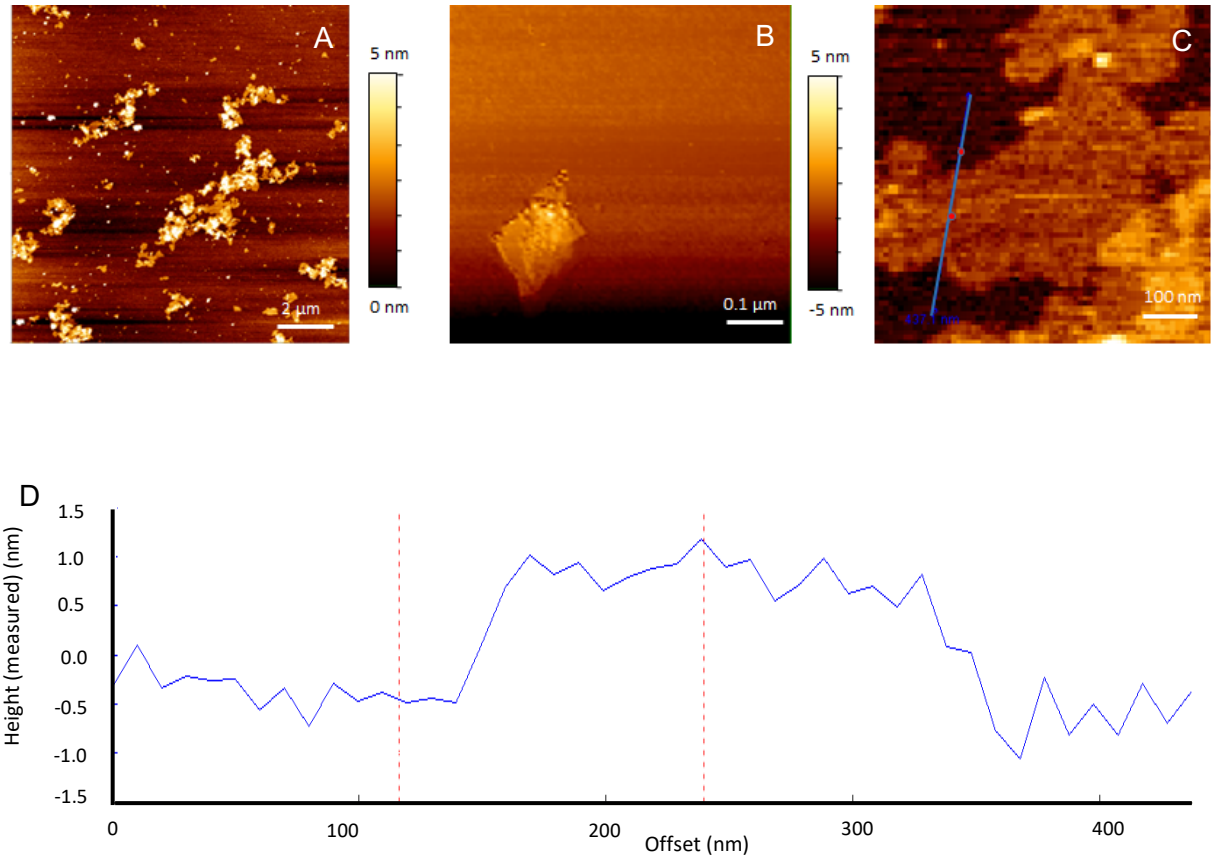

Figure 2.5 AFM of GO sheets. (A) shows a top view of GO sheets on silicon wafer (B) high-resolution image of a single GO sheet showing the sharp edges of GO (C) and (D) a cross-section analysis along the blue line of GO.

The results show that GO was thicker than theoretical graphene sheet 0.34 nm (Kano et al., 2017). This is because of pristine graphene has no functional group. Graphene sheets with 10 layers is considered as a graphene while less than that it will be considered as an ultrathin graphite (Jasim et al., 2016).Most studies reported a wide range of GO thickness for a single layer average of 0.7-1.2 nm (Mukherjee et al., 2016), 1.2 -1.3 nm (Rathnayake et al., 2017), 1.5 ± 0.3 nm (Chu et al., 2018), 1.2 nm (Huang et al., 2011) 0.8 –1.2 nm (He et al., 2015a) and 1.4 nm (Perreault et al., 2015). These results are in agreement with ours 1.6-2.0 nm. The reason for these differences is not clear but it may have something to do with the time of the graphite exfoliation. The longer exfoliation the thinnest GO sheets. These results are similar to those reported by other studies (Ali-Boucetta et al., 2013; Shao et al., 2015; Gao et al., 2017).

Initially, the **Raman scattering** of GO was compared to that of graphite in the region of 1000-3000 cm^{-1} after excitation at 633 nm (**Figure 2.6**). As shown in **Figure 2.6**, both GO and graphite shown a clear D and G bands which are around the wavelength of 1360 and 1560 cm^{-1}, respectively (Sur et al., 2016; khan et al., 2017). The presence of the D & G bands is a clear confirmation of the existence of poly-aromatic hydrocarbons and defects at the aromatic rings surface (Ferrari et al., 2007; Eda and Chhowalla, 2010). The G band is attributed to the sp^2 bonded carbon regions while the D band reflects the disorder and the defects in the crystalline structure (Perreault et al., 2015). It has been reported that 2D band corresponds to the number of layers of graphene sheets and their relative orientation (López-Díaz et al., 2017). Some studies reported that GO has a low 2D intensity because GO has 1-2 sheets of graphene therefore it is common to have a reduced 2D intensity in GO compared to graphite (López-Díaz et al., 2017).

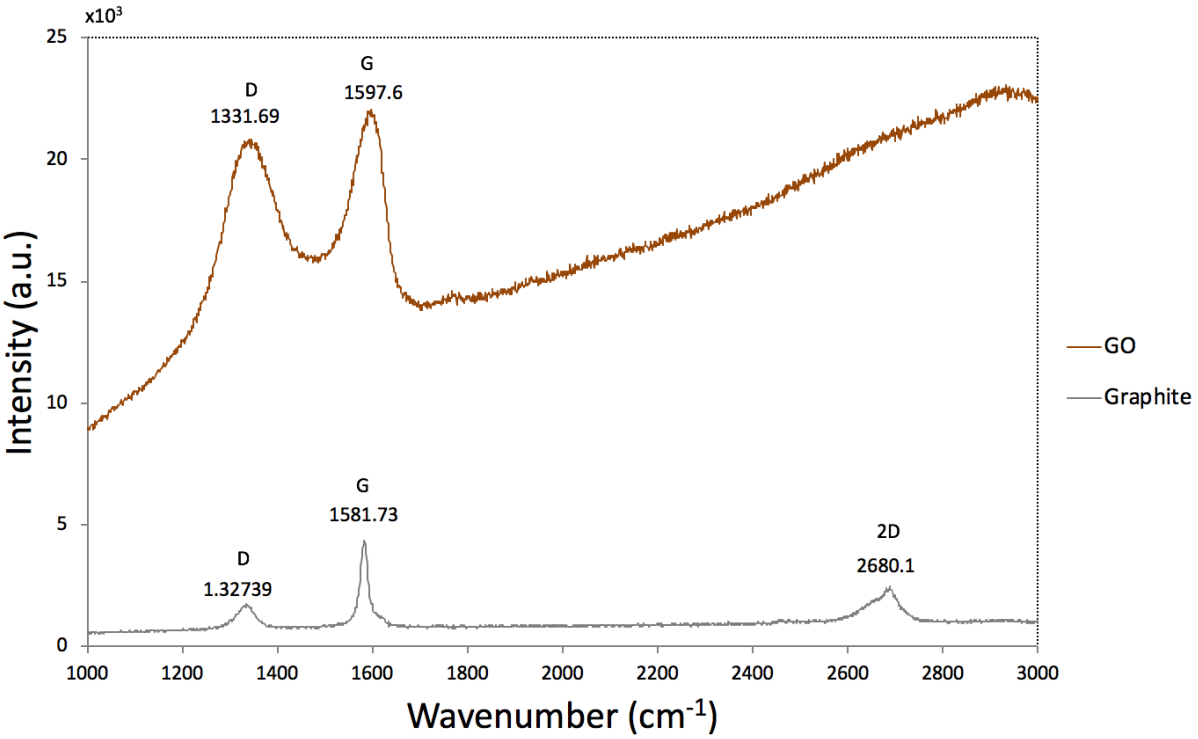

Figure 2.6 Raman spectra with D, G and 2D-band after the oxidation an exfoliation processes for graphite and GO. The spectra correspond to an exciting laser wavelength of 633 nm laser. GO and graphite both exhibited the D and G-band.

2.4.3. Chemical properties

In order to understand further what functional groups gave rise to the negative charge of GO, FTIR was used to further probe the GO surface. **Figure 2.7** illustrates the FTIR spectra of GO and highlights the presence of multiple oxygen functionalities at the GO surface which aligns with the attributed negative charge and confirms the successful isolation of GO. The sample shows a broad band around 3405 cm^{-1}, which correspond to the hydroxyl group O-H stretching. The peak around 1729 cm^{-1} corresponds to a carbonyl group while the peak around 1640 cm^{-1} is an aromatic ring with carboxyl substitution (Jasim et al., 2016). While the peak around 1450 cm^{-1} represents C=C bonds (Ţucureanu et al., 2016). The absorption at 1383 cm^{-1}, represents to a C-OH stretching groups (Herrera-Alonso et al., 2007).

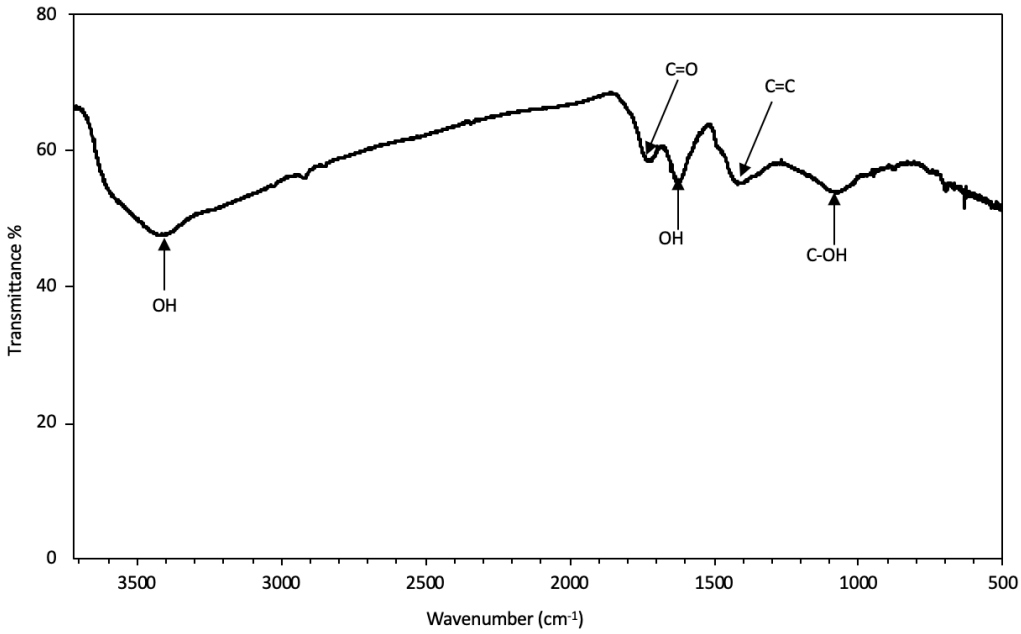

Figure 2.7 The FTIR spectra of GO in the full range of wavenumbers.

.

The UV-vis spectrum of the GO confirms its strong absorption peak at 235 nm as shown in **Figure 2.8** which is due to the transition of π to π^* of the aromatic C=C bonds. In addition there is a weak broad absorption band (shoulder peak) around 300 nm which highlights transitions of C=O bonds. Together these confirm the oxidation of graphite and is in agreement with the literature (Ali-Boucetta et al., 2013; Jasim et al., 2016).

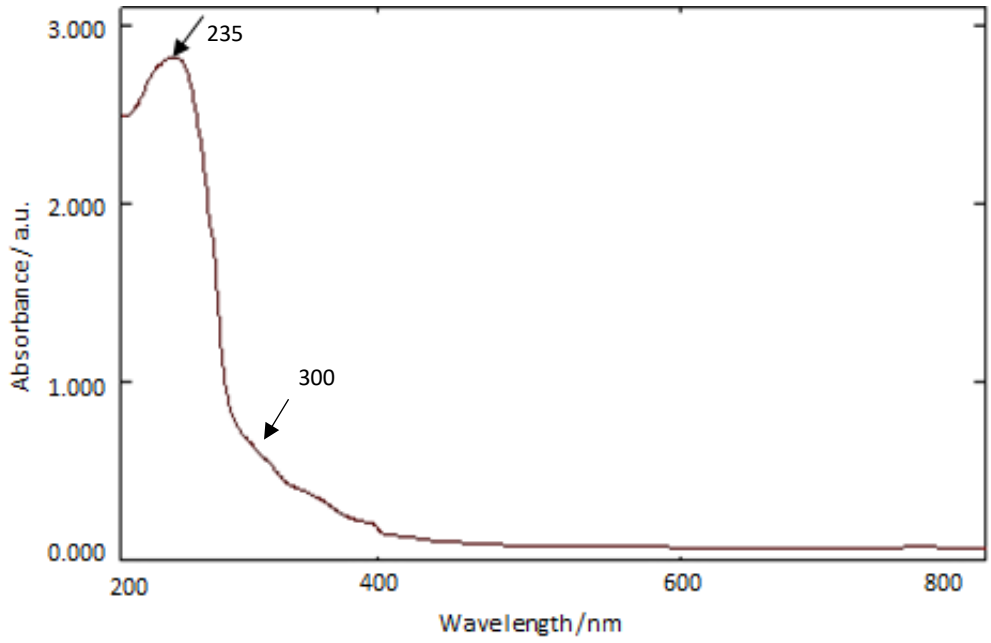

Figure 2.8 UV-Vis absorption spectra of GO exhibits a maximum absorption peak at about 235 nm, corresponding to the transition of π to π^* of C=C bonds.

To further analyse the surface and chemical content of GO, XPS analysis was performed. The carbon to oxygen ratio (C:O) was found at 2:1 correlates very well with the literature (Bianco, 2013, Hummers & Offeman 1958). As shown in **Figure 2.9A** and **Table 2.1**, carbon and oxygen are clearly the main elements in the GO sample with (68.845 and 30.54 %), respectively. A minimal percentage of sulphur and nitrogen were detected (0.48 and 0.13 % respectively).

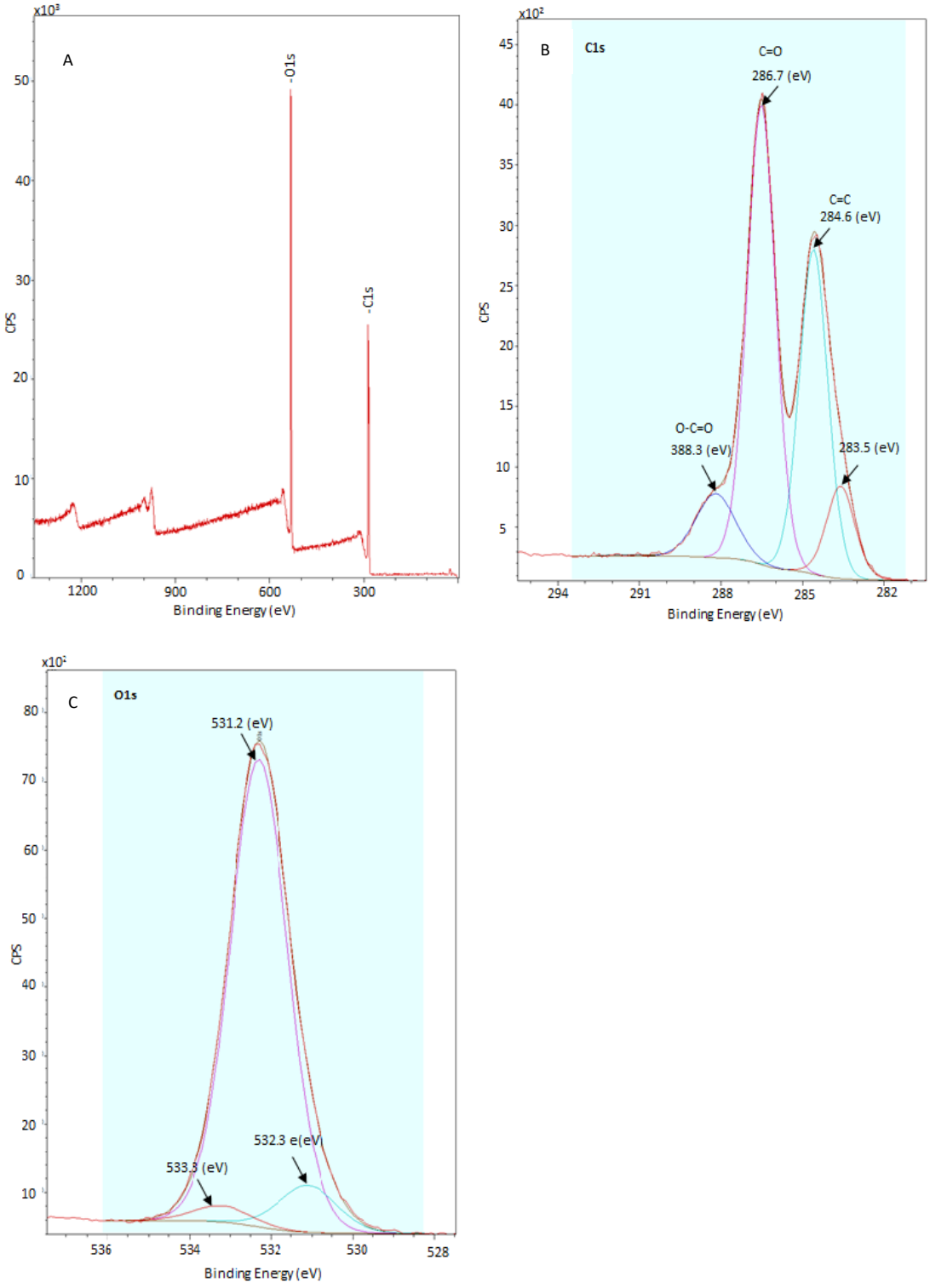

Figure 2.9 XPS result for GO Chemical contamination by XPS survey spectra (A); and quantification of functional groups by high resolution C1s XPS spectra (B) and O1s XPS spectra (C)

Table 2. 1 Atomic composition data from XPS analysis

Elements	%AT Concentration average of 3 replicates
C1s	68.845
O1s	30.54
S2p	0.4825
N1s	0.1325

In addition, the carbon chemical states show information about the surface chemical composition of GO. **Figure 2.9 B** shows the **C1s** spectra of GO. The lower binding energy at 283.5 eV represents the sp^2 carbon bond C-C in aromatic rings (Cheng et al., 2013). The double bonds between carbons C=C showed at 284.6 eV. While the carbon peaks at 286.7 and 288.3 eV represent C=O and O-C=O, respectively. These assignments agree with the literature (Cheng et al., 2013; Sarawutanukul et al., 2018). The C=O groups mainly arise from ketones which present on the edges of GO sheets but may also be bound to the sheets as carbonyl (Song et al., 2014).

Moreover, the **Os1** spectra in **Figure 2.9 C** shows information about the oxygen states on the surface of GO. Three components are found at 532.3, 531.2 and 533.3 eV corresponding to COO (531.2 eV), C=O (532.2 eV) and OH (533.3 eV) (Geng et al., 2013). While the OH could be due to water vapour that covers the sample surface from the environment or from the oxidation process of graphite, it is clear that the carbonyl C=O group was the most dominant group formed within the oxidation.

2.4.4. Surface charge

The surface charge of GO was determined by zeta potential analysis. The zeta potential GO in water was found to be – 36.4 mV as shown in **Figure 2.10** and indicate that GO is negatively charged.

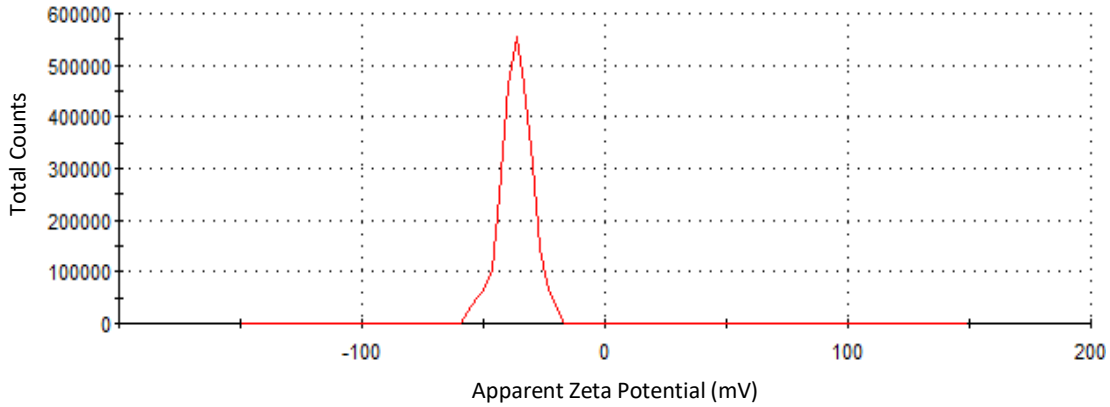

Figure 2.10 Shows the surface charge data of GO expressed as Zeta potential values from Zetasizer ζ = -34.6 ± 0.9 mV. Values are mean ± SD; n= 3

The GO dispersions in this study had a highly negative charge because of the oxygen group was added on the surface. Oxygen-containing functional groups present on GO particles make them highly hydrophilic (Kashyap et al., 2014).This confirms that acid treatment places oxygen-containing functional groups on the graphene surface (Manafi et al., 2017).

In conclusion, highly purified GO sheets were prepared through the exfoliation of graphite flakes using the modified Hummers' method. The structural, chemical and optical properties of GO were characterized by TEM, AFM, Raman spectroscopy, FTIR spectroscopy, UV-vis, XPS and Zeta potential. GO of 1-2 layers was prepared and confirmation of GO identity was achieved using a range of characterisation techniques. The presence of oxygen groups on the GO sheets gave it an overall negative charge. In the next chapter, the effect of the prepared GO will be tested against planktonic cells and biofilms.

Chapter 3. Antibacterial Effect of Graphene Oxide (GO) against Bacterial Biofilms of Variable Age

3.1. Abstract

GO has been reported to possess antibacterial activity, therefore, its accumulation in the environment could affect microbial communities such as biofilms. The susceptibility of biofilms to antimicrobials is known to depend on the stage of biofilm maturity. The aim of this chapter was to investigate the effect of GO nanoparticles (NPs) on *Pseudomonas putida* KT2440 and *Acinetobacter* sp. NCIMB 8250 biofilm of variable age. Biofilms varying in maturity (24, 48, and 72 h) were formed using a CDC reactor and were treated with GO (85 μg/mL or 8.5 μg/mL). The viability of both strains was monitored by culture on media and the bacterial membrane integrity was assessed using flow cytometry and staining with propidium iodide (PI). Biofilm biomass and thickness were observed using confocal microscopy combined with SYTO 9 and PI staining while SEM investigated morphological changes of bacteria cells. In contrast to previous studies showing no susceptibility or enhancement of biofilm growth in response to GO, our results showed that GO significantly reduced the viability of 48 h *P. putida* biofilms while the viability was not affected in 24 and 72 h biofilms. *Acinetobacter* sp. showed the reduction at 72 h but not at 24 or 48 h. The membrane integrity of *P. putida* cells from 48 h biofilm was compromised and *P. putida* cells showed flattened morphology indicative of cell membrane damage. Interestingly, *P. putida* cells detached from 48 h biofilms and cells detached from *Acinetobacter* sp. biofilm at 72 h showed susceptibility to GO. No antibacterial effects were observed in planktonic cells. The results showed that susceptibility of biofilms to GO varied

according to age which may be due to changes in the physiological state of the cells during maturation.

3.2. Introduction

Since the discovery of GO, it has shown promising applications in various areas in industry used as metal free catalysts for degradation of organic matters in water and can be used in polymer membranes for water purification and medical cloths for wound disinfection, and also coating of silicone tubes of catheters to prevent biofilm formation (Wang et al., 2013; Zheng et al., 2018). Such applications may increase the release of non-biodegradable GO into the environment posing risks of biological toxicity (Guo and Mei, 2014).

In comparison to rGO, GO contains more reactive groups that interact strongly with bacteria by covering cell surfaces, and thus presents higher antibacterial activity (He et al., 2015b; Liu et al., 2012b, 2011; Gurunathan, 2015; Hui et al., 2014). Previous mechanisms suggested for the antibacterial activity of GO include oxidative stress (Mangadlao et al., 2015; Perreault et al., 2015), trapping of bacterial cells within GO sheets (Yadav et al., 2017), cell membrane damage by the sharpened edges of GO sheets (Gao et al., 2017), and electron transfer from microbial membranes to GO (Li et al., 2014). Nevertheless, there is contradiction in the literature as some studies suggested that GO has no antibacterial activity (Bianco, 2013).

In nature bacteria attach themselves to surfaces to form communities known as biofilms by generating extracellular polymeric substance (EPS) mainly consisting of polysaccharides, proteins, and nucleic acids. In the environment biofilms actively participate in organic matter decomposition and biogeochemical cycling, being a key component of ecosystem functioning (Balcázar et al., 2015). Since environmental

biofilms affect crucial ecosystem processes it is important to understand the effect of GO accumulation on biofilm growth and survival. In aqueous environments GO can be sustained as homogenous colloidal suspensions (Zhao et al., 2010). Studies have reported that GO decreases bacterial activity and viability in soil (Jamialahmadi et al., 2018; Gurunathan, 2015). The presence of GO in activated sludge reduced the metabolic activity and viability of bacteria and inhibited their essential microbial functions needed in activated sludge processes such as removal of organic matter and nutrients including nitrogen and phosphorus (Ahmed and Rodrigues, 2013). These studies showed that GO has a negative impact on environmental bacteria.

There are four main stages that occur dynamically during biofilm formation: planktonic cells; attachment (reversible and irreversible); maturation (micro- and macro-colonies along development of EPS); and dispersion (Monds and O'Toole, 2009). Cells in each stage are physiologically different to cells in the other stages (Bester et al., 2005). Moreover, biofilms at different stages of maturity showed different susceptibility to antibiotics (Tré-Hardy et al., 2009), sanitizers (Shen et al., 2011) and silver nano-particles (Thuptimdang et al., 2015).

The presence of EPS makes the biofilm resistant to detergents, antibiotics and other chemicals as it protects the interior of the community (Hall-Stoodley et al., 2004). The removal of the EPS matrix has enhanced the antibacterial activity of rGO against *E. coli* biofilms suggesting that the presence of EPS protects the cells (Guo et al., 2017). There is controversy in the literature regarding the effects of GO on biofilms. The growth of *E. coli* biofilms was inhibited on GO coated surfaces (Mejías Carpio et al., 2012; Yadav et al., 2017). In contrast, Guo et al., (2017) reported that the formation of *E. coli* biofilm was enhanced in the presence of GO. *E. coli* and *Bacillus subtilis* biofilm

formation was encouraged at low concentrations of GO while it was inhibited at high concentrations of GO (Song et al., 2018). Furthermore, there are many factors that determine the antibacterial activity of GO including the size of GO sheets (Liu et al., 2012b; Yadav et al., 2017), purity of GO dispersion (Barbolina et al., 2016), bacterial species(Gao et al., 2017; Yadav et al., 2017) and growth media (Hui et al., 2014).

Studies that investigated the impact of GO on biofilms were limited to GO-coated surfaces which do not reflect GO within environmental systems i.e. colloidal suspensions. Moreover, studies that assessed the development of biofilms in the presence of a GO colloidal suspension have either reported no susceptibility or enhancement of biofilm growth. The aim of this study was to investigate the susceptibility of biofilm to GO at different stages of maturity, based on *P. putida* KT2440 and *Acinetobacter* sp., both of which are well-characterised bacteria and are known to be effective biofilm-producers. High and low concentrations of GO were tested assuming low and high accumulation.

3.3. Materials and methods

3.3.1. Materials

Phosphate buffered saline (PBS) pH 7.45, tryptic soy agar (Oxoid Ltd. CM0131) and broth (Oxoid Ltd. CM0129) were purchased from Fisher Scientific (United Kingdom). 40g of TSA and 30g TSB powder were dissolved in 1000 ml dH_2O then autoclaved for 15 min at 121^oC to prepare media. Stains SYTO 9 and propidium iodide (PI) were purchased from Thermo Fisher Scientific (United Kingdom).

3.3.2. Synthesis of Graphene oxide

The GO preparation and the characterisation is described previously in section 2.3.1. GO-120 was used thought this chapter (section 2.4.2; figure 2.4)

3.3.3. Preparing GO-coated surface

To test the antibacterial activity of GO-coated surface, 300 µL of 85 µg/mL GO was added to sterilized stainless coupons and were air dried. Coupons where then placed in CDC bioreactor with *P. putida* then were sampled every 24 for three days.

3.3.4. Biofilm formation using CDC reactor

Pseudomonas putida KT2440 and *Acinetobacter* sp. NCIMB 8250 were stored in -80^oC with glycerol and were streaked on TSA and incubated at 30^oC for overnight. From the overnight culture, one colony was transferred in 100ml of TSB and incubated for 24 h at 30^oC shaking at 150 rpm. This procedure has been done twice. maintained on TSA plates at 4 ^oC. Cells were transferred into 100 ml of TSB, incubated at 30 ^oC for 24 h shaking at 150 rpm. Stationary phase cells were harvested by centrifugation (10,000g for 10 min), washed and resuspended in phosphate buffered saline (PBS) to inoculate the CDC reactor.

A sterile CDC reactor (model 90-2, BioSurface Technologies, Bozeman, MT) CRB vessel containing 500 mL of sterile TSB (300 mg/mL) and with 24 polycarbonate coupons was inoculated with both species *P. putida* and *Acinetobacter* sp. cells (10^8 CFU/mL) separately, and stirred at 125 rpm at 25 ^oC for 24 h providing a batch stage for cells to attach to the coupons. The temperature was maintained at 25 ^oC using a water bath and a silicon tube blanket. Continuous-flow was operated by connecting the vessel to a 20 L TSB (100 mg/mL) and an empty carboy for feeding and waste respectively. Sterile medium was pumped into the vessel at a rate of 11.67 ± 0.2 mL/min using a peristaltic pump (Watson Marlow Inc., Wilmington, MA). Eight coupons μμwere sampled every 24 h and washed with PBS. The removed rods were replaced with blanks to maintain hydrodynamic conditions within the bioreactor.

3.3.5. Viability of *P. putida* and *Acinetobacter* sp. after treatment with GO

Biofilms on coupons from the CDC reactor at 24, 48 and 72 h were incubated with either 4 mL of sterile de-ionised water (control) or 4 mL of 85 μg/mL GO at 25 ^oC for 24 h under shaking at 80 rpm. For cell counts, the coupons were vortexed for 30 seconds and then bath sonicated (40 kHz) for 30 seconds, three times. Bacterial counts were determined in PBS using the Miles & Misra technique (Miles et al., 1938). Each dilution was plated in triplicate on TSA agar and incubated at 25 ^oC for 48 h and colonies were counted. Each experiment was conducted in triplicate (N = 3).

The effect of GO was studied on free-floating cells detached from biofilms and was compared to control planktonic cells. Coupons were vortexed and sonicated as described above at 24, 48 and 72 h and the detached cells were incubated with either 4 mL of sterile de-ionised water (control) or 4 mL of 85 μg/mL GO at 25 ^oC at 80 rpm for 5 days. The bacterial counts (CFU/cm^2) were determined on each day as described above and each experiment was conducted in triplicate (N = 3). For planktonic cells,

200μL of 10^8 CFU/mL were inoculated in 4 mL dH_2O or 85μg/mL GO and incubated the same condition of free-floating cells detached from biofilms.

3.3.6. Scanning electron microscopy (SEM)

The morphological changes to the membrane of *P. putida* cells were observed using a scanning electron microscope. Cells were mounted on a stub and coated with gold-palladium alloy (100Å and 50Å thickness respectively) sputter module in a vacuum evaporator in argon atmosphere in order to minimize surface charges and increase resolution. The samples were observed under a Quanta 3D FEG dual-beam FIB-SEM microscope operated at 15kV.

3.3.7. Confocal microscopy analysis

Coupons of *P. putida* and *Acinetobacter* sp. biofilm were washed by gentle immersing and agitating in PBS to remove unattached cells. The biofilms on the coupons were stained by adding 10 μL of PI (100 μM) and SYTO 9 (100 μM) on their surface and incubated in the dark for 5 minutes. The samples were gently covered with a cover slip and were observed at room temperature using a Leica SPE-II confocal microscope (Leica) equipped with solid state lasers for excitation. Images were acquired under 60x magnification oil immersion objective lens with a Leica DFC500 camera and Leica LAS AF software. Samples were excited using a 488 nm laser and fluorescence was detected at 617 nm (PI) and 503 nm (SYTO 9). The thickness (μm) of biofilms was measured using the Leica LAS AF software. The confocal images were Z-stacks of optical sections using 512 x 512-pixel resolution tagged image file format. From the Z-stacks of the 3D biofilm structure the biomass volume ($\mu m^3/\mu m^2$) was calculated using COMSTAT software (Heydorn et al., 2000; Vorregaard, 2008) and the percentage of live/dead cells was determined.

3.3.8. Assessment of *P. putida* and *Acinetobacter* sp. membrane integrity with flow cytometry analysis

P. putida and *Acinetobacter* sp. biofilms on CDC reactor coupons at 24, 48 and 72 h were exposed to either 4 mL of sterile de-ionised water (control) or 4 mL of 85 µg/mL GO, following their removal from the CDC reactor, at 25 ^{o}C for 24 h shaking at 80 rpm. Coupons were then placed in PBS and vortex for 30s and bath sonicated (40KHz) for 30s, three times. Dispersed *P. putida* or *Acinetobacter* sp. cells (1 mL) were stained with PI to a final concentration of 4 µL/mL and incubated in the dark for 5 minutes. Flow cytometric analysis was conducted using the BD Accuri C6 flow cytometer (BD Biosciences, UK) and samples were excited using a 488nm solid state laser and particulate noise was eliminated using a Forward scatter height (FSC-H) threshold while 20,000 data points were collected at a maximum rate of 2500 events/s. PI fluorescence was detected using 670 LP filters and data was analysed using CFlow software. Each experiment was conducted in triplicate (N = 3).

3.3.9. Statistical analysis

The generated results were collected in Excel (Microsoft Corp.) for calculating means, standard deviations, and error bars. For student's *t*-test to compare two means or one-way analysis of variance (ANOVA) and the Tukey's HSD *post hoc* test to compare several means were used for checking whether there is significant difference among samples using IBM SPSS Statistics software version 23. Differences were considered significant at $P < 0.05$.

3.4. Results

3.4.1. Effect of GO on *P. putida* and *Acinetobacter* sp. biofilms

The activity of GO against 24, 48 and 72 h mature *P. putida* and *Acinetobacter* sp. biofilms in water were monitored by plate counting (CFU/cm^2) (**Figure 3.1A and 3.1B**). In **Figure 3.1 A** there were no significant differences in viability of *P. putida* biofilm treated with 85 µg/mL GO after 24 and 72 h development compared to controls; however, the viability at 48 h was significantly ($P < 0.05$) lower indicating an age dependency of the biofilm susceptibility to GO. *Acinetobacter* sp. biofilms showed significant difference ($P < 0.05$) in CFU at 72 h after the treatment with GO 85 µg/mL GO. However, the viability showed no any significant difference at 24 h and 48 h compared to control.

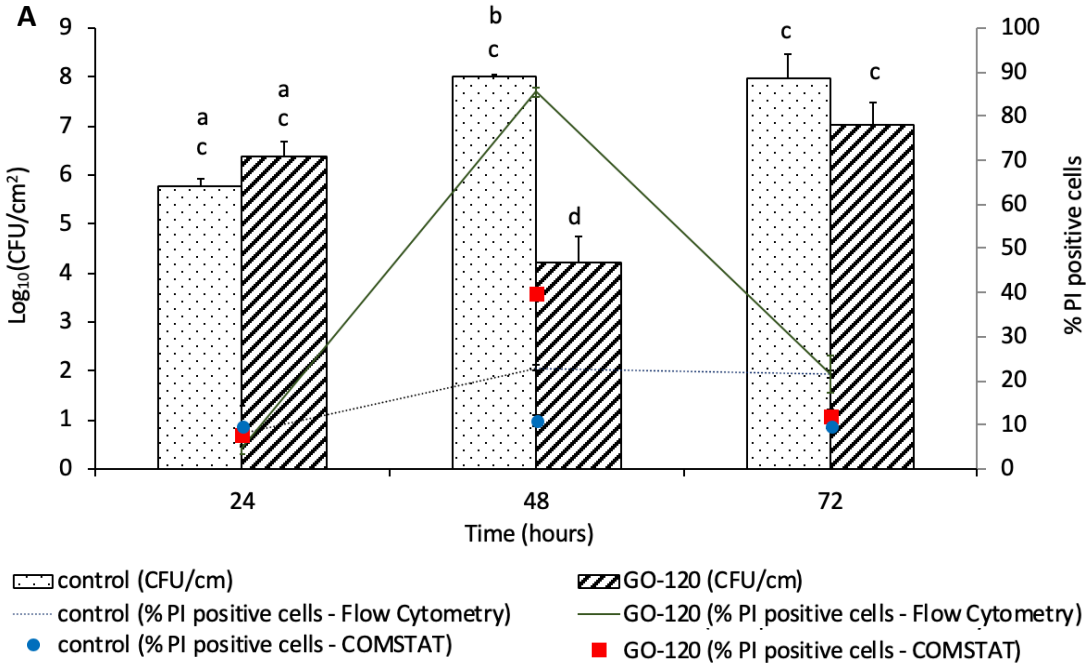

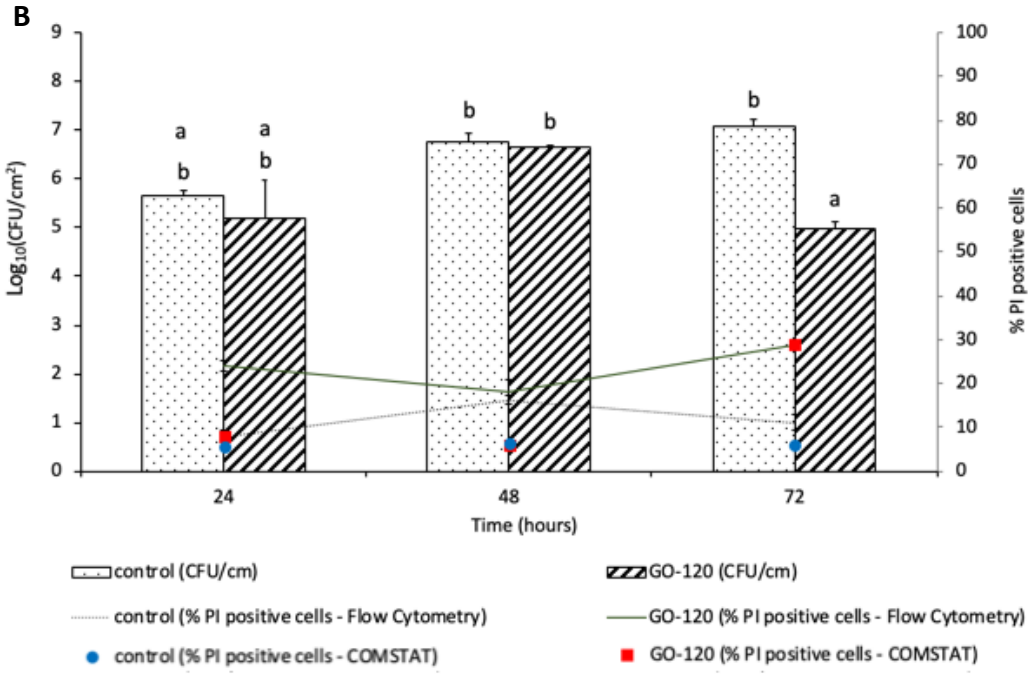

Figure 3.1 Bacteria growth in CFU/cm^2 (bars) and percentage of PI positive cells after developing biofilms for 24, 48 and 72 h then treated with GO (85 µg/mL) or dionized H_2O measured using flow cytometry and confocal microscopy with COMSTAT analysis Bars represent mean ± SEM taken from a minimum of 3 independent experiments. Mean values with different letters are significantly different (P < 0.05). The data was analysed with one-way ANOVA (A) *P. putida* (B) *Acinetobacter* sp.

Flow cytometry and confocal microscopy were employed to assess the membrane integrity for both strains cells as an indication of cell damage or death after treatment with GO. PI is a membrane-impermeable dye and is commonly used to stain cells with damaged or compromised membranes, whereby it binds to DNA and emits red fluorescence, indicative of dead cells. To establish if GO sheets would interfere with flow cytometric analysis, a solution of GO was stained with PI and analysed by flow cytometry to measure the background noise. The percentage of GO sheets detected at concentration of 85 µg/mL GO and 8.5 µg/mL GO was 3.1-1.3% and 0.4-0.06%, respectively (**Figure 3.2**) showing that background noise was too low and should not

interfere with the analysis of cells. Regarding *P. putida*, n the control samples, the percentage of PI positive cells was 2.8-fold higher in 48 and 72 h biofilm compared to 24 h biofilm (**Figure 3.1 A**). Flow cytometry data revealed that after treatment with GO, the percentage of PI positive cells was 18.8-fold higher in 48 h *P. putida* biofilm compared to 24 h *P. putida* biofilm and 4.4-fold higher compared to 72 h *P. putida* biofilm. Furthermore, in 24 and 72 h biofilms, the percentage of PI-positive cells was similar in the control and after GO treatment, but in the 48 h biofilm the percentage of PI positive cells was 4-fold higher after GO treatment compared to the control **(Figure 3.1A and 3.3**). While the flow cytometry data for *Acinetobacter* sp. showed after treatment with GO, the percentage of PI positive cells was 1.2-fold higher in 72 h biofilm compared to 24 h biofilm and 1.6-fold higher compared to 48 h *Acinetobacter* sp. biofilm. In GO treated 72 h biofilm the percentage of PI positive cells was 3.07-fold lower than 24h bioflm after GO treatment and 2.59-fold lower than 24 h biofilm control but was similar to 48 h biofilm. **(Figure 3.1B and 3.4**).

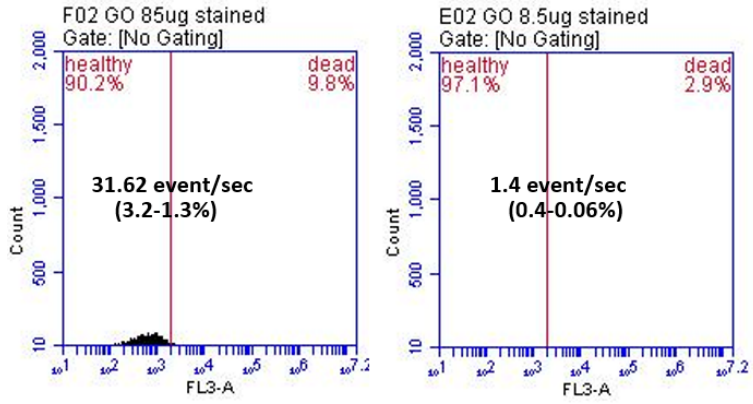

Figure 3.2 Flow cytometry scatter plots showing the events per second of GO stained with PI and an estimated percentage of GO at concentrations of 85 µg/mL (left) and 8.5 µg/mL (right) during the analysis of biofilm. The estimated percentage was calculated based on the optimal number of events per second recommended by the manufacturer which is 1,000-2,500 events per second

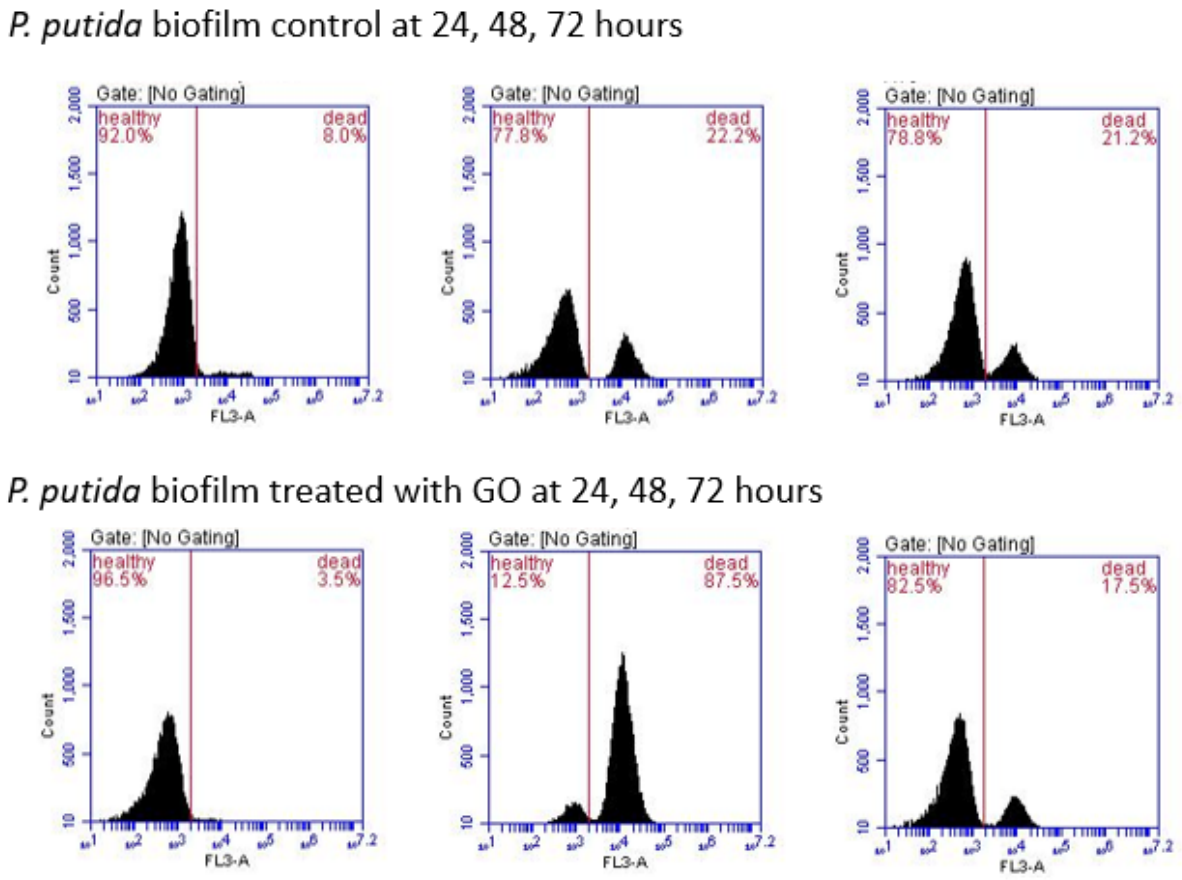

Figure 3.3 Representative flow cytometry scatter plots showing the percentage of PI-positive *P. putida* cells from a 24h (left), 48h (middle) and 72h (right) mature biofilm without (top) or with (bottom) GO-120 (85 µg/mL).

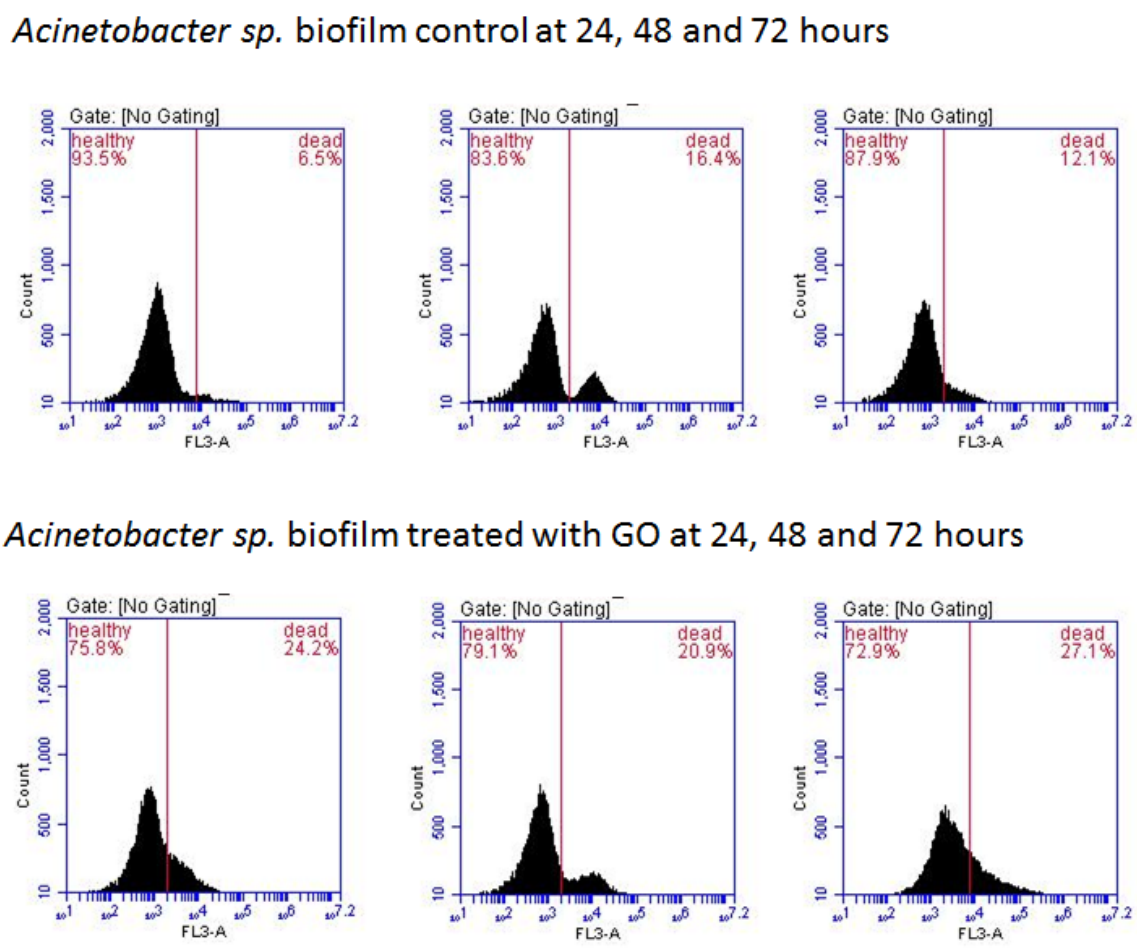

Figure 3.4. Figure S6. Representative flow cytometry scatter plots showing the percentage of PI-positive *Acinetobacter* sp. cells from a 24h (left), 48h (middle) and 72h (right) mature biofilm without (top) or with (bottom) GO-120 (85 µg/mL).

The primary goal of using confocal microscopy is to show the deployment and viability of bacteria in biofilm structure. Labelling using PI and SYTO9 shows that biofilms contained live and dead bacterial cells (**Figure 3.5**). In addition, these results shows that the biofilms developed over time and became more confluent. In the earliest stages, at 24 h, a large number of bacterial cells were observed in both strains and they appear mostly as single cells or microcolonies, indicating the initial attachment (**Figure 3.5**). The images also indicated an increase in PI intensity after GO treatment for *P. putida* biofilm at 48 h compared to 24 and 72 h (**Figure 3.5A** and **Figure 3.6**). While the intensity of PI for *Acinetobacter* sp. increased at 72 h but not at 24 or 48 h (**Figure 3.5B and Figure 3.6**). These results are consistent with the biofilm cell count results in **Figures 3.1**.

The developing biofilm was also observed using the side images of confocal analysis. At 24 h the biofilm was thin, and became thicker over time at 48 and 72 h for both strains as seen in (**Figure 3.6**) indicating biofilm was formed and developed.

The image stacks for both strains of the 3D biofilm structure were analysed using COMSTAT software to obtain the percentage of live/dead cells. In the control, the percentage of PI positive cells was similar in all samples. After GO treatment, the percentage of PI positive cells in 48 h *P. putida* biofilm was 5.2-fold and 3.3-fold higher compared to 24 and 72 h *P. putida* biofilm, respectively. Furthermore, in 24 and 72 h biofilm the percentage of PI positive cells was similar after GO treatment and control but in 48 h biofilm the percentage of PI positive cells was 3.6-fold higher after GO treatment compared to control **(Figure 3.1A).**

The COMSTAT data for *Acinetobacter* sp. biofilms is shown in **Figure 3.1B**. In the control, the percentage of PI positive cells was similar in all samples. After GO

treatment, the percentage of PI positive cells in 72 h *Acinetobacter* sp. biofilm was 3.8-folds and 5.8-folds higher compared to 24 and 48 h *Acinetobacter* sp. biofilm, respectively. Furthermore, in 24 and 48 h biofilm the percentage of PI positive cells was similar after GO treatment and control but in 72 h biofilm the percentage of PI positive cells was 4.7-folds higher after GO treatment compared to control. These results are further confirmed flow cytometry data showing an increase of PI positive cells that only occurs in 48 h for mature *P. putida* biofilm and 72 h for *Acinetobacter* sp. after GO treatment.

.

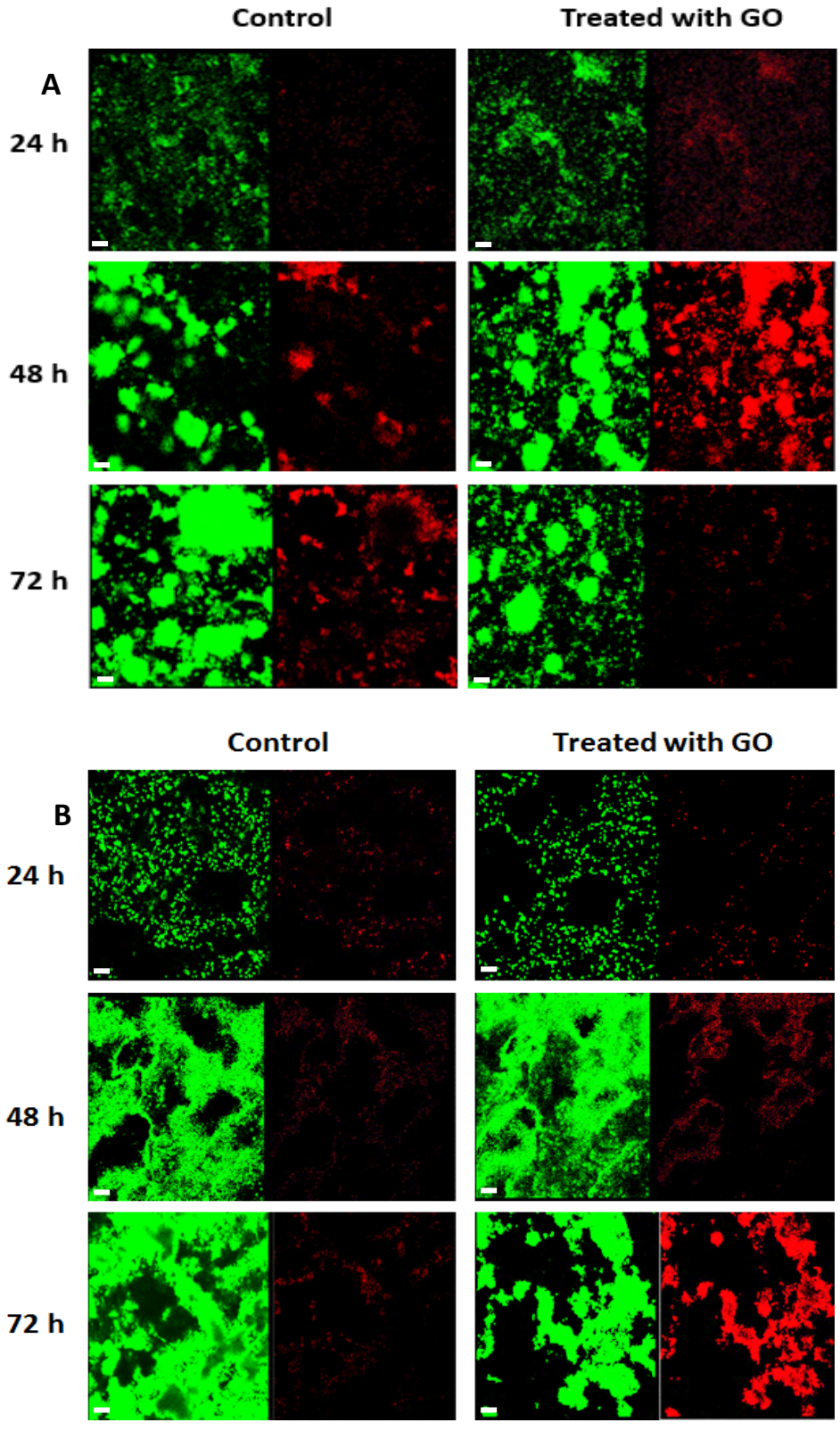

Figure 3.5 Confocal images (top view) of (A) *P. putida* and (B) *Acinetobacter* sp. biofilm with or without GO (85 μg/mL) at 24, 48 and 72 h. The biofilms were stained with SYTO 9 (left, green) and PI (right, red). Scale bar: 20 μm.

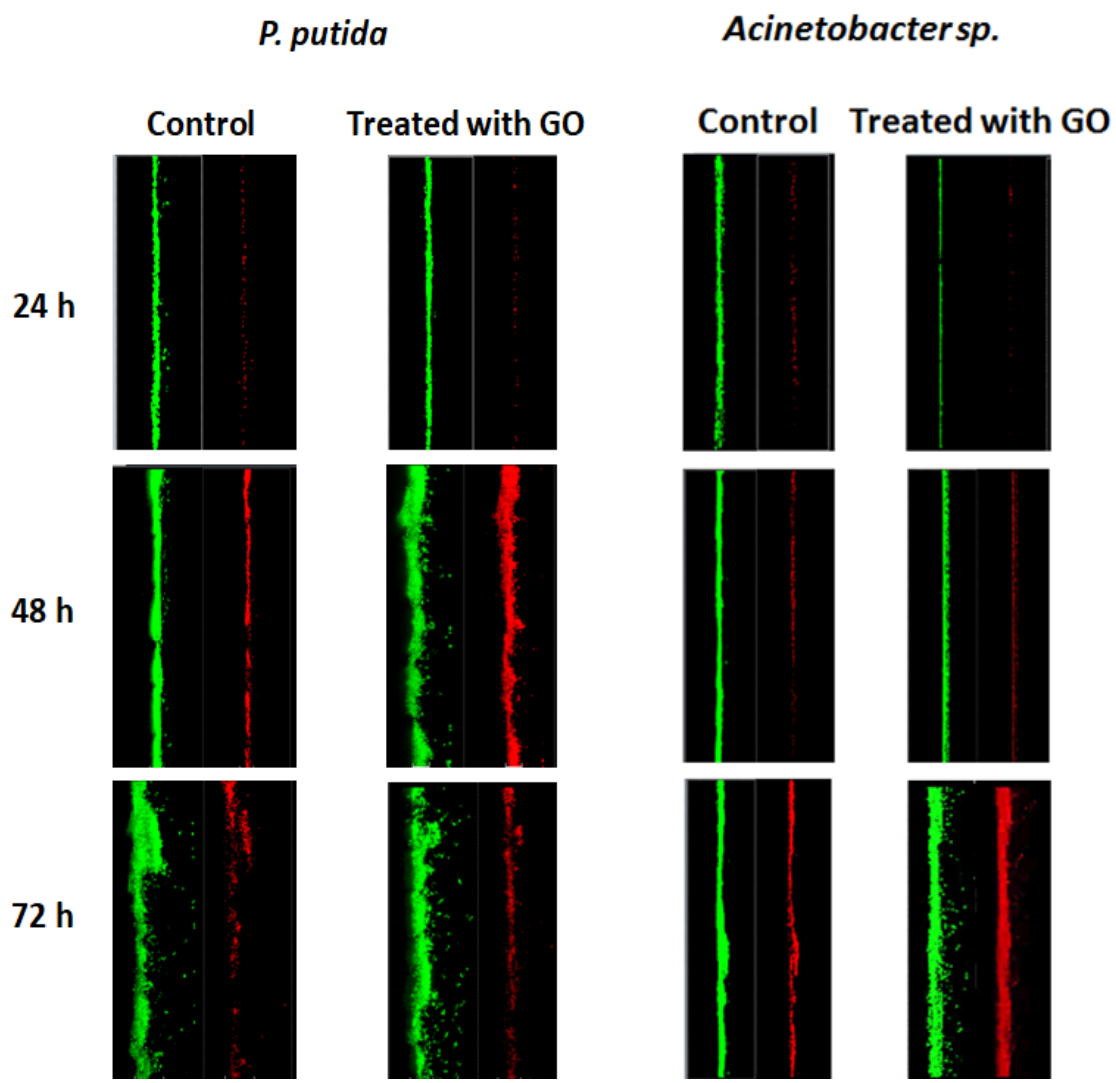

Figure 3.6 Confocal images (side view) of *P. putida* and *Acinetobacter* sp. biofilm with or without GO (85 μg/mL) at 24, 48 and 72 h. The biofilms were stained with SYTO 9 (left, green) and PI (right, red).

To further investigate the mechanism of GO affecting the cellular membrane of *P. putida,* SEM analysis was carried out on 48 h biofilm after GO treatment (**Figure 3.7**). Most GO-treated *P. putida* cells had a flattened morphology instead of being rod-shaped while the control showed unchanged cell morphology. These results suggest that the loss of cell viability was associated with membrane damage.

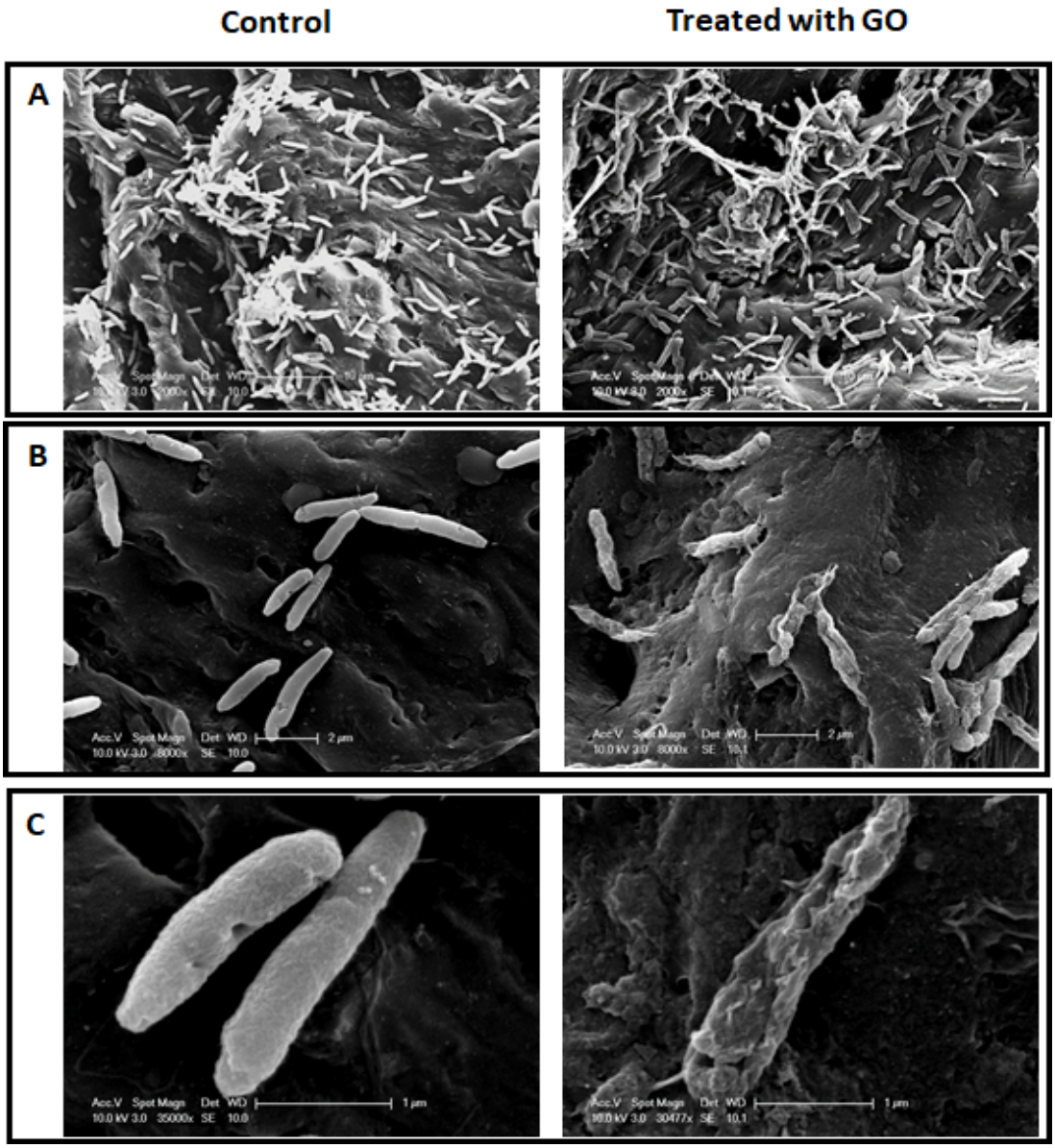

Figure 3.7 Scanning electron microscopy (SEM) images of 48 h mature biofilm of *P. putida* without (left) and with GO (85 µg/mL) (right) treatment. Scale bar: A) 10 µm, B) 2 µm and C) 1µm.

3.4.2. Effect of GO concentration, exposure time, lateral size and GO coated surface

There was no observed antibacterial activity at lower concentration of GO (8.5 µg/mL) against 48 h *P. putida* or 72 h *Acinetobacter* sp. biofilms (**Figure 3.8**) and the membrane integrity was not compromised either species (**Figure 3.9 and 3.10**). The confocal analysis for both strains after treatment was similar with control and after GO treatment at all times for either species.

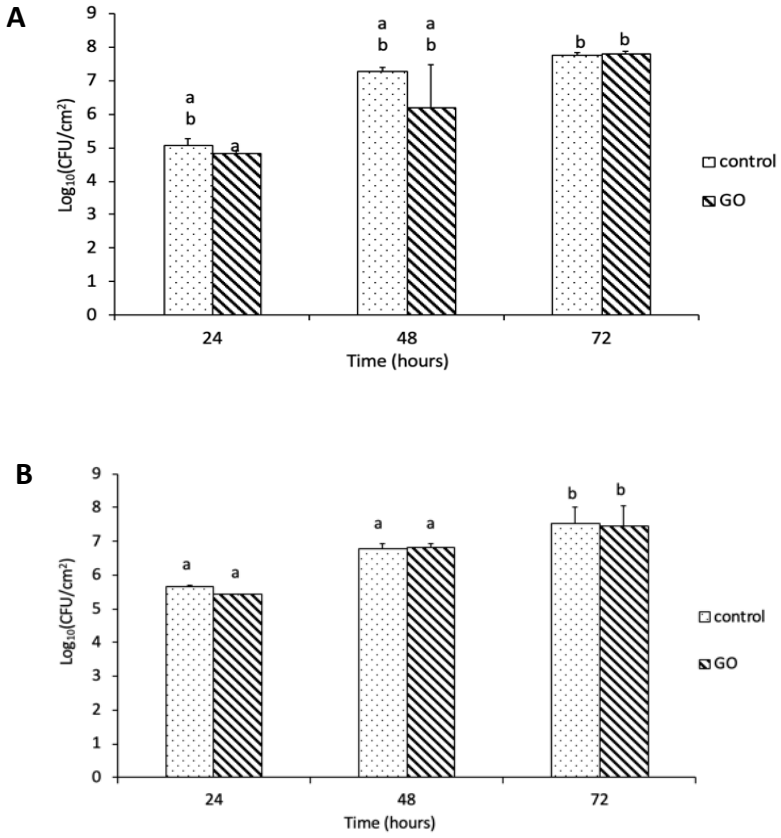

Figure 3.8 Growth of biofilm grown for 24, 48 and 72 h then incubated with GO (8.5 µg/mL). Bars represent mean ± SEM taken from a minimum of 3 independent experiments. Mean values with different letters are significantly different (P < 0.05). The data was analysed with one-way ANOVA. (A) *P. putida* (B) *Acinetobacter* sp.

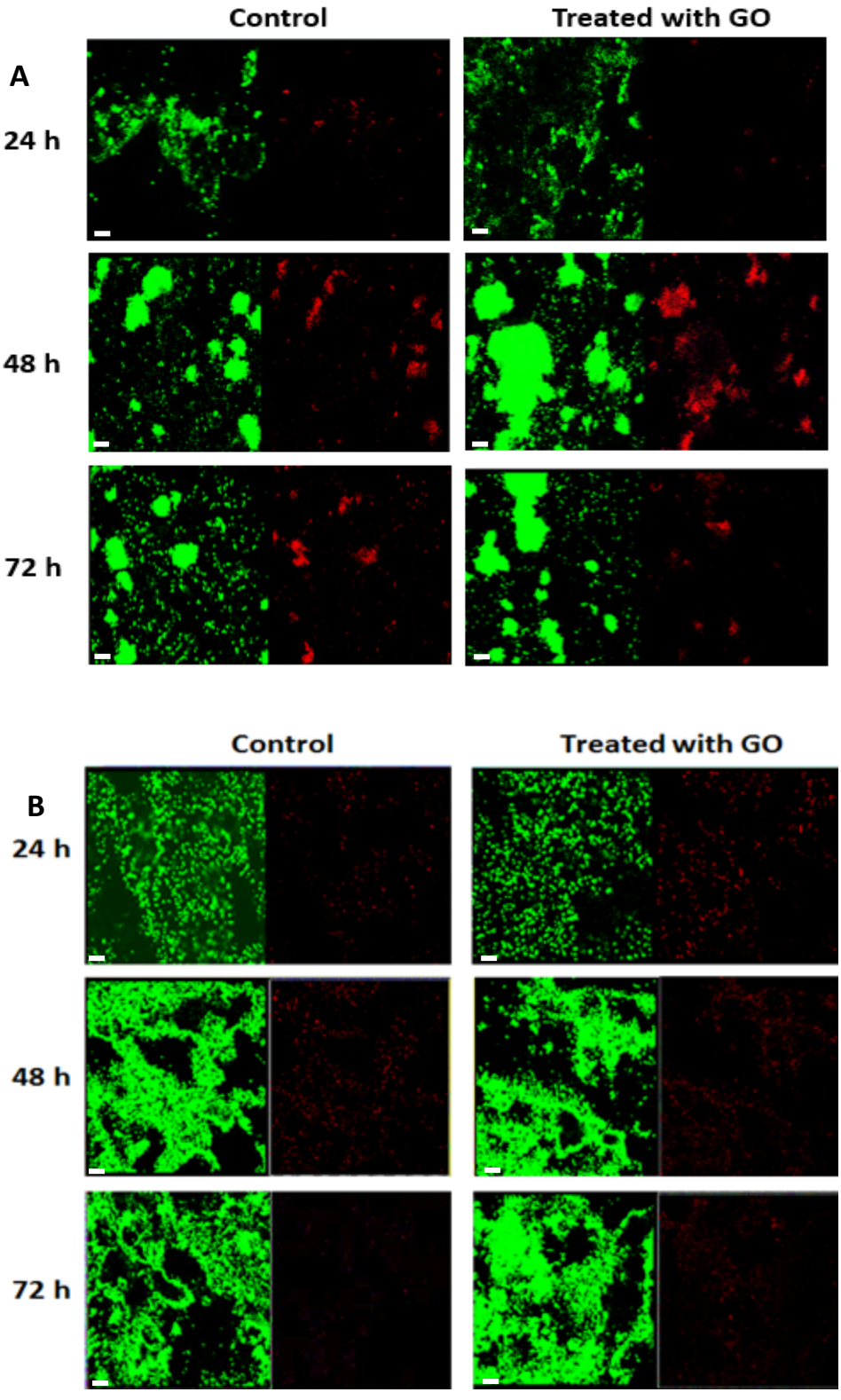

Figure 3.9 Confocal images (top view) of (A) *P. putida* and (B) *Acinetobacter* sp. biofilm with or without GO-120 (8.5 µg/mL) at 24, 48 and 72 h The biofims were stainted with SYTO9 (left, green) and PI (right, red) Scale bar 20 µm.

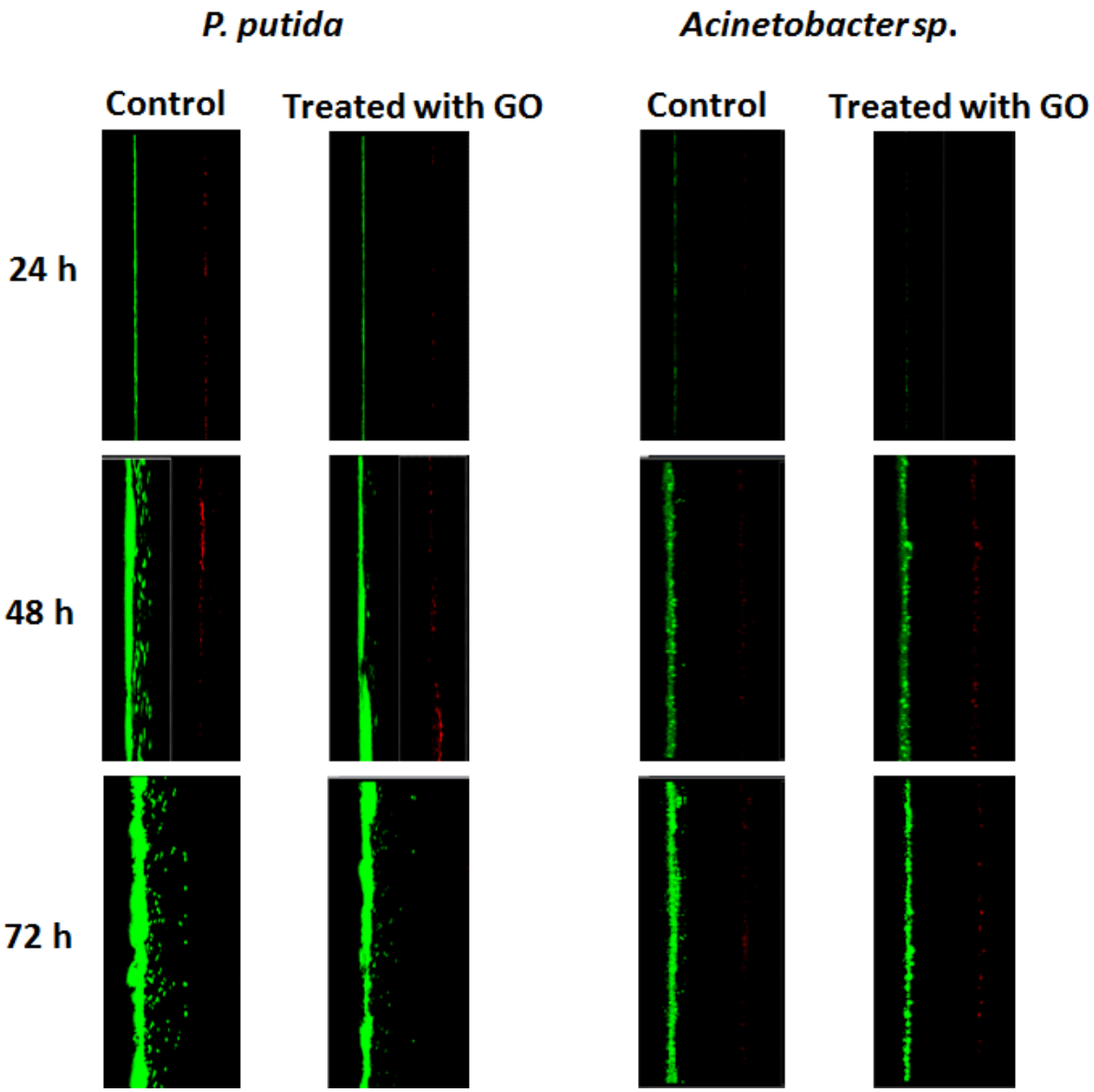

Figure 3.10 Confocal images (side view) of *P. putida* and *Acinetobacter* sp. biofilm with or without GO-120 (8.5 μg/mL) at 24, 48 and 72 h. The biofilms were stained with SYTO 9 (left, green) and PI (right, red).

To test the effect of prolonging the time of GO exposure, the viability of 48 h *P. putida* biofilm was assessed after GO-treatment for 24 and 48 h. The viability of 48-h mature *P. putida* biofilm with GO was significantly ($P < 0.05$) lower compared to control after 24 and 48 h (**Figure 3.11**). However, there was no significant difference in viability of 48 h mature *P. putida* biofilm exposed to GO for 24 h compared to 48 h; therefore, prolonging exposure to GO did not result in further reduction in viability.

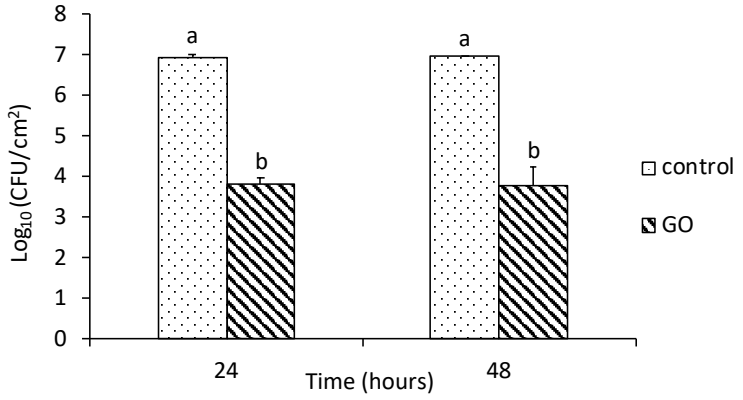

Figure 3.11 Viability of 48 h mature *P. putida* biofilm incubated with GO-120 (85 µg/mL) for 24 or 48 h. Bars represent mean ± SEM taken from a minimum of 3 independent experiments. Mean values with different letters are significantly different ($P < 0.05$). The data was analysed with one-way ANOVA.

The antibacterial activity of large and small GO sheets was compared against a 48 h *P. putida* biofilm. The lateral size of GO sheets had no effect as there was no significant difference in viability of *P. putida* biofilm treated with large sheets GO-10 compared to small sheets GO-120 (**Figure 3.12**). GO-10 and GO-120 are detailed in Figure 2.4.

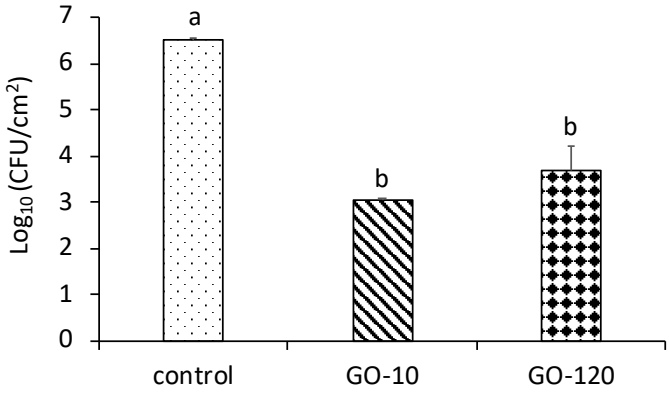

Figure 3.3 Viability of 48 h *P. putida* biofilm incubated with GO (85 µg/mL) with large (GO-10) and small (GO-120) sheet size for 24 h. Bars represent mean ± SEM taken from a minimum of 2 independent experiments. Mean values with different letters are significantly different (P < 0.05). The data was analysed with one-way ANOVA.

The growth of *P. putida* biofilm on GO-coated surface was investigated to study the antibacterial activity and the development of biofilm on stainless surface. Results showed that biofilm was developed and there was no significant difference in the concentration of viable biofilm cells compared with non-coated surface at all ages (24, 48 and 72 h) (**Figure 3.13**).

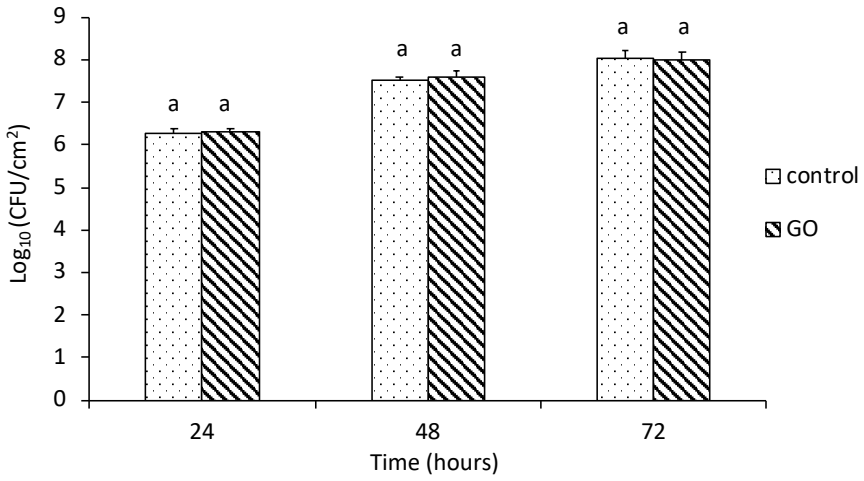

Figure 3.13 Bacteria growth of *P. putida* biofilms in CFU/m^2 (bars) incubated on GO surfaces for 24, 48 and 72 h. Mean values with different letters are significantly different (P < 0.05). The data was analysed with one-way ANOVA

3.4.3. Effect of GO on detached-biofilm and planktonic cells

To investigate the role of EPS and the biofilm maturity-related susceptibility of *P. putida* and *Acinetobacter* sp., 24, 48 and 72 detached-biofilm cells were treated with GO and viability was assessed over time (**Figure 3.14**). There was no significant difference in viability between 24 and 72 h detached *P. putida* treated with GO compared to control after 1, 2, 3, 4 and 5 days. Similarly, to *P. putida*, no significant difference was found in the viability between 24 and 48 h detached *Acinetobacter* sp. treated with GO compared to control after 1, 2, 3, 4 and 5 days. The viability of 48 h of *P. putida* and 72 h for *Acinetobacter* sp. detached-biofilm cells treated with GO was significantly ($P < 0.05$) lower compared to all the other samples after 1 and 2 days and was completely inactivated from day 3 onwards. Therefore, as with 48 h for *P. putida* and 72 h for *Acinetobacter* sp. biofilm for these strains, the detached-biofilm cells were also susceptible to the same concentration of GO showing similar reduction in viability.

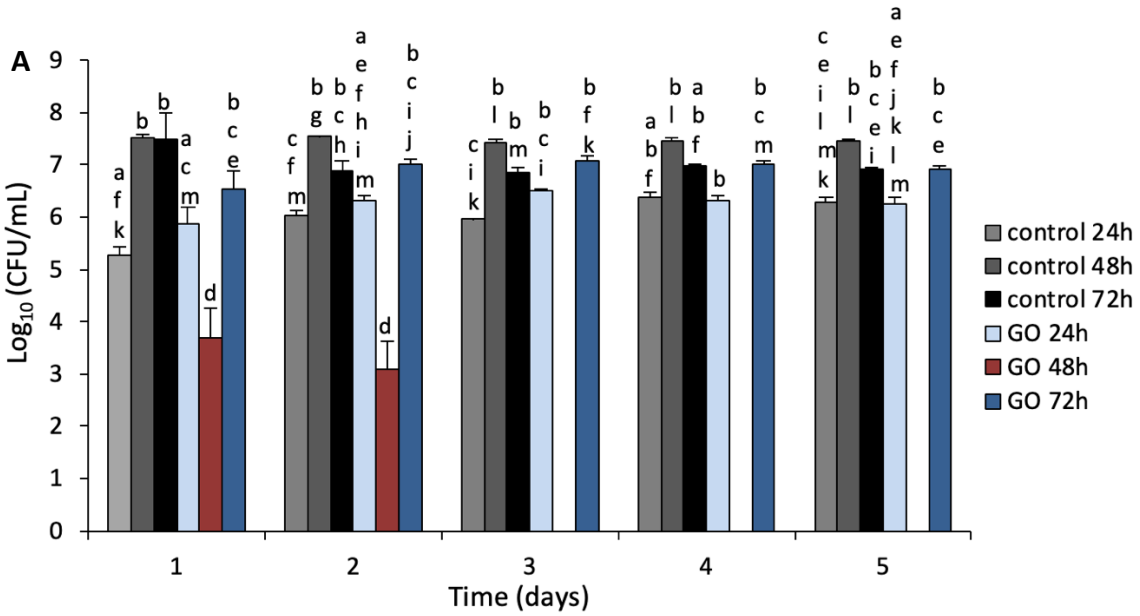

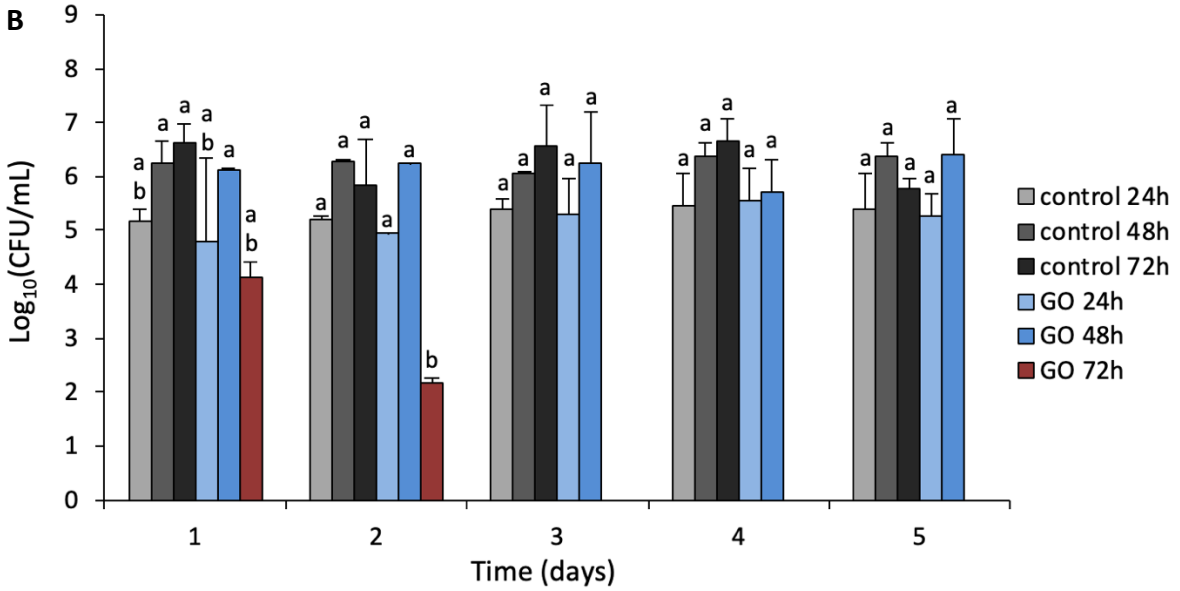

Figure 3.14 Viability of free-floating cells detached from 24, 48 and 72 mature biofilm and incubated with GO (85 µg/mL) or dionized H_2O (control) for 1, 2, 3, 4 and 5 days. Bars represent mean ± SEM taken from a minimum of 3 independent experiments. Mean values with different letters are significantly different ($P < 0.05$). The data was analysed with one-way ANOVA. (A) *P. putida* (B) *Acinetobacter* sp.

In addition, GO was tested against planktonic cells for both strains and viability was assessed over time (**Figure 3.15**). There was no significant change in viability of planktonic cells for the strains after GO treatment with a concentration ranging from 100-1600 µg/mL at 0, 1 and 5 days. These results further confirm that only 48 h *P. putida* biofilm cells were susceptible to GO and only 72 h *Acinetobacter* sp. biofilm were susceptible. **Figure 3.16** shows the aggregation of GO in TSB media with the attachment of bacterial cells on the GO aggregates.

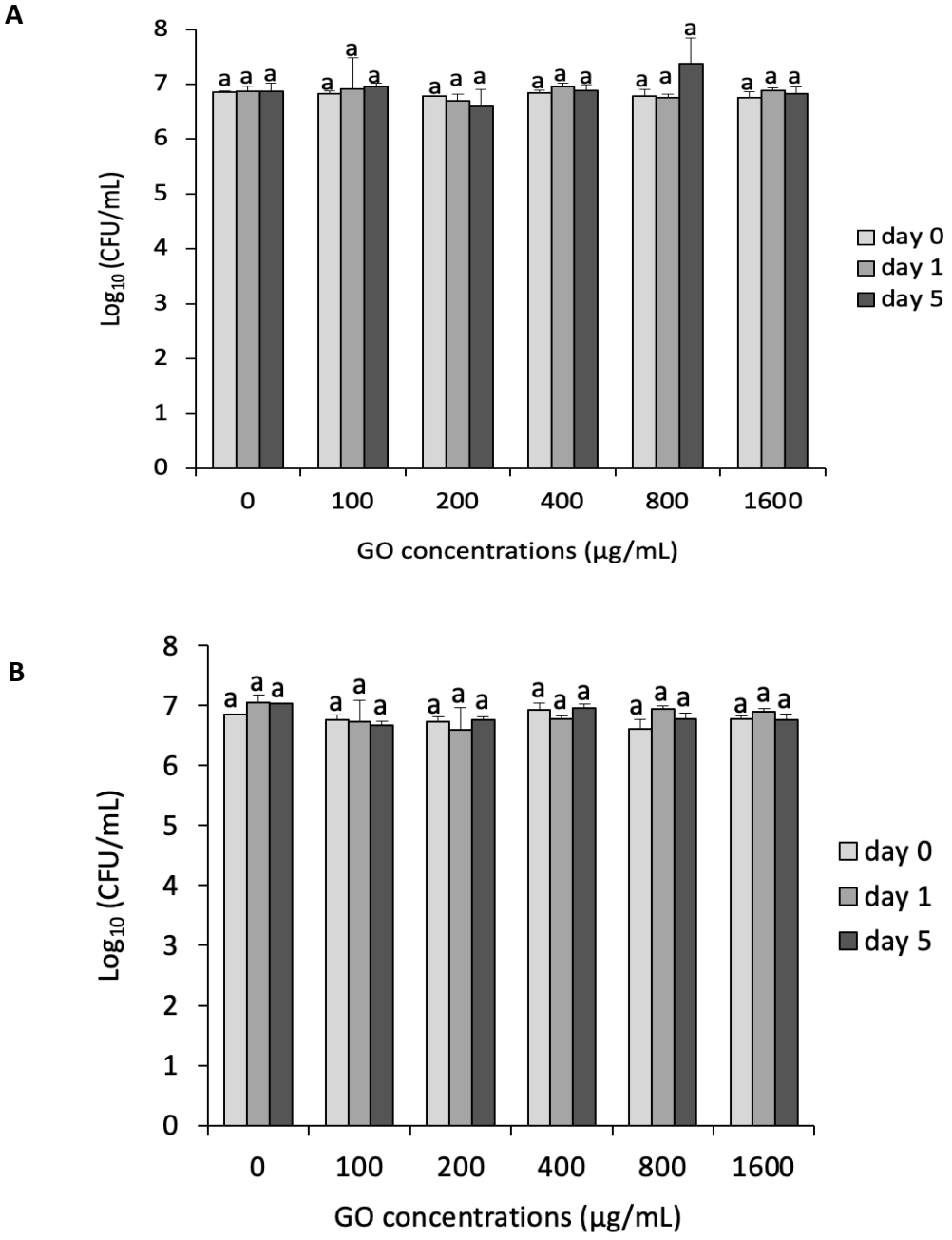

Figure 3.15 . Viability of planktonic cells incubated with varying concentrations of GO at day 0, 1 and 5. Bars represent mean ± SEM taken from a minimum of 2 independent experiments. Mean values with different letters are significantly different (P < 0.05). The data was analysed with one-way ANOVA. (A) *P. putida* (B) *Acinetobacter* sp.

.

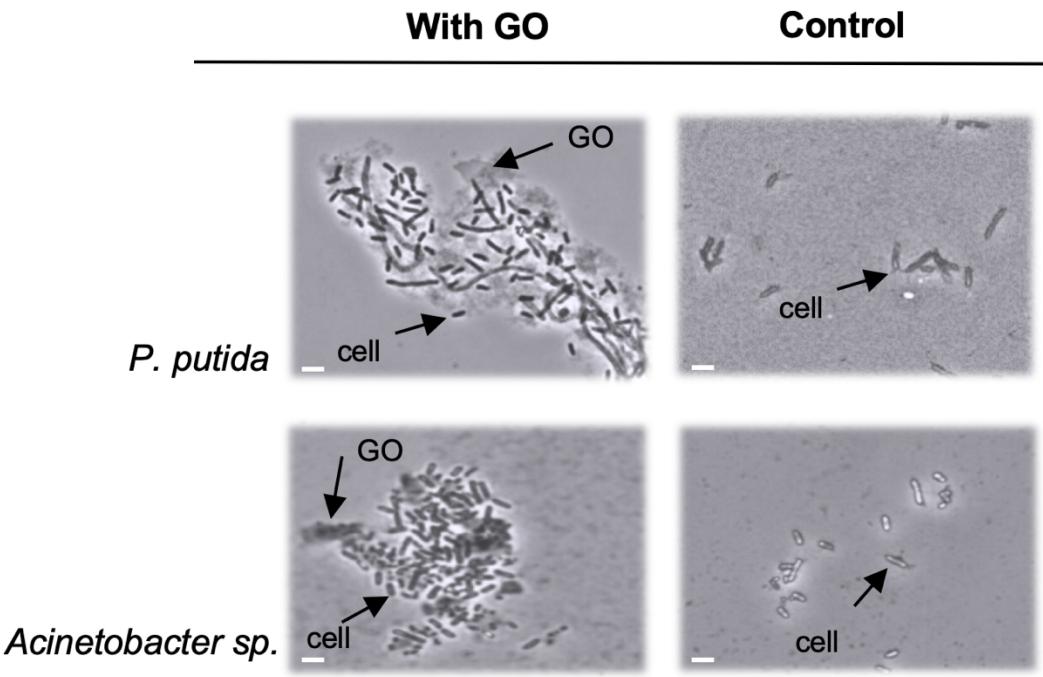

Figure 3.16 Images taken from light microscopy (X100) show bacterial cells of *P. putida* and *Acinetobacter* sp. cells grown in media with/without the addition of GO. Scale bar 2 µm

3.5. Discussion

3.5.1. Effect of GO on *P. putida* and *Acinetobacter* sp. biofilms

In this study, the effect of GO on biofilms of different ages were tested. Very few studies investigated the antibacterial activity of GO against bacterial biofilms and in contrary to our results they suggested that GO has no effect against biofilms. In a study by Ruiz et al., (2011) GO at a concentration of 25 µg/mL was shown to promote faster growth of *E. coli* in rich LB media resulting in dense biofilm formation. They observed GO precipitation and aggregation in LB media which suggested that may be acting as a scaffold for bacterial attachment, proliferation, and biofilm formation. In a recent study Guo et al., (2017) investigated the impact of GO against *E. coli* and *Staphylococcus aureus* biofilms in LB media. They found that GO promoted biofilm formation and development and possessed no antibacterial activity on mature 48 h biofilms with concentrations ranging from 0.5-500 mg/mL. However, all these studies investigated the antibacterial effects of GO in LB media. According to Hui et al., (2014) the antibacterial activity of GO (200 µg/mL) against *E. coli* was completely inhibited in LB-supplemented saline compared to saline solution due to components in LB adsorbing onto GO basal planes deactivating its antibacterial activity. In the present study experiments were done in de-ionised water as opposed to LB media and therefore it is not possible to compare the results. Also, the antibacterial effects of GO may vary against different bacterial species. Gao et al., (2017) found that the membrane integrity of *E. coli* and *S. aureus* was compromised after exposure to GO. However, the amount of RNA released from *S. aureus* was higher than that from *E. coli* which was attributed to the smaller size of the *S. aureus* which makes it more susceptible to the “cutting” and “wrapping” mechanisms of GO sheets. Yadav et al., (2017) found selectivity in antimicrobial activity of GO due to size differences, smaller

GO sheets showed higher antibacterial activity against *E. coli* compared to *S. aureus* due to having thinner cell wall which could be easily pierced by the GO sheets. These studies show that the antibacterial activity of GO varies depending on the bacterial species.

The pH of GO depends on its purity and this may affect its antibacterial activity. In a recent study Barbolina et al., (2016) showed that adding several washing steps can change the pH of GO solution from acidic to neutral. Exposure to un-washed GO reduced the survival of *E. coli* and *S. aureus* in a concentration dependent manner (10-250 µg/mL) while the washing steps during the purification process diminished the antibacterial effects of GO. The authors suggested that the acidic pH was responsible for the antibacterial activity of un-washed GO. However, in this study the highly purified GO was obtained using a modified Hummers' method in accordance to (Ali-Boucetta et al., 2013) and the pH of samples after adding GO was ~6.5 which is not low enough to damage the bacteria.

There is inconsistency in the literature regarding the effects of antibacterial agents against biofilms of different ages. Several studies reported that mature biofilms are more susceptible to antimicrobial agents compared to young biofilms (Anwar et al., 1989; Frank and Koffi, 1990; Leriche and Carpentier, 1995; Høiby et al., 2001; Tré-Hardy et al., 2009; Shen et al., 2011; Pandit et al., 2015). In Thuptimdang et al., (2015) 48 h *P. putida* biofilms showed higher resistance to silver NPs compared to 6-, 12- and 30 h *P. putida* biofilms. In contrast, Chumkhunthod et al., (1998) found that there was no significant difference in susceptibility between 1, 2, and 3-day *P. putida* biofilm to non-foaming acidic and liquid hypochlorite sanitizers. However, in this study it was shown that antibacterial activity of GO depended on the age of the biofilm and only

occurred at a specific time during its developmental stage. Furthermore, the growth of cells and formation of EPS is also dependent on the type of media, pH, temperature, and strain of bacteria (Combrouse et al., 2013) which may explain the variability observed between the different studies.

The study also investigated the biofilms at lower concentration of GO (8.5 µg/mL). It shows that low concentration of GO had no antibacterial activity against biofilm for both strains in all ages and the membrane integrity was not compromised. These results are in agreement with studies that show a dose dependent antibacterial activity of GO against planktonic bacteria (Liu et al., 2011; Ahmed and Rodrigues, 2013; Chen et al., 2014b; He et al., 2015a; Combarros et al., 2016; Gao et al., 2017). It can therefore be assumed that the antibacterial activity only occurs at higher GO concentration and it depends on the maturity stage of the biofilm.

3.5.2. Effect of GO exposure time, and lateral size on *P. putida* biofilm

In this study the effect of varying the lateral size of GO sheets (GO-10 vs GO-120) had no effect on the viability of 48 h *P. putida* biofilm (**Figure 3.12**). These results are in contradiction to findings by Liu et al. (2012) that antibacterial activity of GO sheets against *E. coli* increased in a size dependent manner ranging from 0.753-0.01 μm^2. Similarly, Campos-Delgado et al., (2016) reported that GO sheets with larger lateral size (> 2 µm) showed higher antibacterial activity against *E. coli* compared to GO sheets with smaller lateral size (100 nm). The authors suggested that GO wraps the bacterial cells and prevents them from being able to uptake nutrients and proliferate on agar plate leading to reduced counts. Yadav et al., (2017) found a selectivity in antibacterial activity of two types of GO sheets (GO_I and GO_H) prepared using different

methods against *E. coli* and *S. aureus*. Since oxidative stress was found to be similar in both it was suggested that the selectivity in antimicrobial activity of each GO was due to size differences of GO_l and GO_H (200 nm and 1200 nm, respectively). The authors suggested that smaller GO_l sheets pierce the thin cell wall in *E. coli* cells while the cell wall in *S. aureus* is difficult to pierce by GO_l and therefore wrapping of the bacterial cells by larger sheets of GO_H is the predominant mechanism of killing. However, these studies investigated the effect of GO sheets against planktonic bacteria and not biofilm. Also, the size difference between the large and small GO sheets was greater in those studies compared to this study (GO-10 and GO-123).

It has been observed that NPs can penetrate and deposit in biofilms (Miller et al., 2013). Biofilm and specifically EPS enhance the retention of GO NPs due to the surface roughness and physical straining (He et al., 2015a). Once inside the biofilm GO may come in contact with bacteria and expresses antibacterial activity. Several mechanisms have been suggested in regards to the antibacterial actions of GO against planktonic bacteria including “sharp” edges of the GO nanosheets cutting through the cell membrane leading to leakage and death (Chen et al., 2014b; Gurunathan, 2015; Nanda et al., 2016), wrapping of large GO sheets around the cells to block interactions isolating them from the environment (Mejías Carpio et al., 2012; Perreault et al., 2015) and ROS-dependent and -independent oxidative stress (Ahmed and Rodrigues, 2013; Li et al., 2014). In addition to the loss in cell viability many studies reported flattening and loss of cellular structure in bacteria treated with GO (Liu et al., 2011; Chen et al., 2014b; Perreault et al., 2015; Nanda et al., 2016; Combarros et al., 2016; Farid et al., 2018) which corroborate these findings. Tu et al., (2013) showed that GO can induce the degradation of the inner and outer cell membranes of *E. coli* and reduce their viability. Using molecular dynamics simulations,

the authors suggest that two types of molecular mechanisms drive the degradation of *E. coli* cell membranes: one by severe insertion and cutting and the other by destructive extraction of lipid molecules. Since in this study there was no differences in the antibacterial activity between different sizes of GO sheets the mechanism of membrane cutting due to sharp edges is unlikely. Also, the size of the GO sheets is not large enough to wrap the cells. Therefore, the most probable mechanism would be oxidative stress, however, further investigation is required to understand which mechanism is responsible for the antibacterial activity of GO.

The study of *P. putida* biofilm on GO-coated surface was investigated using plate count measurements. In this experiment GO was dried on stainless steel surfaces and clear stainless steel used as control. The number of biofilm cells on stainless steel was similar to polycarbonate. GO-coated surfaces had no impact on the viability of *P. putida* biofilms. Results also showed there was no reduction on the viability of biofilms on these surfaces. This observation is similar to Mokkapati et al., (2018) who tested the response of *P. aeruginosa* and *E. coli* on plate-integrated GO and rGO. Their data showed that rGO was toxic to the bacteria while GO was harmless. However, other study contradict these finding. To investigate the interaction of bacteria on GO and rGO, Hu et al., (2010) investigated the interaction of *E. coli* with GO and rGO in a LB culture plate for 12 h then colony was counted. Results showed a significant reduction in the viability of *E. coli* with GO and lost of the cellular integrity, leading to a viability reduction of more than 98%. Again the authors suggested that GO damaged the bacterial membrane through direct contact with GO or oxidative stress (Hu et al., 2010).

This study confirms the previous observation where bacterial cells were grown around GO aggregation in broth media. However, more investigation and characterisation is

needed to confirm that the GO is adhered to the coupons during the experiment and not dispersed in media. This experiment can be modified by adding bacterial suspension on GO surfaces and study the bacterial cells adhesion by counting the CFU and the use of microscopy techniques such as confocal microscopy and scanning electron microscopy (SEM).

3.5.3. Effect of GO on detached-biofilm *P. putida* and planktonic cells

In a recent study by Guo et al., (2017) the removal of EPS in biofilm enhanced the antibacterial activity of rGO suggesting that EPS acts “as a barrier” to protect the cells from physical damage and “acts as a sink” of ROS by limiting their damaging activity on the cells. GO may also adsorb the components of EPS and aggregate preventing it from coming in contact with bacterial cells.

Antibacterial studies of graphene materials have mainly focused on modifying their chemistry, but the physiological state of bacteria as a factor in susceptibility was not investigated. Biofilm formation is regulated by genetic and environmental factors and occurs through several developmental stages (Acemel et al., 2018). In each stage the bacterial cells physiologically differ from cells in the other stages and biofilm cells may differ phenotypically from planktonic cells (Bester et al., 2005). The results in this study are in contrast to the belief that planktonic bacteria are more sensitive to GO than biofilms. These results were obtained with bacteria harvested in the stationary phase before GO treatment. However, bacteria in the exponential phase may respond differently to the GO treatment and therefore more work needs to be done in the future.

During the early stages of *P. putida* biofilm development (1 to 3 days), cells are non-motile and reside inside the micro-colonies. After 3 days of growth the micro-colonies reach a critical size and the bacteria start to swim rapidly in circles and the compact micro-colonies are dissolved to begin the formation of loose structures containing bacteria from different micro-colonies (Tolker-Nielsen et al., 2000). Actively dividing or exponentially growing bacteria are more susceptible to antibiotics compared to non-dividing or stationary phase bacteria (Mascio et al., 2007). After 48 h of maturation the cells were likely to be more actively dividing and at this stage may become susceptible to GO. However, further work is required (e.g. gene expression analysis) to understand the physiological state of *P. putida* cells in biofilm at different developmental stages.

Also, the production of EPS leads the micro-colonies to maturation, making the highly ordered structure of the biofilm. In *P. putida* biofilm the EPS is comprised of polysaccharides (e.g. cellulose), xanthan, dextran (Camesano and Abu-Lail, 2002), alginate (Chang et al., 2007), and proteins (e.g. LapA protein, a cell-to-surface adhesin) (Klausen et al., 2006). Also, *P. putida* has been reported to produce substantial amounts of extracellular DNA in the sessile mode of growth (Steinberger and Holden, 2005). In this study the thickness of the EPS increases dramatically from 24 to 48 h and slightly increase from 48 to 72 h. From these results it can be deduced that at 48 h, most of EPS constituents are being secreted from the cellular membrane which may become susceptible to the destructive actions of the GO sheets.

In conclusion, antibacterial activity of GO against biofilms was observed and this activity only occurred at a specific stage of biofilm maturity. GO was found to have

antibacterial effect against 48 h *P. putida* biofilms, but no effect was observed with cells detached from 24 and 72 h biofilms or planktonic cells. However, *Acinetobacter* sp. showed the antibacterial activity of GO at 72 h but not at 24 or 48 h. Moreover, similar trends were observed when the GO was tested against both strains cells detached from biofilm for both species. This age-related susceptibility to GO may be linked to the physiological state of the cells which differs at each maturation stage. For example, gene expression or secretion of molecules by the bacteria at a certain stage of biofilm maturity may be responsible for the observed susceptibility to GO, however, further investigation is required to fully understand this link. This may explain the inconsistencies of GO activity against bacteria reported in the literature. These findings present important implications of GO accumulation for environmental systems where biofilm maturity varies.

Chapter 4. Impact of environmental stresses and graphene oxide against *P. putida*

4.1. Abstract

The production of graphene-based materials such as GO is increasing, therefore it is expected that a large amount of GO wastes will be generated. The environment (i.e. soil, aquatic systems) will be among the final repositories of these wastes and it is known that microbial communities in such environments are exposed to various stresses. However, little is known about how these communities respond to environmental disturbances in the presence of GO. Thus, it is important to investigate any potential toxic effect of GO in soil bacteria. In this chapter, the effect of three different stress condition; temperature (4, 5 and 40 ^{o}C); pH (5, 6, 7, 8 and 9); and osmotic stress (51, 219 and 320 mM NaCl) against *P. putida* was investigated before GO treatment. The viability was monitored by plate counting and physiology was investigated by confocal microscopy. It was found that planktonic cells are more resistant to GO compared to biofilms but not to pH or osmotic stress. Temperature was not found to influence the survival of biofilm cells with or without exposure to GO. However, low pH caused a slight reduction in CFU at pH 5 (~ 1.5 log) and pH 6 (~ 1 log) for the pre-treated samples, while biofilms at pH 7-9, did not show a decrease in the CFU. The post-treatment samples with GO showed a reduction in all pH ranges of ~3 log. The effect of osmotic stress at higher concentrations of NaCl (219 and 320 mM) with GO showed a significant reduction in CFU of ~3.5 and 4.5 log, respectively for biofilms. These results show that NaCl enhances the antimicrobial activity of GO against *P. putida*.

4.2. Introduction

The increase in GO applications will increase the possibility of its discharge into the environment (Du et al., 2015) and soil ecosystems are more likely to be a large recipient of nano-material contamination when compared with water and air (Du et al., 2015). Bacterial biofilms are widely distributed in soil and play a major role in nutrient recycling such as carbon, nitrogen, phosphorus and sulphurs and they are frequently exposed to environmental changes such as temperature, pH and osmotic changes (Reva et al., 2006). Generally, bacteria have the ability to grow at a wide range far from the optimal conditions and they have to adapt to these changes in order to survive and grow (Beales, 2004).

Bacteria in biofilms are more resistant to extreme environmental conditions or antimicrobial agents than those grown under planktonic conditions, making them more robust and difficult to destroy (Ricker and Nuxoll, 2017). Since bacterial cells are embedded in EPS, this may limit the transport of antibacterial agents (e.g. antibiotics) to cells (Thuptimdang et al., 2015).

It was shown that the amount of EPS increases with high stresses which makes biofilms even more resistant. Lin *et al.* 2014 studied the EPS production of biofilm in response to temperature, pH and osmotic stresses in *P. putida* CZ1. The amount and compaction of EPS increased during specific conditions (low pH, high temperature and certain osmotic stresses), and showed that the EPS production is approximately linearly positively correlated with culture time, while number of cells decreased to cope with nutrient depletion during aging (Lin et al., 2014). Moreover, the study showed that EPS production formed a more hydrated microenvironment around cells, therefore, increasing the tolerance of the cells.

It was shown that combined treatment of increase of temperature and antibiotics (ciprofloxacin, tobramycin and erythromycin) has synergistic effects against *P. aeruginosa* biofilms (Ricker and Nuxoll, 2017). It has been suggested that the transport of antibiotics through the EPS increase with increasing the temperature suggesting synergistic effect on *P. aeruginosa* biofilms (Ricker and Nuxoll, 2017). In addition, when the osmotic stress of the surrounding cells increased, the tolerance of cells to high hydrostatic pressure decreased (Molina-Höppner et al., 2004).

Many studies investigated the impact of environmental stresses on biofilms during its developing stages (Abdallah et al., 2015; Akiyama et al., 1998) however, few studies investigated these impact on mature biofilms (van der Waal et al., 2011). Moreover, GO has been shown to have a significant effect against mature biofilm but not planktonic cells (Chapter 3). However, no study so far has investigated the combined effect of environmental stresses and GO on biofilm.

One objective of the study is to determine the impact of the environmental stresses: temperature (5, 25 and 40 ^{o}C), pH (5, 6, 7, 8 and 9) and NaCl (51, 219 and 320 nM) on 48 h *P. putida* biofilm and compare the impact of these stresses to the corresponding planktonic cells. The aim of the study is to determine the impact of the environmental stresses on biofilm or planktonic cells and to determine the impact of GO on biofilms and planktonic cells after exposure to these environmental stresses.

4.3. Materials and Methods

4.3.1. Preparation of Graphene Oxide and Buffers

Graphene oxide: Graphite was purchased and prepared for GO as described in section 2.1 and 2.2.

Citrate–phosphate Buffers: These buffers were used to obtain acid solutions. Three pH values were used (5.0, 6.0 and 7.0) by mixing 0.1 M citric acid; and 0.2 M dibasic sodium phosphate in the proportions indicated in **Table 4.1** and adjusting the final volume to 100 mL with deionized water.

Tris-HCl Buffers: These buffers were used to obtain alkaline solutions at pH values of 7.0, 8.0 and 9 by mixing 0.1 M Tris(hydroxymethyl)aminomethane; and 0.1 M hydrochloric acid (HCl). To achieve these pH values, 50 ml of Tris(hydroxymethyl)aminomethane was used and known volumes of HCl as described in **Table 4.2** were mixed and adjusted to the final volume of 200 ml with deionized water. A pH meter (Beckman) was used to adjust the final pH.

NaCl solutions were used to stimulate osmotic stress by preparing 51, 219 and 320 mM (equivalent to 0.3, 1.3 and 1.9%) NaCl by initially dissolving 58.44 g of NaCl in final volume of 1 litre to make a 1 M solution. Then dilutions were made to obtain these concentrations.

Table 4. 1 Final volumes needed to achieve the acidic buffers

pH	***5.0***	***6.0***	***7.0***
mL of sodium phosphate (0.2 M)	25.7	33.1	43.6
mL of citric acid (0.1 M)	24.3	16.9	6.5
deionized water (mL)	50.0	50.0	49.9
final volume (mL)	100.0	100.0	100.0

Table 4. 2 Final volumes needed to achieve the basic buffers after making 50 ml of Tris(hydroxymethyl)aminomethane (0.1M)

pH	***7.0***	***8.0***	***9.0***
mL of HCl (0.1 M)	44.2	29.2	5.0
deionized water (mL)	155.8	170.8	195.0
final volume (mL)	200.0	200.0	200.0

4.3.2. Bacterial strain, culture conditions and biofilm cultivation

The bacterial strain used for this study was *Pseudomonas putida* KT2440 and was maintained as described in section 3.3.4 *P. putida* biofilm was grown in TSB media using CDC bioreactor as described in section 3.3.4.

4.3.3. Environmental stresses and quantification of biofilm incubated with GO

To study the effect of temperature, biofilms were developed in the CDC reactor as described in Chapter 3 and the coupons were collected after 48 h. Coupons

carrying biofilm bacteria onto them were incubated at 4, 25 or 40^{o}C with sterilised de-ionised water (control) or 4 mL GO 85 µg/mL for 24 h with shaking at 80 rpm. The viability was tested by plate counting as described in Chapter 3. For planktonic cells, CFU were enumerated was taken after incubation with water or GO at the same temperatures and for the same times. One colony was transferred from a plate agar into TSB 100 mL and incubated for overnight. 10^{8} CFU/mL from the culture was added to 4 mL H_2O or GO 85 µg/mL for 24 h with shaking at 80 rpm and incubated at the same temperatures. CFU were enumerated after incubations.

To study the effect of pH and osmotic stress, biofilms were grown in the CDC reactor for 48 h and were rinsed with PBS; pH 7.0 to remove the non-adherent cells followed by adaptation at different pH (5, 6, 7, 8 and 9) or for different osmotic stress NaCl (51, 219 and 320 mM) for 3 h at room temperature. For the pH experiment, two groups were used; the acid group included pH 5, 6, and 7 using citrate–phosphate buffers while the alkaline group included pH 7, 8 and 9 using tris-HCl buffer.

Six coupons were used for each pH in this experiment; two coupons were exposed to different stresses for 3 h and called pre-treatment. The other four coupons were also exposed to the same stresses for 3 h then incubated with either deionised water (control) or GO 85 µg/mL for 24 h at 25 ^{o}C with shaking at 80 rpm., called post-treatment. For planktonic cells, they were treated similarly to biofilms (Figure 4.1). One colony was transferred from plate agar into TSB 100mL and incubated for overnight. 10^{8} CFU/mL from the culture was added to 4 mL the different pH (5,6,7,8 and 9) and (51, 219 and 320 mM) NaCl.

However, the free cells were washed with PBS two times after the incubation with pH or osmotic stress solutions, then incubated with either deionised water or 85 µg/mL GO.

4.3.4. Confocal microscopy analysis

Biofilms were observed using confocal microscopy as described in section 3.3.7.

4.3.5. statistical analysis

The statistical analysis was done as described in section 3.3.9.

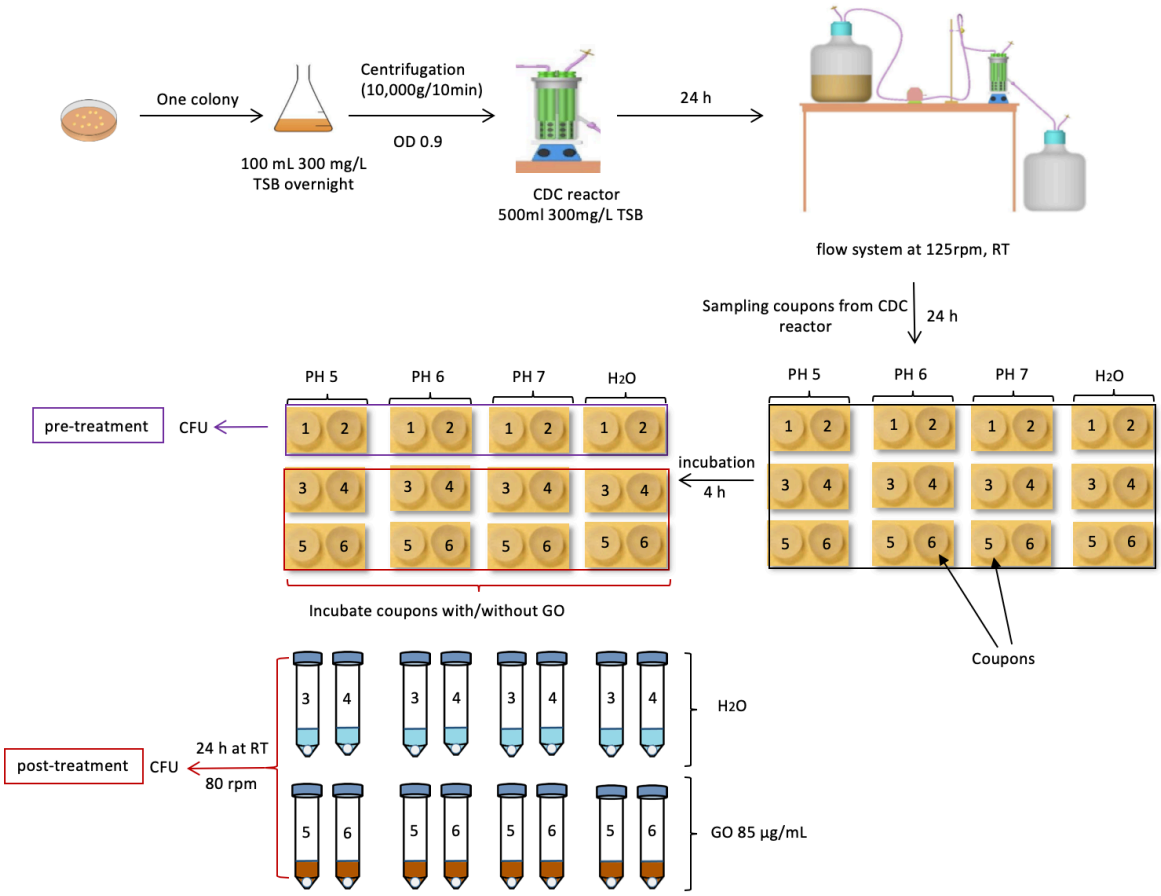

Figure 4.1 Flow chart illustrating the experimental steps in the study used to detect the viability of biofilm in pH ranges 5, 6, and 7

4.4. Results

4.4.1. Effect of Temperature and GO on viability of planktonic and biofilm cells

The effect of temperature on the viability of 48 h biofilms and planktonic cells was monitored by plate counting, (CFU/m^2) for biofilms and (CFU/mL) for planktonic cells. The controls in biofilms were not significantly affected at low or high temperatures as seen in **Figure 4.1**. Then the biofilms exposed to 85 μg/mL GO were compared and there is no effect of different temperature on viability. However, when the exposed biofilms were compared to controls, the growth decreased (~3-log) after 24 h incubation with GO at 4 and 25^{o}C. The number of CFU decreased more at 40^{o}C (~3.5-log) compared with the initial biofilm and ~3-log compared with the control biofilm at 40^{o}C.

Similar to biofilms, planktonic cells showed no reduction in CFU number for controls at all temperatures 5 °C, 25 °C and 40 °C (~log 6.5) as shown in **Figure 4.2**. In addition, there was no significant effect on planktonic cells when the cells were exposed to 85 μg/mL GO at all temperatures or compared with the other controls.

A

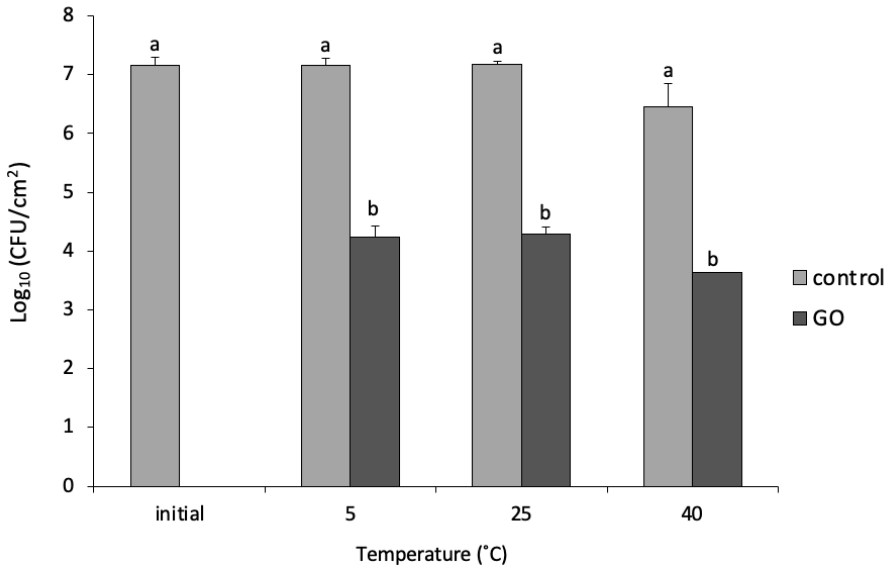

B

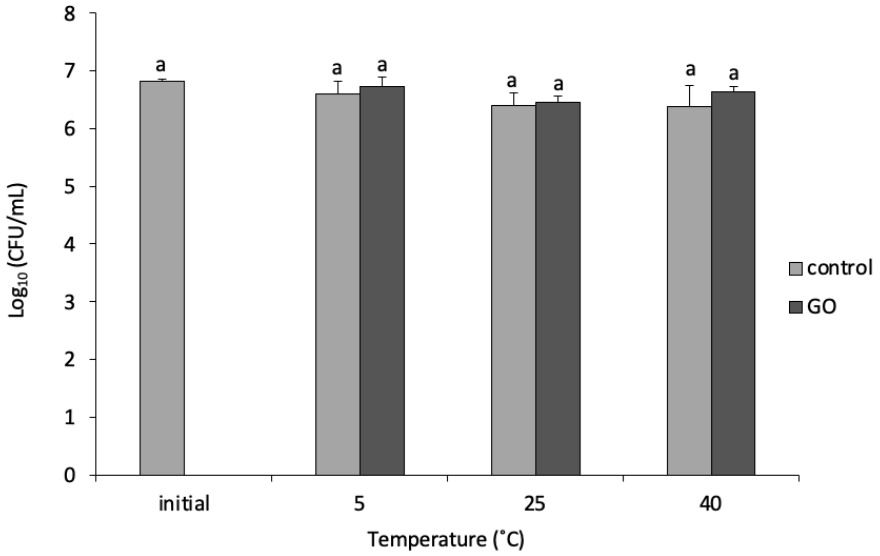

Figure 4.2 The viability of 48 h *P. putida* with/without GO incubated at 5, 25 and 40°C (A) biofilm and (B) planktonic cells. The initial indicates the viability of *P. putida* after sampling form CDC bioreactor. Mean values with different letters are significantly different ($P < 0.05$). The data was analysed with one-way ANOVA

.

4.4.2. Incubation of GO on pH and NaCl solutions

To find out if GO can be incubated with the bacterial cells during the environmental stresses, the stability of GO at different pH and NaCl concentrations were tested. GO at 85 μg/mL GO was added to different pH buffers and solution containing NaCl of similar concentrations used for the environmental stress and incubated for 24 h to identify the stability of GO in these solutions. **Figure 4.3** shows an aggregation of GO at pH 5 and at 320 mM NaCl after incubation at room temperature and illustrates that the top of the solution was clear. In acidic buffer (pH 5), GO becomes protonated and hydrophobic, thus it aggregates, and the buffer becomes more transparent, while in alkaline buffer (pH 9), GO becomes deprotonated and remains hydrophilic, thus it remains homogeneous. These results suggest that GO is not stable at pH and NaCl concentrations used in this study and therefore the bacterial cells would be treated with GO in de-ionised water after they have been exposed to the environmental stresses.

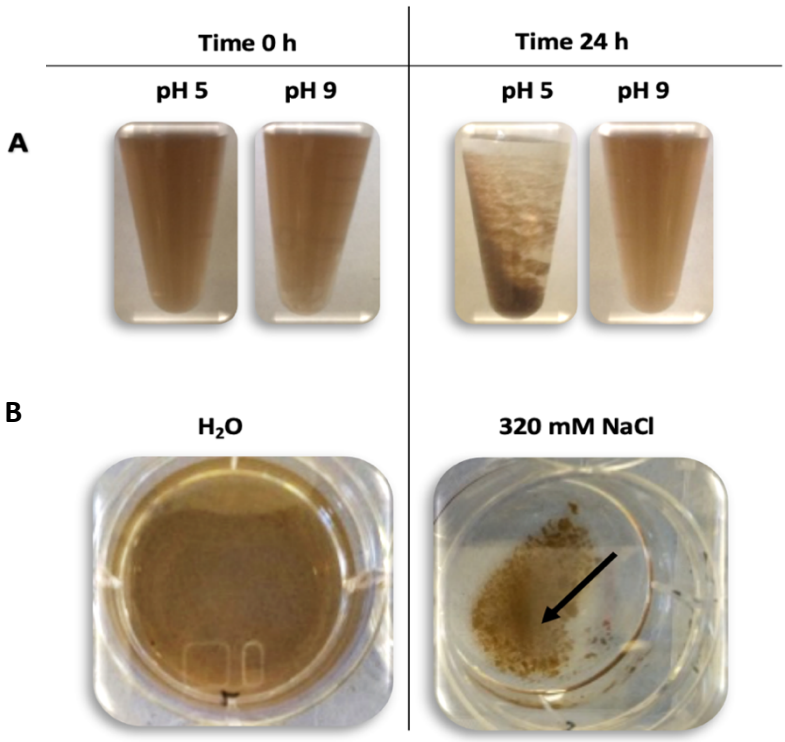

Figure 4.3 Images of GO incubated in low and high pH; and NaCl for 0 and 24 h (A) Shows the GO in pH 5 and 9 . At 24 h, pH 5 showed aggregations of GO (B) A top photo of a 6-welll plate shows the interaction of GO in water with 320 mM NaCl. At 24 h GO aggregates with NaCl. The black arrow indicates the aggregation.

4.4.3. Effect of pH and GO

To study the combined effect of pH and GO on the biofilm, the mature biofilm was incubated for 3 h at different pH values and then further incubated for 24 h with either H_2O (control) or 85 µg/mL GO. One sample was used for an additional control called pre-treatment right after the pH incubation but before addition of either H_2O or GO. The reason for applying these conditions to biofilms and planktonic cells before applying GO is to study the effect of the pH and osmotic stress on bacteria.

The impact of pH on biofilms is demonstrated in **Figures 4.4 A and B** which compares biofilms shocked with different pH values (pre & post-treatment). There was a direct correlation between the cell viability and pH; the lower the pH value the lower the viability of bacterial cells and *vice versa* until pH 7. The pre-treatment samples showed a slight but not significant reduction in CFU at low pH such as pH 5 (~ 1.5 log) and pH 6 (~ 1 log) after incubation for 3 h compared with the initial sample (**Figure 4.4 A**). However, at neutral or higher pH (pH 7, 8 and 9) it showed little or no effect on biofilm cell viability. The post-treatment samples incubated with 85 µg/mL GO showed a significant reduction in CFU in all pH ranges ~ 3 log. Nevertheless, pH was not found to significantly influence the anti-biofilm activity of GO as shown in **Figure 4.4 C**. At pH 5 the differences between pre-treatment and GO was (2.60±0.29) and the differences between pre-treatment and GO at pH 7 or 9 were (3.35±0.41; 3.15±0.35), respectively.

A

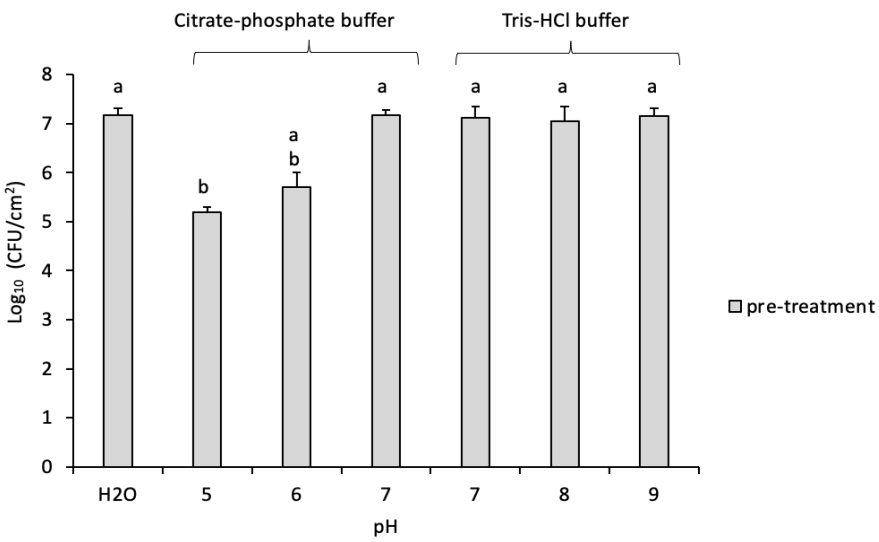

B

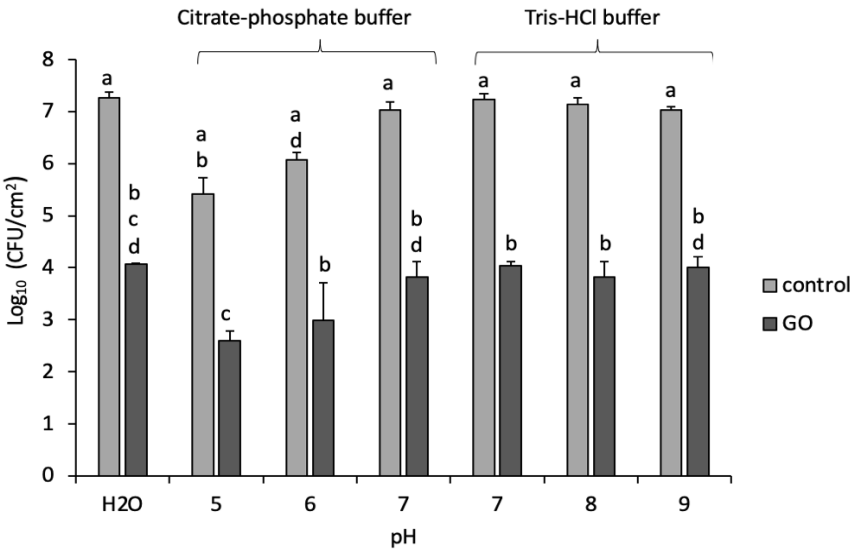

C

	H_2O	5	6	7	7	8	9
(Pre-)-GO	3.10±0.15	2.60±0.29	2.71±1.02	3.35±0.41	3.08±79	3.22±0.61	3.15±0.35
Cont-GO	3.36±0.12	2.82±0.13	3.07±0.57	3.19±0.03	3.02±0.28	3.21±0.46	3.32±0.17

Figure 4.4 Impact of different constant pH values on *P. putida* biofilm (A) Represents the viability of biofilm after exposure to different pH values (pre-treatment). (B) Represents the viability of biofilm after the exposure to constant pH and incubation with either deionized water (control) or 85 mg/mL for 24 h (post-treatment). (C)The table shows the differences in log_{10} CFU/m^2 viability between pre-treatment and GO; and control and GO. Mean values with different letters are significantly different (P < 0.05). The data was analysed with one-way ANOVA

The effect of pH stress and GO on planktonic cells is shown in **Figure 4.5A and B**. Unlike biofilms, the CFU of pre-treatment planktonic cells was significantly ($P<0.05$) reduced at lower pH (~ 3 log) at pH 5 and (~ 0.5 log) at pH6 compared with the initial ~ 6.5 log CFU/mL. This is potentially due to the EPS layer in biofilm protecting the cells from the acidity. At the other pH values studied there was no significant difference in the CFUs. The exposed cells to 85 µg/mL GO, also showed no significant difference in CFU compared to pre- or post-treatment control samples in the same pH values.

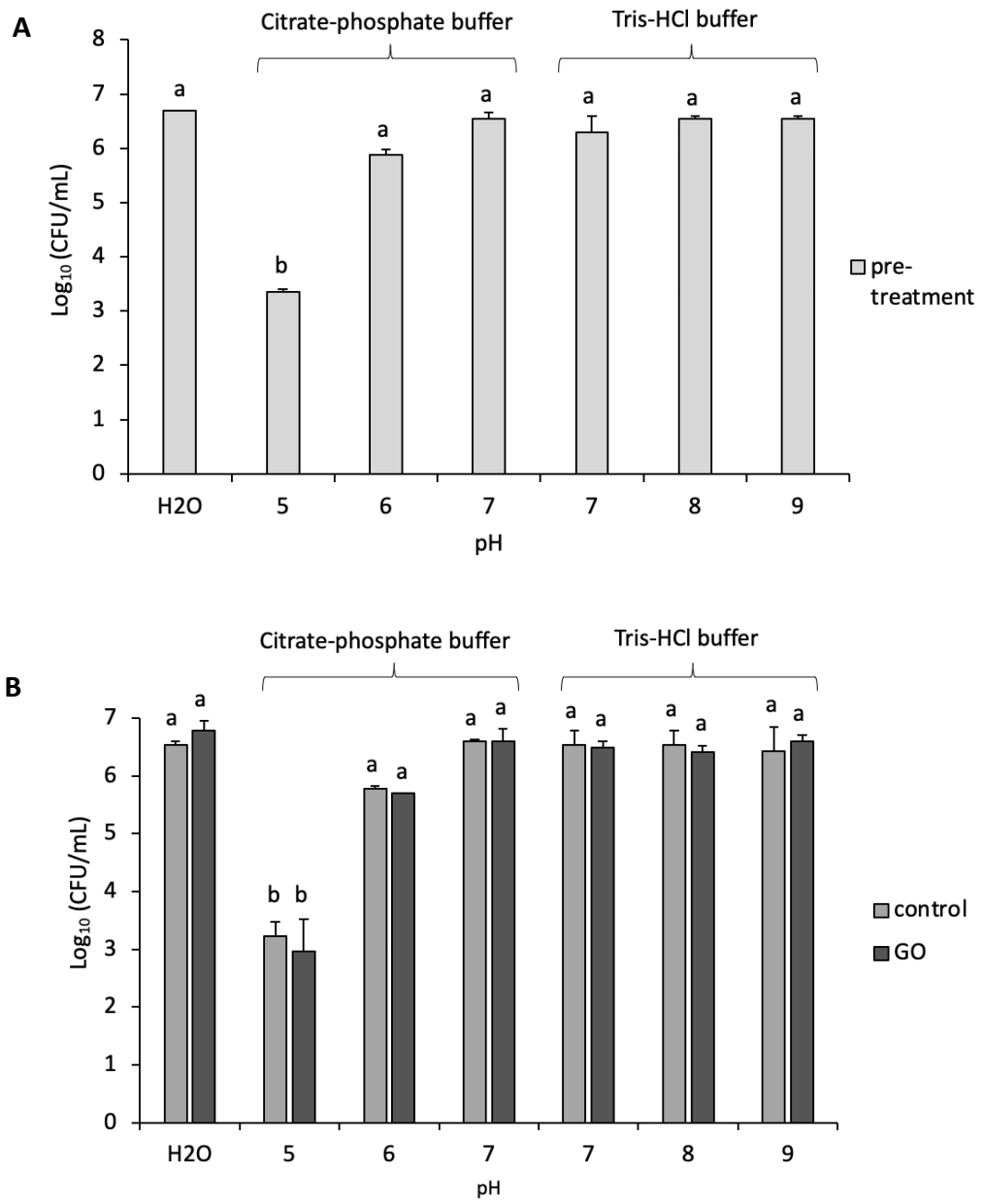

Figure 4.5 Impact of different pH values on *P. putida* planktonic cells (A) Represents the viability of planktonic cells after the exposure of different pH values (pre-treatment). The initial is the planktonic viability before the exposure. (B) Represents the viability of biofilm after the exposure with constant pH and incubation with either deionized water (control) or 85 mg/mL GO for 24 h (post-treatment). Mean values with different letters are significantly different (P < 0.05). The data was analysed with one-way ANOVA

4.4.4. Effect of osmotic stress

To study the effect of osmotic stress and GO on the biofilm, the mature biofilm was incubated for 3 h at different NaCl concentrations (pre-treatment) and then further incubated for 24 h with either H_2O (control) or 85 µg/mL GO (pre-treatment). The influence of osmotic stress on bacteria is shown in **Figure 4.6**. At concentrations 51 mM and 219 mM NaCl, the viability of the cells remained similar to control in water, which was not exposed to the stress. However, at a higher concentration (320 mM NaCl), there was a slight reduction (~0.5 log) in CFU/cm^2 (**Figure 4.6 A**).

In contrast, biofilms treated with GO after the exposure to NaCl stress for 3 h (post-treatment) showed a significant ($P<0.05$) decrease in CFU for all NaCl concentrations. This reduction was significantly ($P<0.05$) higher when NaCl concentration increased. The CFU/cm^2 for biofilm exposed to GO at 219mM was ~2.8 log and was 1.6 log at 320 mM as shown in **Figure 4.6 B**.

Further calculation was used to investigate the reduction between pre & post-treatment (**Figure 4.6 C**). For example, the reduction in CFU at 0 and 51 mM NaCl was 2.64±2.74 log and 2.74±0.13 log, respectively. However, the CFU decreased to 3.52±0.22 for 219mM and 4.45±0.71 for 320 mM, when compared with pre-treatment samples.

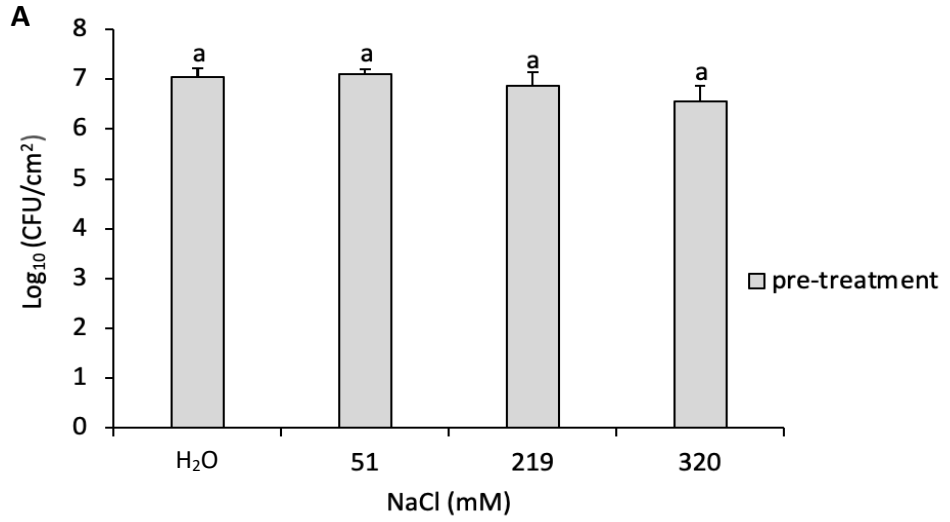

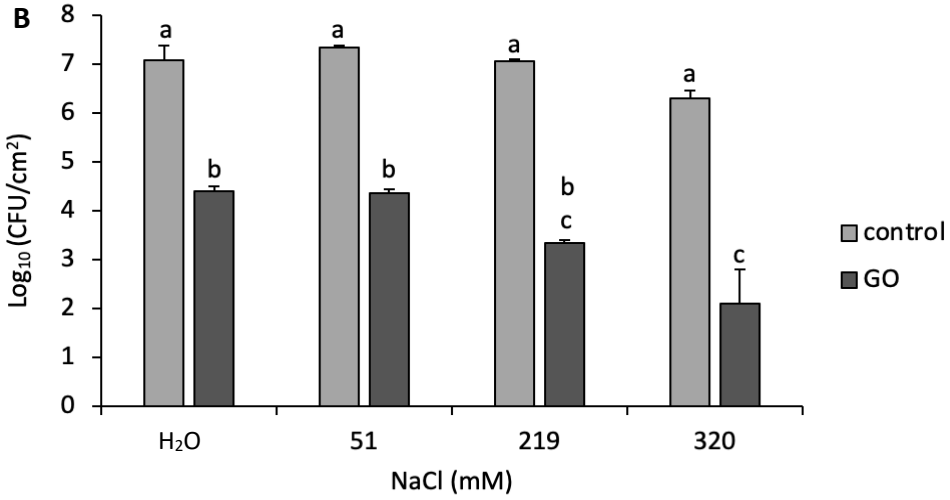

C

	H_2O	51mM	219mM	320mM
(Pre-)-GO	2.64±0.06	2.74±0.13	3.52±0.22	4.45±0.71
Cont-GO	2.69±0.27	2.98±0.04	3.52±0.01	4.45±0.38

Figure 4.6 Impact of different osmotic presure on *P. putida* biofilm cells (A) Shows the viability of biofilm after the exposure of different NaCl concetration (pre-treatment). (B) Shows the viability of biofilm after the exposure with constant NaCl and incubation with either deionized water (control) or 85 mg/mL GO for 24 h (post-treatment). (C)The table shows the differences in log_{10} CFU/cm^2 between (pre-treatment)-GO and control-GO. Mean values with different letters are significantly different (P < 0.05). The data was analysed with one-way ANOVA

The impact of GO on planktonic cells in different concentrations of NaCl is shown in **Figure 4.7**. The CFU of pre-treated cells at high concentrations of NaCl showed a reduction of ~ 1.2 log for 219mM and ~ 4.6 log for 320mM. The controls in post-treatments showed no differences when compared with pre-treatment samples. Moreover, the samples exposed to GO showed no significant differences when compared to the controls in post-treatment. However, when comparing the exposed sample with GO at 320 mM NaCl to the control at 0 mM NaCl, the number of CFU reduced from ~ 6.5 log to ~ 1.5 log. However, this high log reduction was solely due to the presence of the high NaCl content (i.e 320 mM) regardless of GO.

The differences between the planktonic cells and biofilms in the high NaCl concentrations are obvious. The survival decreases at 219 and 320 mM in planktonic cells. However, the survival of biofilm cells were not affected at the same concentrations. This could be due to EPS gives protection to cells.

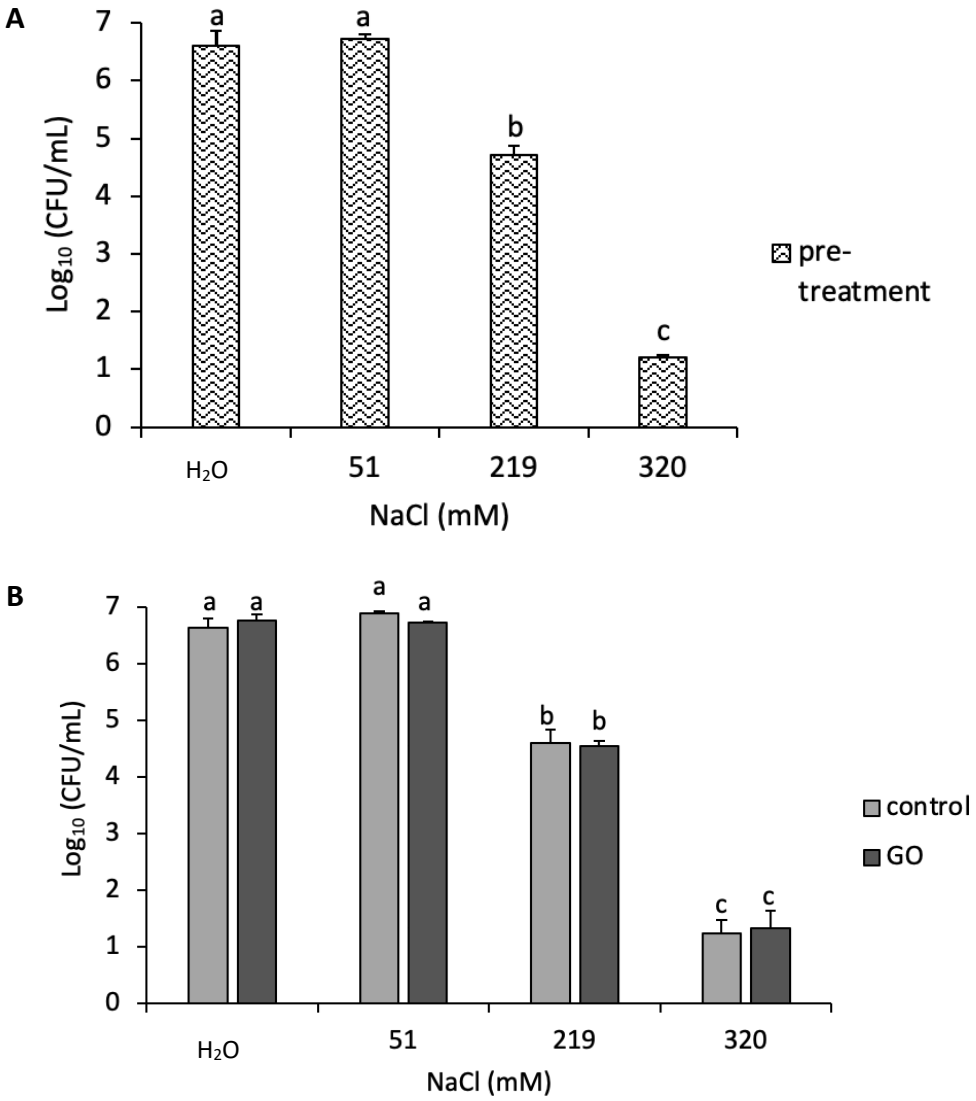

Figure 4.7 Impact of different osmotic pressure (using NaCl) on *P. putida* planktonic cells. (A) Represents the viability of planktonic cells after the exposure to different NaCl concentration (pre-treatment). (B) Represent the viability of planktonic cells after the exposure to constant NaCl and incubation with either deionized water (control) or 85 mg/mL for 24 h (post-treatment). Mean values with different letters are significantly different ($P < 0.05$). The data was analysed with one-way ANOVA

Confocal microscopy was used to assess the membrane integrity of *P. putida* biofilm cells to indicate the damage or the death of bacterial cells. **Figure 4.8** shows biofilms after treatment with 320 mM NaCl with and without the presence of GO. The images from confocal microscopy showed there was an increase of PI stain after GO treatment compared to the control, indicating decreased membrane integrity. These results confirm the CFU data (**Figure 4.6 B**) that showed reduced viability after GO treatment compared to the control.

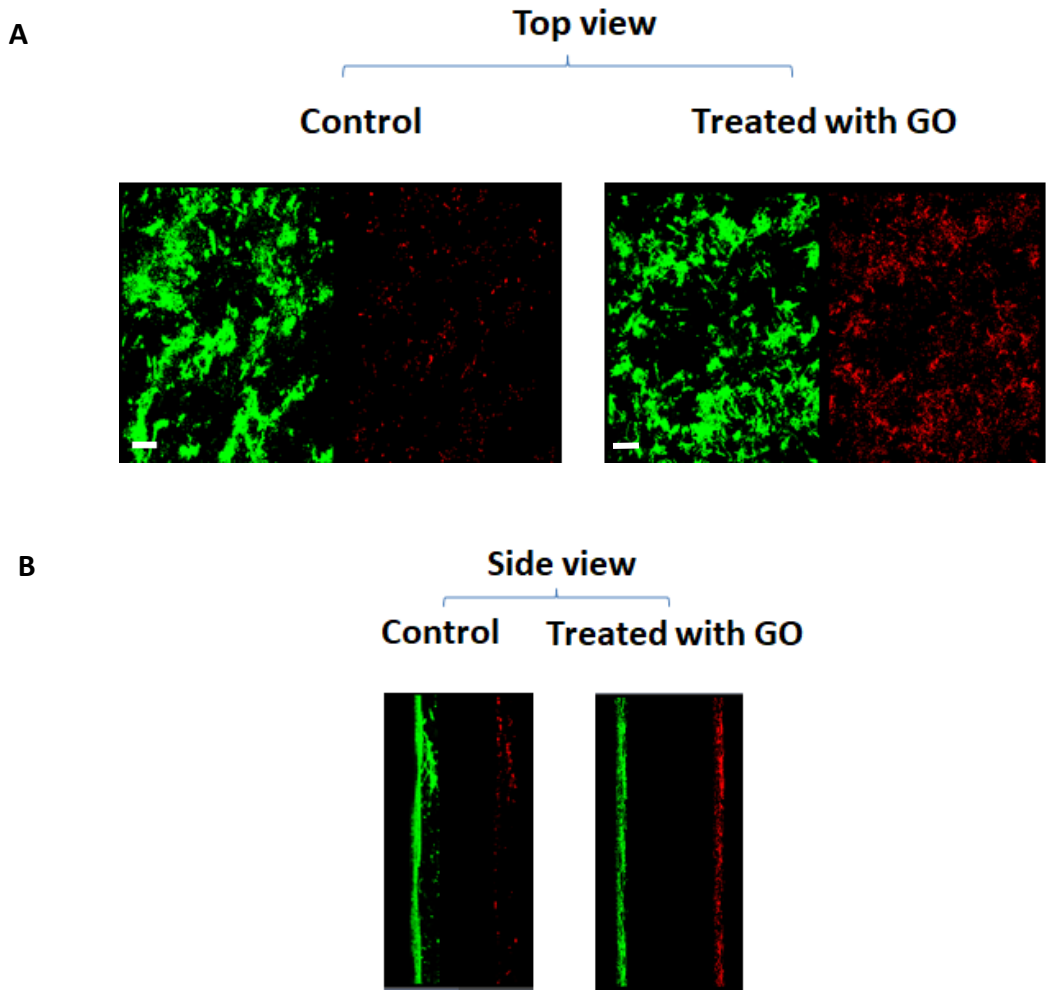

Figure 4.8 Confocal images of *P. putida* biofilm with or without GO (85 µg/mL) at 48 h incubated with 320 mM NaCl. The biofilms were stained with SYTO 9 (left, green) and PI (right, red). Scale bar: 20 µm (A) top view (B) side view

4.5. Discussion

4.5.1. Temperature

This study aimed to investigate the antibacterial activity of GO on planktonic and biofilm *P. putida* with or without pH, osmotic or temperature shock. The effect of temperature on biofilms and planktonic cells incubated with GO was studied. Most *P. putida* form biofilms at 25 ^{o}C (Antoniou and Frank, 2004). In the literature, 5 and 40 ^{o}C were used as the lowest and highest temperatures respectively to investigate the effects of temperature on *P. putida* biofilms (Munna et al., 2015; Morimatsu et al., 2012; Karpouzas and Walker, 2000; Reva et al., 2006; Srivastava et al., 2008) and based on that those temperatures were chosen in this study. As expected, at all temperatures the viability of *P. putida* biofilm was significantly ($P < 0.05$) reduced after exposure to GO compared to control. However, temperature was not found to influence the viability of *P. putida* biofilm cells upon their in parallel exposure to GO.

In this study, temperature was not shown to affect the viability of *P. putida* biofilm cells. Ricker and Nuxoll, (2017) studied the effect of antibiotic after heat shock (ranging from 37 to 80 ^{o}C for 1 to 30 min) on the viability of *Pseudomonas aeruginosa* biofilms. The viability of *P. aeruginosa* biofilms was reduced synergistically after shock treatment combined with antibiotics. The contradiction between our data and literature may be due to the difference in the mechanism of killing that is induced by GO. However, further work needs to be done to confirm if this is true.

The lowest and highest temperatures (5 and 40^{o}C) tested in this study did not show any effect on planktonic cells. This observation is similar to a previous study (Karpouzas and Walker, 2000). However, biofilms showed a slight reduction in number of biofilm cells at 40^{o}C. This reduction was also observed in other studies such as Lin

et al. (2014), whose results showed a reduction in the survival of *P. putida* biofilms at higher temperatures. They demonstrated there is a reduction at 35^{o}C for the bacterial growth while the component of the exopolysaccharide (EPS) increased such as carbohydrates, DNA, and proteins. In biofilms the maintaining of a healthy EPS is essential to prevent cells from drying at high temperature. Furthermore, high temperatures may cause cell lysis and death in biofilms and planktonic cells. *P. aeruginosa* biofilms have been shown to be more resistant to heat and antibiotic treatments compared to planktonic cells (Ricker and Nuxoll, 2017). In this study GO showed no effect on planktonic *P. putida* but was able to significantly reduce the viability of *P. putida* biofilm cells.

4.5.2. pH Stresses

Due to the aggregation of GO in low pH solution, biofilm had to be pre-treated before exposure to GO in water. These results are similar to those found in Shih et al. (2012) who studied the behaviour of GO at different pH values and found that at low pH, GO forms aggregates. This is due to the carboxyl groups in GO which become extremely protonated and became less hydrophilic. However, GO does not aggregate in water and shows a GO-water-GO structure that make it stable instead of precipitating. On the contrary carboxyl groups are deprotonated and become very hydrophilic in high pH, which make it dissolve in water and the solution will be homogeneous with a dark brown colour (Shih et al., 2012).

It has been also reported that GO sheets in water are negatively charged due to the oxygen functional group attached (Wang et al., 2016). The repulsive electrostatic interactions between the GO particles, which is greater than van der Walls attractive

forces, prevents the accumulation of GO particles and makes the GO dispersion steady (Wang et al., 2016).

This study shows the strong impact of pH on *P. putida* biofilm and planktonic cells. The pre-treated samples, whether biofilms or planktonic, have been affected by low pH which reduced the viability of cells more than high pH. Lee et al. (2011) used *P. putida* KT2440 to study the effect of pH ranges from 4.0 to 10.0 on the EPS production using HCl or NaOH. At higher pH, it enhanced the production of polysaccharide and pellicle formation while the acidic buffers changed the morphology and reduce pellicle formation. A similar study found that at low pH *P. putida* biofilm production was inhibited while the amount of EPS increased (Lin et al., 2014). Thus, lowering of the pH of the surrounding biofilms using citrate-phosphate might be sufficient to supress *P. putida*.

However, high pH did not show any statistically significant toxicity on the cells. These results agreed with van der Waal et al. (2011) who investigated the effect of alkaline on mature *P. aeruginosa* biofilms using calcium hydroxide $Ca(OH)_2$ at pH 12.1. The study showed that alkaline broth did not reduce the number of bacterial cells. This was due not only to genetic adaption but also the increase of EPS production in which the cells can be protected from the alkaline environment (van der Waal et al., 2011; Lee et al., 2011). However, this finding is contrary to previous studies which have suggested that high pH similar to ones used in this study can exert a killing effect on planktonic forms of Gram-negative bacteria (Mendonca et al., 1994; Pearson et al., 1987). A study by Mendonca et al. (1994) used NaOH to give buffers of pH 9.0 – 12.0 on two Gram-negative bacteria (*E. coli* and *Salmonella* Enteritidis) and found these bacteria lost their viability at high pH values more than the Gram-positive bacteria (*Listeria monocytogenes*) . The study suggested that the destruction of bacteria is

more likely due to disruption of cytoplasmic membrane, which causes the internal contents to leak. This discrepancy may be due to species difference and also due to biofilm cells being less susceptible to higher pH compared to planktonic cells.

4.5.3. Osmotic Stress

Similar to pH, osmotic stresses were chosen according to the tolerance of the cells without being totally destroyed (Lin *et al*., 2014). Aggregation of GO in NaCl was seen as in **Figure 4.3**. Previous studies have suggested that dispersed GO will aggregate in the presence of an electrolyte such as NaCl (Li et al., 2008). The electrolytes decreased significantly the electrostatic repulsion between the GO particles, which results in destabilization of the GO dispersion by electrostatic double layer attraction (Li et al., 2008). Wang et al. (2016) studied the behaviour of different GO sizes in common inorganic-salt electrolytes, such as NaCl, $MgCl_2$ and $AlCl_3$ at different concentrations. They found that GO dispersions started to form coagulations over 24 mM NaCl, but the dispersions remained stable in lower concentrations. $MgCl_2$ also aggregated GO from 2.50 (mM). However, in the presence of $AlCl_3$ GO started to aggregate at 0.25 mM and remained clear above this concentration. This is due to electrostatic repulsion which makes the zeta potential more than +30 mV which makes GO stable. A similar phenomenon was found in other nanoparticles such as carbon nanotubes (Niyogi et al., 2007) and gold nanoparticles (Jiao et al., 2014). A study showed the effect of NaCl concentration on absorption efficiency and found that the efficiency increased with the increase of GO aggregation (Xu et al., 2016). Thus, the study of osmotic stresses on bacteria and GO was completed after the bacterial incubation with NaCl.

In this study, biofilms were slightly affected at higher concentration of NaCl (**Figure 4.6A**). Biofilms and planktonic cells were not affected at low concentration of NaCl. However, at higher concentration, the number of planktonic cells decreased comparted with biofilms. The salts can alter the membrane fatty acid composition (Beales, 2004). Moreover, the cells will shrink due to osmotic pressure being higher outside the cell (Csonka, 1989).

Thus, the number of planktonic cells decreased as NaCl concentration increased. Lin et al., (2014) showed that EPS create a more hydrated microenvironment around the cells, which therefore, increase adaptation of *P. putida* to osmotic stress without decreasing the growth rate. However, the EPS production cannot protect the cells from plasmolysis caused by NaCl. Biofilm were convoluted (morphologically altered) under AFM, which indicates that NaCl exerted an osmotic pressure on the cytoplasmic membrane even though the cells were surrounded by EPS. Moreover, (Lin et al., 2014) found the surface morphology of *P. putida* biofilms changed clearly under different osmotic stresses. However, the cells volume decreased slightly. When biofilms were exposed to 120 mM NaCl, the surface was extremely rough. Therefore, it is possible that at higher osmotic pressure, bacterial membrane changes its activities due to increased membrane fluidity that can make the cells in biofilm more susceptible to damage with GO as observed here, a significant decrease in viability with GO at higher NaCl concentrations as shown in **Figure 4.6 B**.

Confocal microscopy images confirmed the CFU results at high concentration of NaCl which indicated the death or damage of the cells. This suggest that the tolerance of biofilm to GO depends on the concentration of NaCl. The mechanism of destroying the bacterial cells by hyperosmotic stress has been reported earlier by (Lee, 1972; Facklam, 1973). Microorganisms organise the intracellular concentration by

counteracting the emigration of water from inside to outside the cells. This happens because of the uptake or producing molecules and ions that do not affect the metabolism inside the cells. In case of high osmotic stress outside the cells, toxicity depends on the capability of the bacteria cells to adapt to the changed osmotic stress, resources of solutes and energy outside cells during hyperosmotic stress change. Microorganisms will be affected and destroyed when solutes or energy resources are low (Csonka and Hanson, 1991). The phenomenon of osmotic stress depends on the solute's concentrations which cause movement of solvents between the cell and its environment until the solute's concentrations reaches equilibrium.

In conclusion, the effects of temperature, pH and osmotic stresses on biofilms followed by GO exposure were studied. The GO exerted the same effect at all temperatures. However, the combined exposure to low pH and GO affected biofilms. Moreover, the biofilms were affected by the combined exposure to high osmosis and GO. In general, planktonic cells were not affected by GO.

The results showed that exposure to GO had no additional or synergistic antibacterial activity against biofilms and planktonic cells that have been subjected to temperature and pH stresses. Conversely, higher concentrations of NaCl reduced the population of biofilms. The findings suggest that *P. putida* can survive in a wide range of environmental stresses. Moreover, some of these stresses, such as osmotic stress, could also lead to biofilms becoming more susceptible to GO toxicity probably due to physiological changes in the cell membrane. To better understand how these stresses, along with exposure to GO, affect *P. putida,* it is important to study changes that occur to the bacteria at the molecular level, such as genes and proteins. Besides molecular effects the higher toxicity of GO in the presence of osmotic stress against biofilm cells may be related to changes in some biofilm specific features such as changes in EPS

consistency. It is also important to study and investigate the bacterial cell membrane to understand the mechanism of GO toxicity. These findings can be interesting for other researchers investigating the toxicity of GO on bacteria.

Chapter 5. The Effect of EPS on the Susceptibly of *P. putida* Biofilm to GO

5.1. Abstract

The extracellular polymeric substances (EPS) have a protective effect on microbial cells in adverse environmental conditions. The removal of EPS may increase bacterial susceptibility to antimicrobial agents such as GO. In this chapter, the effect of GO on *P. putida* biofilm in the presence or absence of EPS (after removal using standard methods) was assessed by plate counting. The method of EPS removal involves inculcation of biofilm with EDTA and preliminary data showed that this treatment had no effect on *P. putida*. The removal of EPS increased the susceptibility of *P. putida* cells to GO which confirms the protective effects of EPS in biofilms mentioned in literature. Also, the mechanism of GO's antibacterial activity was investigated by characterising the bacterial cell wall after exposure to GO. FTIR using fingerprint spectra was used to study the chemical compounds and the functional groups in the cell wall. Infrared spectroscopy is a technique used to detect the functional groups in organic compounds according to their variation and wave numbers. Any changes in these groups can be detected by analysing the position and the intensity of the bands. Moreover, it is considered a non-destructive method, where the living cells can be monitored. In this study, FTIR was used to characterize bacterial cells by identifying their functional groups. Using FITR with bacteria shows bands corresponded to lipids, proteins, polysaccharides and polyphosphate groups (Ojeda and Dittrich, 2012).

5.2. Introduction

The use of FTIR spectroscopy was used to identify bacteria for over 100 years (Coblentz, 1911). Recently, it has started to be used as a tool to analyse chemical changes in bacteria (Parikh et al., 2014). It is a quick method to study the chemical compounds and the functional groups in the envelope. Infrared spectroscopy is a technique used to detect the functional groups in organic compounds according to their variation and wave numbers. Any changes in these groups can be detected by analysing the position and the intensity of the bands. Moreover, it is considered a non-destructive method, where living cells can be monitored (Ojeda and Dittrich, 2012). The FTIR spectra of bacteria show four major groups of bands corresponding to lipids, proteins, polysaccharides and nucleic acids (Parikh et al., 2014). The three most common FTIR-based methods used for bacteria are: Transmittance FTIR, attenuated total reflectance (ATR-FTIR) and micro-spectroscopy FTIR (Faghihzadeh et al., 2016); in this chapter, the first two are used.

Transmittance FTIR analysis can be used with liquid, solid or gas samples. Solid samples have to be mixed with highly polished salts such as NaCl, AgCl or KBr to make a transparent pellet and placed between two infrared-transparent plates. ATR-FTIR can be used with liquid or dried samples placed on a crystal surface (Faghihzadeh et al., 2016). It has been widely used to study the toxicity of nanoparticles such as silver (Ansari et al., 2014) and carbon nanomaterial (Riding et al., 2012). Ansari et al. (2014) used ATR-FTIR to characterize the impact of AgNPs on *E. coli*. FTIR data revealed damage of the cell membrane after treatment with AgNPs as both lipopolysaccharides (LPS) and the membrane component phosphatidylethanolamine (PE) were affected leading to the destruction of the membrane. Hydrogen bonding was found as a result of interaction of AgNPs with the

O-antigen part of LPS and the phosphodiester bond of PE was broken by AgNPs forming monoesters resulting in highly disordered alkyl chain. Another study investigated the toxicity impact of long and short nanotubes on Gram negative bacteria using ATR-FTIR (Riding et al., 2012). The study reported that the toxicity of these nanoparticles depends on their size. For instance, the smallest nanotubes had greater toxicity than longer nanotubes, according to the signature of lipids, amide II and DNA in the cells.

It is known that EPS structure plays a major role in protecting bacteria and can bind to nanoparticles (Guo et al., 2017). Studies showed that the accumulation of NPs occurred in EPS (Yeo and Nam, 2013; Ikuma et al., 2015). When Ag was added to *P. fluorescens* biofilms, it showed that it accumulates in the EPS (Peulen and Wilkinson, 2011). Functional groups on EPS have the potential to bind charged molecules, ions and nanoparticles (Ikuma et al., 2015). Therefore, this interaction can change the functional groups of EPS.

In order to better understand the role and the nature of EPS and its interaction with GO, it is important to understand the actual functional groups' location in the cell wall and the mechanisms of interaction. The composition of EPS is complex, as it consists of many complicated compounds. The biochemical properties of these compounds still elusive since they have their own unique monomer linkages and complex structures (Jiao et al., 2010).

The general observation from the previous chapters was that only the biofilm cells were affected by GO. Therefore, this chapter focuses on the EPS and its role on the cells' protection from GO by studying the effect of GO on biofilms after EPS. Moreover, it analyses the chemical compounds of EPS to understand its interaction with GO.

5.3. Materials and methods

5.3.1. Growing biofilms

P. putida biofilms were grown in CDC bioreactor as descried in section 3.3.4 and the coupons were collected after 48 h.

5.3.2. Synthesis of Graphene oxide

GO was synthesised as described in section 2.3.1 and 85 µg/ml GO was used.

5.3.3. Effect of GO on *P. putida* biofilm after removing EPS

To examine the susceptibility to GO of *P. putida* biofilms, the experiment was conducted in a falcon tube after biofilm was developed using CDC bioreactor. EPS was removed as described by Thuptimdang et al. (2015) with some modification by adding 1% (w/v) instead of 2% (w/v) of ethylene diamine tetra acetic acid (EDTA) for 3 h at 4^{o}C before rinsing samples with PBS and treating with 85 µg/mL GO at 25^{o}C at 0, 3 and 24 h. For control, the biofilm had been previously incubated with dH_2O for 3 h at 4^{o}C instead of with EDTA. Coupons were vortexed for 30 seconds and then bath sonicated (40 kHz) for 30 seconds, three times. CFU was used to determine the viability at different times: 0, 3 and 24 h by plate counting.

To test the susceptibility of planktonic cells against EDTA and GO, cells were grown in LB overnight then centrifuged at 12,000g. After removing the supernatant, the pellet was washed with PBS then 1% EDTA was added for 3 h at 4^{o}C. EDTA was removed by centrifugation at 10,000g before adding H_2O or 85 µg/mL GO for 24 h at 25^{o}C.

5.3.4. Extraction of EPS

EPS was extracted using the EDTA method for chemical composition analysis. This method shows a better extraction compared with other methods such as alkaline, heating and high-speed centrifugation since this method showed low amount of cell lysis and high extraction productivity (Elayatt and Romero-Gonzalez, 2016). *P. putida* biofilm was dissociated by vortexed for 30 seconds and then bath sonicated (40 kHz) for 30 seconds, three times and centrifuged at 12,000g for 10 min. The pellet was transferred to 10 ml ddH_2O and spun; then the pellet was put in 1% EDTA for 3 h at 4^oC. The supernatant was filtered by 0.022μm cellulose membrane. The EPS was precipitated using 3 volumes of 100% cold ethanol overnight at -20^oC. EPS was then collected by centrifugation at 12,000g for 30 min followed by adding ddH_2O to the pellet to remove the ethanol. It was dried at 50^oC overnight.

5.3.5. Chemical composition analysis

FTIR is a rapid method used to identify chemical compounds in bacteria. 12 coupons of *P. putida* biofilms were washed with PBS and they were broken by vortexing and sonication. Then it was centrifuged at 17,500g for 20 min at 4^oC and the pellet was resuspended in 20µl PBS to obtain a highly concentrated suspension which is required for further analysis.

Attenuated Total Reflection ATR-FTIR

For liquid samples, small drops of the sample were used such that the crystal was covered using Pasteur pipette. Then, using software and Nicolet 380 FTIR (Thermo

FisherScientific) the infrared spectrum of the sample was scanned using diamond or zinc glasses.

Transmittance FTIR analysis

FTIR was used for dried sample. The 20 µl of the sample was transferred to a clean microscope slide and dried at room temperature. To analyse cells with FTIR, a transparent disc was used by gently mixing 5mg cells with 5mg KBr before adding an additional amount of KBr (95mg) to homogenize the sample. The mixture was then placed into a die to make the disc using hydraulic press (15 tonnes). Each disc was subjected to 64 scans (averaged at a resolution of $2cm^{-1}$) in a Nicolet 380 FTIR (Thermo FisherScientific, Waltham, MA, USA) in direct beam mode.

5.4. Results

5.4.1. Susceptibility of *P. putida* to GO

The effect of removing the EPS from *P. putida* biofilms on susceptibility to GO was tested. Untreated biofilms and biofilms treated with EDTA to remove the EPS, were incubated with water (control) or GO. **Figure 5.1** shows the reduction of the viability after using 1% EDTA and exposing the cells to GO. Results showed that there was a significant reduction in CFU for biofilms with GO at time 3 and 24 h, approximately 3-log compared with controls. In addition, samples treated with EDTA also showed a significant reduction compared with the control and further reduction around 6-logs was observed when GO was applied to these samples in times 3 and 24 h.

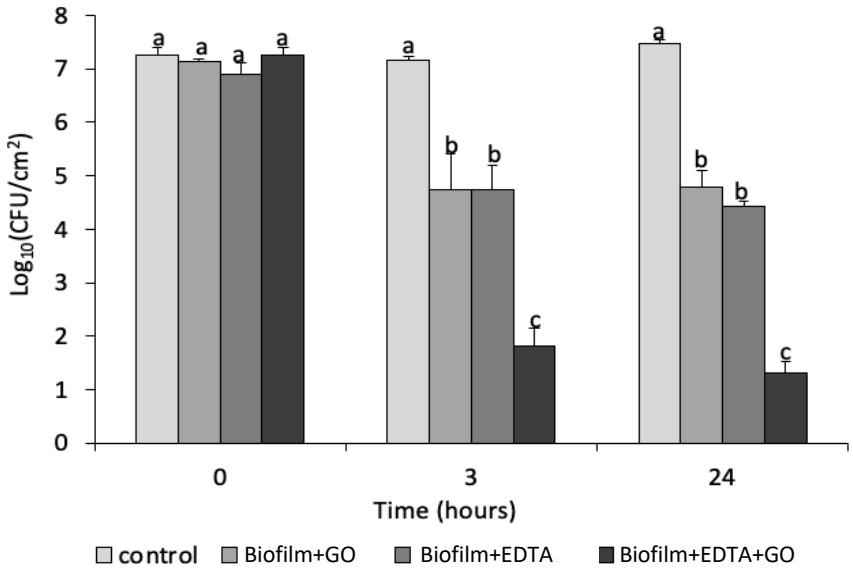

Figure 5. 1 shows the viability in CFU after removing EPS using 1% EDTA from *P. putida* biofilms. Control: the viability of biofilm after sampling and incubation with dH_2O. Biofilm+GO: the viability of biofilm after exposing to 85 µg/mL GO for 24 h. Biofilm+EDTA: viability of biofilm after exposing to EDTA for 3h. Biofilm +EDTA+GO: viability of biofilm after exposing to EDTA for 3h then being incubated with 85 µg/mL GO for 24 h. Mean values with different letters are significantly different ($P < 0.05$). The data was analysed with one-way ANOVA

To confirm that EDTA did not affect the susceptibility of planktonic cells to GO treatment, planktonic cells were also exposed to EDTA and there was no significant difference in the CFU between control cells and those treated with GO or EDTA. **Figure 5.2** shows that EDTA did not affect the viability of planktonic cells. Moreover, this treatment did not affect the susceptibly of these cells.

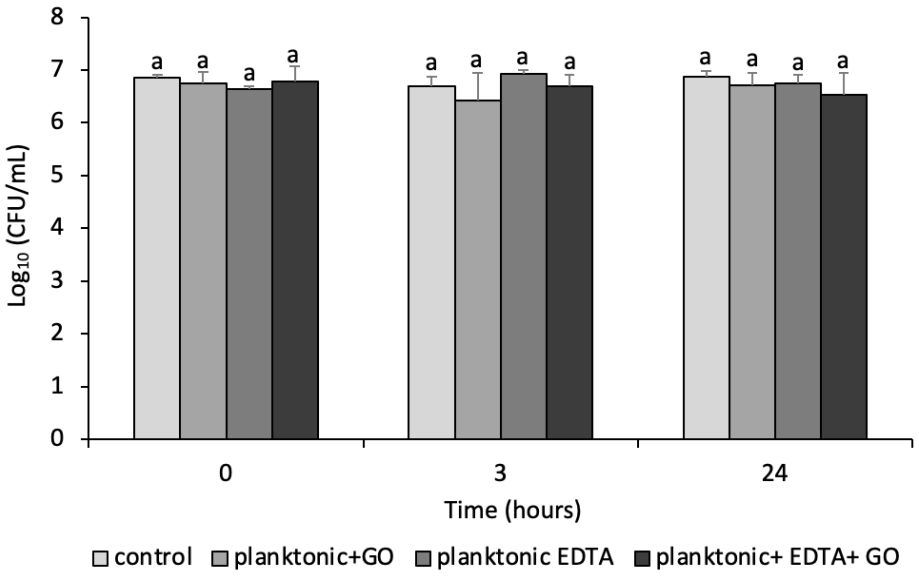

Figure 5. 2 shows the impact of EDTA and 85 µg/mL GO on *P. putida* planktonic cells. Control: the viability of planktonic cells after sampling and incubation with dH_2O. Planktonic cells+GO: the viability of biofilm after exposing to 85 µg/mL GO. Planktonic cells+EDTA: viability of biofilm after exposing to EDTA for 3h. Planktonic cells+EDTA+GO: viability of planktonic cells after exposing to EDTA for 3h then being incubated with 85 µg/mL GO. Mean values with different letters are significantly different ($P < 0.05$). The data was analysed with one-way ANOVA

5.4.2. Characterization of *P. putida* planktonic cells by FTIR

The region of an FTIR spectra between 4000 and 500 cm^{-1} holds characteristic bands for microorganisms (Schmitt and Flemming, 1998). Different methods were used to characterize biofilms with FTIR. The sandwich method where samples are placed between two discs of KBr and clamped together, then scanned with FTIR, was used first.

However, this method is not suitable as the bands in this method were unclear and difficult to observe (**Figure 5.3 A**). Bacteria have distinct bands corresponding to protein, carbohydrate and lipids. The bands here do not correlate with those in other studies (Ojeda et al., 2008). This is due to the KBr disc being dissolved in the water in the sample. A good example (*P. putida* biofilm grown using a flow-cell system) of good bands is presented in **figure 5.3 C**.

Another method was used to get the bacteria specra is by the ATR-FTIR. A few drops of bacterial suspension were placed on ATR-FTIR. After the scan, the bacteia bands were not clear (**Figure 5.3 B**). This could be due to the small amount of bacterial cells which makes it difficult to identify.(why not use higher amount?) since all the 24 coupunds are needed for one expermental setteing, it will be a limatation of the study. Moreover, different methods to obatin higher concentation bofilm biomass could be used in the future.

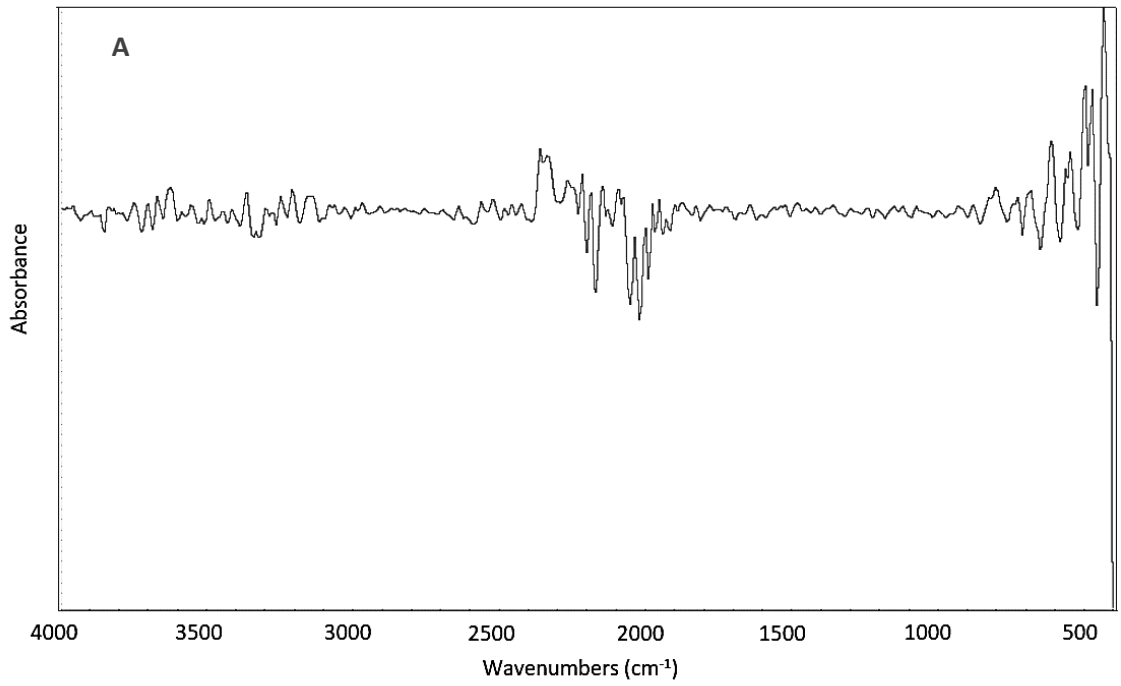
A
Absorbance
4000
3500
3000
2500
2000
1500
1000
500
Wavenumbers (cm-1)

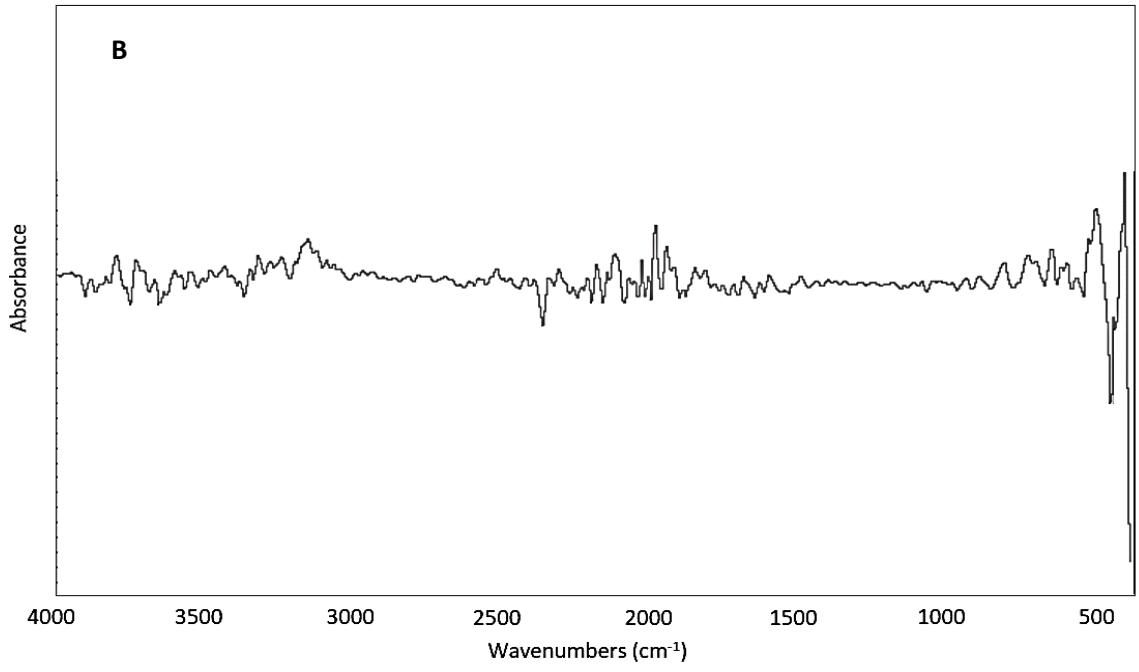
B
Absorbance
4000
3500
3000
2500
2000
1500
1000
500
Wavenumbers (cm-1)

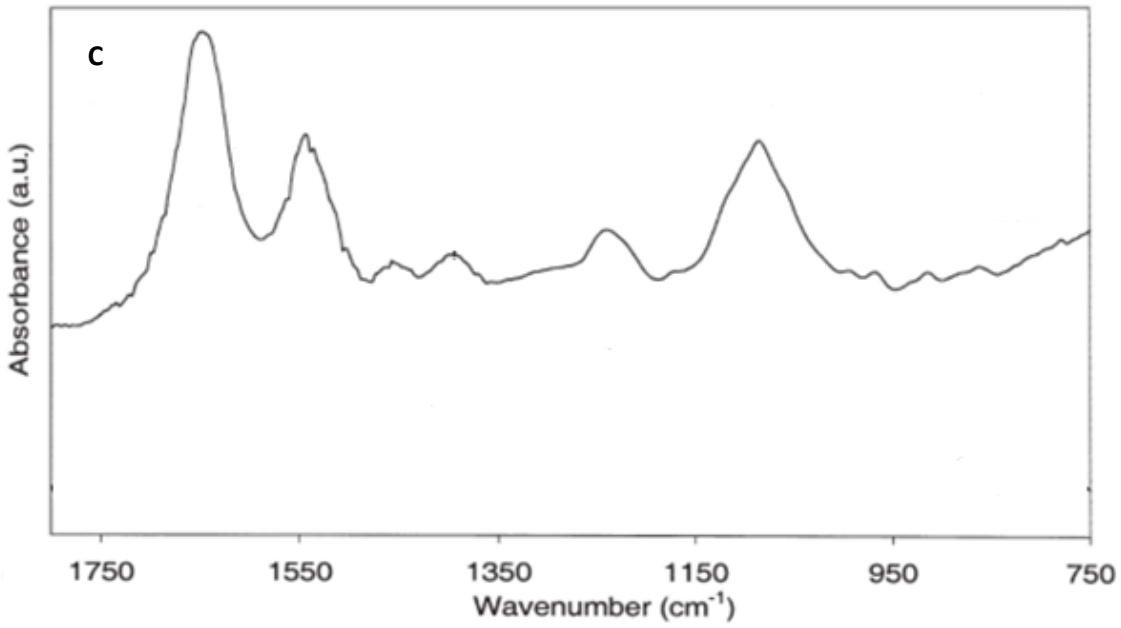

Figure 5. 3 *P. putida* (grown using CDC bioreactor)spectra with FTIR using A) sandwich method B) liquid sample on ATR-FTIR C) an example a good bands of *P. putida* biofilm grown using flow-cell system from Ojeda et al., (2008).

Infrared absorbance of both GO treated and untreated *P. putida* planktonic cells was monitored by ATR-FTIR. *P. putida* was grown on LB media overnight in a flask and centrifuged 10,000g for 10min. The pellet was then dried and mixed with KBr.

The typical bacterial spectra has five groups of bands corresponding to biomolecules: 1) Water with streaking modes of O-H in the region between 3800-3000 cm^{-1}; 2) Protein mainly identified by the N-H stretching and vibrations of peptide in amide I which come from C=O stretching and amide II which come from N-H and C-N stretching; 3) Lipids and phospholipids with methylene stretching and phosphate groups and 4) Polysaccharides which appear in region between 1200-900 cm^{-1}; and 5) nucleic acids which is liked to phosphate groups (Humbert and Quilès, 2011).

Figures 5.4 A and B show the functional group contributions of *P. putida* planktonic cells compared with those exposed to GO. The IR spectra for GO-treated and untreated samples are very similar. No new absorptions band were found on the sample with GO. However, most of the bands for treated samples shifted to the left in wavenumbers by around 1-4 cm^{-1} probably because of GO treatment. The region from 3000-2820 cm^{-1} is assigned to symmetric and asymmetric stretching of methylene and methyl groups derived from lipids (Mihoubi et al., 2017). The bands at region 2926.1 and 2925.6 cm^{-1} are similar for treated and untreated, respectively. The region between 1652 and 1540 cm^{-1} is dominated by amide I and II. The treated *P. putida* showed two bands at 1653.5 and 1543.0 cm^{-1} which are associated to C=O, C-N and N-H stretches. While the untreated *P. putida* showed the bands at 1652.1 and 1540.0 cm^{-1}, respectively (Parikh and Chorover, 2005).

The region between 1460 and 540 cm^{-1} is associated with macromolecules such as carbohydrate and polysaccharide and nucleic acids (Omoike and Chorover, 2004; Filip et al., 2008). The band at 1451.6 and 1399.2 cm^{-1} are assigning to CH_2 and C-H stretching of methyl group. The absorption band at 1237.2 cm^{-1} links to PO_2 stretching of nucleic acid or phosphorylated protein. The list of the IR absorption bands and their assignments are represented in (**Table 5.1**).

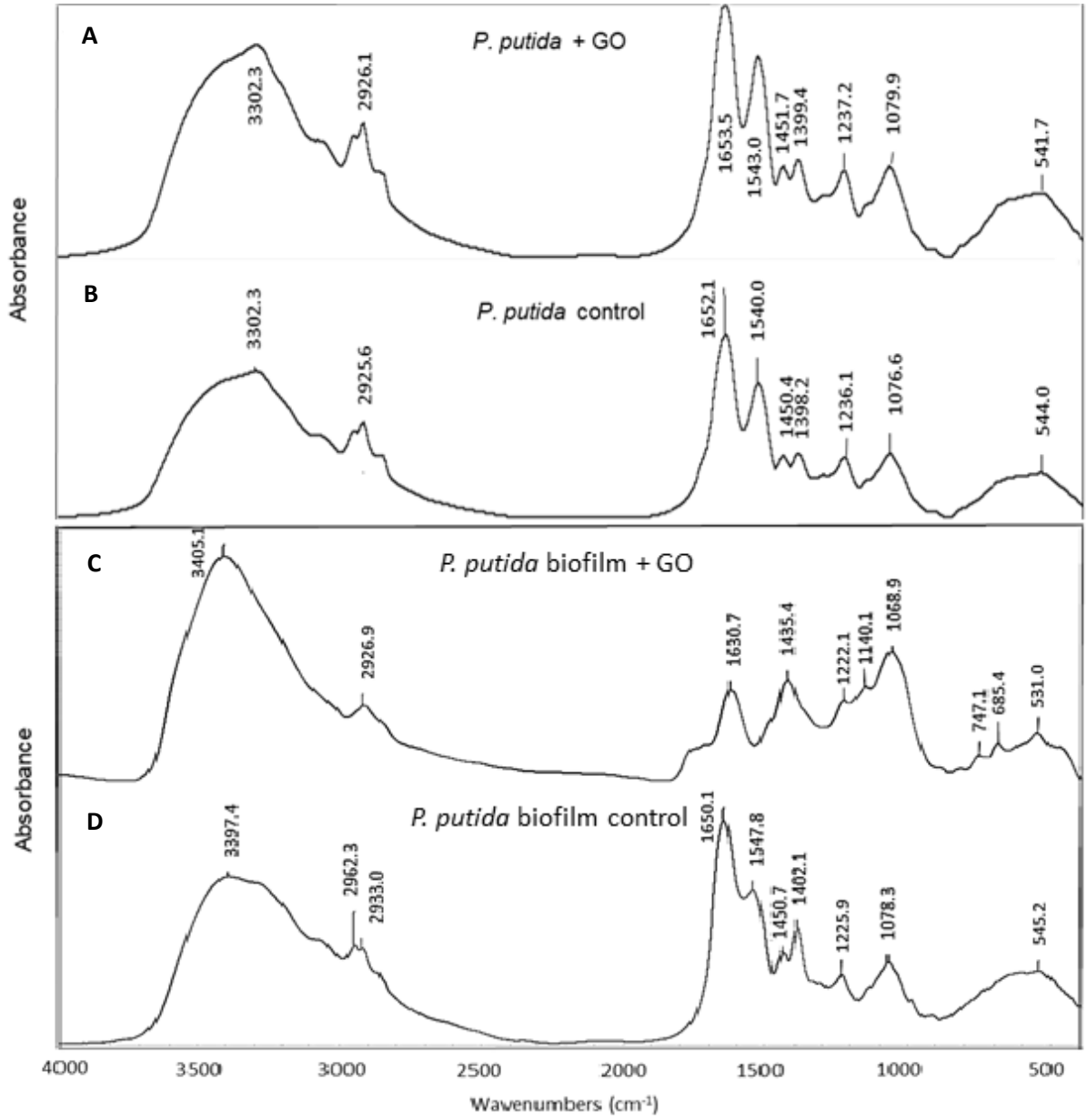

Figure 5. 4 ATR_FTIR spectra of GO-treated and untreated *P. putida*. Spectrum A) is for the GO-treated planktonic cells, B) is for untreated planktonic cells, C) is for GO-treated biofilm and D) is for untreated biofilm. The numbers on the graphs represent the absoption bands.

Table 5. 1 Functional groups of *P. putida* planktonic cells treated/untreated with GO and the corresponding infrared absorption wavelengths

Wavelength for *P. putida* control (cm^{-1})	Wavelength for *P. putida* with GO (cm^{-1})	Wavelengths (cm^{-1})	Assignments	References
3302.3	3302.3	3500-3200	O-H	(Radhika and Mohaideen 2015)
2925.6	2925.6	3000-2820 2960-2850	CH_2 (lipds) C-H	(Mihoubi et al., 2017) (Filip et al., 2008)
1653.6	1652.1	1652–1637	C=O,C-N, N-H Amide I	(Parikh and Chorove 2005)
1541.1	1540	1550–1540	N-H, C-N Amide II	(Parikh and Chorove 2005)
1451.6	1450.4	1460-1440	CH_2	(Stelescu et al., 2017)
1399.2	1398.2	1400-1380	C-H	(Devnath et al., 2017)
1237.2	1236.1	1241-1221	P=O	(Omoike and Choroverm 2004)
1079.9	1076.9	1080 1079-1048	C-O-C aliphatic ester C-O-C, C-O-P polysaccharide	(Filip et al., 2004) (Omoike and Choroverm 2004)
541.7	544	650–480	C–O-C, P–O–C	(Filip et al., 2008)

5.4.3. Characterization of *P. putida* biofilm by FTIR

After the previous failed experment with the two methods of FTIR (Figure 5.3) the KBr pellet method was used as it may show the bands that correspond to chemical compounds and obain an accurate FTIR spectrum. In this method the concentrated bacteria was compressed with KBr to form a transparent pellet avoids air bubbles and mositure which interfer with FTIR specturm. The spectra for *P. putida* biofilm treated with GO and untreated are presented in (**Figure 5.4 C and D**). At 3397.4 cm^{-1} showed the O-H vibration (hydroxyl group) which is derived from water. Two small bands apear at 2962.3 and 2933.0 cm^{-1} correspond to NH_2 stretching and O-H group. The amide I and amide II are located at 1650.1 and 1547.8 cm^{-1}, respectively. A band at 1402.1 cm^{-1} assigned to COO^- group stretching and probably C-H bond. The nucleic acid spectra is assigned between 1225.9 - 1140 cm^{-1}.

The main difference between the GO treated and untreated *P. putida* biofiom is shown in (**Table 5.2**) and (**Figure 5.4 C and D**). The amide II band, 1550-1540 cm^{-1}, is not present with the untreated sample. Moreover, two additional peaks appeared in the GO-treated sample at 747.1 and 685.4 cm^{-1} which represent CH_2 stretch. One band was present in GO-treated samples instead of two bands in regions 2960 and 2927 cm^{-1} in the untreated. Some of the bands shifted such amide from 1650.1 for untreated to 1630.7 cm^{-1} and 1405.1 to 1435.4 cm^{-1} for treated sample. This was similar to the nucleic acid band which shifted to 1098.9 cm^{-1}.

In this region, the most noticeable differences between treated and untreated biofilms are the bands that decreased at 1630.7 cm^{-1} for which indicates a loss of amide I content, and the bands at 1547 and 1450 cm^{-1} disappeared, reflecting protein damage.

Table 5. 2 Functional groups of *P. putida* biofilms treated/untreated with GO and the corresponding infrared absorption wavelengths

Wavelength for *P. putida* control (cm^{-1})	Wavelength for *P. putida* with GO (cm^{-1})	Wavelengths (cm^{-1})	Assignment	References
3397.4	3405.1	3500-3200	O-H	(Radhika and Mohaideen 2015)
2962.3 2933.0	2926.9	3000-2820 2960-2927	CH_2 C-H	(Mihoubi et al., 2017) (Filip et al., 2008)
1650.1	1630.7	1652–1637	C=O, C-N, N-H Amide II	(Parikh and Chorove, 2005)
1547.8 1450.7	- -	1550–1540	N-H, C-N Amide II	(Parikh and Chorove 2005)
1402.1	1435.4	1407-1379 1435-1346	C=O (of COO^- group) C-H ($CH_{2/3}$ vibration)	(Omoike and Choroverm 2004) (Christou et al., 2018)
1225.9	1222.1	1242-1221	P=O (nucleic acids or phosphorylated proteins)	(Omoike and Choroverm 2004)
-	1140.1	1000–1140	C-O-P, C-O-H (nucleic acids)	(Sabbatini et al., 2017) (Tarebet al.2017)
1078.3	1068.9	1000–1140	C-O (nucleic acids of polysaccharides)	(Sabbatini et al., 2017) (Tarebet al.2017)
-	747.1 and 685.4	700-750	CH_2	(Kamnev, 2008)
542.2	531.0	630-530	O-C-N (amide VI band)	(Gupta et al., 2011)

Both biofilm and planktonic cells have the O-H stretch in the region between 3800-3000 cm^{-1} and the methyl group in the region between 3000-2800 cm^{-1}. Moreover, the bands of the amide I and II are present for both forms and they located around the region 1652-1637 cm^{-1} and 1550-1540 cm^{-1}, respectively. In addition, the bands around 1450 (CH_2), 1078 (C-O) and 542 (O-C-N) cm^{-1} are present in both forms. However, the bands at 1402.7 cm^{-1} (C-H) and 1225.9 (P=O) cm^{-1} for biofilm are located differently at 1398.2 (C-H) cm^{-1} and 1236.1 (P=O) cm^{-1} for planktonic cells.

The exposed samples both biofilm and planktonic cells to GO showed that the O-H stretch is present but in different location. In planktonic cells the O-H is located at 3302.3 cm^{-1}, while in biofilm is located at 3405.1 cm^{-1}. The C-H stretch located at 2926 cm^{-1} (C-H) is present in both forms. The amide I is located at 1630.7 cm^{-1} for biofilm and at 1653 cm^{-1} for planktonic cells. The amide II is present in planktonic cells at 1543.0 cm^{-1} but it is absent in biofilm. The C-H band is present for both forms, at 1435.4 cm^{-1} for biofilm and 1451.7 cm^{-1} for planktonic cells. New peaks are formed only in biofilms at 1140.1, 747.1 and 685.4 cm^{-1} which represent C-O, C-H_2 and O-C-N.

The EPS was measured by FTIR after extraction and mixed with KBr. FTIR spectra for EPS is presented in **Figure 5.5**. The spectrum is unclear and few peaks are present. This is due to the EPS amount being too low to be detected.

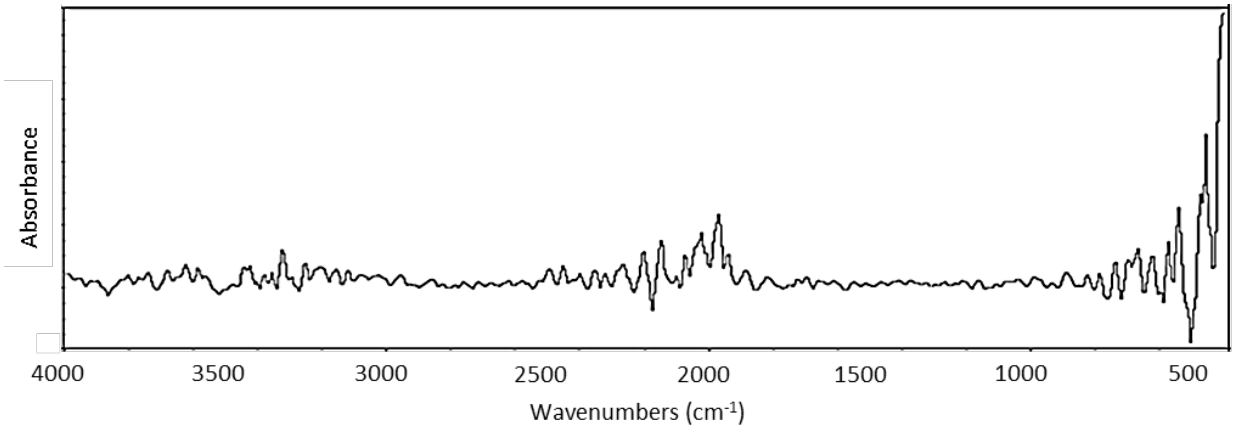

Figure 5. 5 ATR-FTIR spectra of EPS after removal from boifilm

5.5. Discussion

5.5.1. EDTA

In this study, EDTA was used to remove EPS from biofilms to test the effect of GO in the presence or absence of EPS. EDTA is a chemical compound that has destructive effects on the outer membrane of bacteria by chelating cations from LPS, which enables the release of LPS from bacteria and therefore affects the permeability of the outer membrane (Banin et al., 2006; Cavaliere et al., 2014). EDTA can be lethal for bacteria when exposed for a long period of time; however, for a short period of time, it increases the permeability of the outer membrane (Cavaliere et al., 2014). Therefore, EDTA can react as a synergistic agent with other antibacterial compounds (Lambert et al., 2004; Umerska et al., 2018). In this chapter, results showed that EDTA affected *P. putida* biofilms (**Figure 5.2**). The addition of EDTA only reduced the viability of biofilms, but it worked as a synergistic compound when GO was applied.

It has been shown that EDTA killed *P. aeruginosa* biofilm and caused cell detachment from biofilm (Banin et al., 2006). Banin et al. (2006) studied the effect of EDTA on *P. aeruginosa* biofilms. The results showed a reduction in cell number of more than 99% in biofilm cells, when treated with 50 mM EDTA. Furthermore, treatment with EDTA and 50 µg/ml gentamicin together was more effective than ETDA alone.

The experiment in this chapter also in parallel demonstrated that GO has no effect on planktonic cells. Therefore, in this chapter, EDTA was used with planktonic cells as a control to biofilm. Comparing cells exposed to EDTA and non-exposed, there was no significant difference after adding GO. These results are similar to those reported by Thuptimdang et al. (2015).

In this chapter, EDTA with GO shows a synergistic effect against biofilm cells and this might be due to the fact that they both target the cell membrane. Such synergy in antibacterial activity is expected since GO damages the cell membrane as observed previously and EDTA also targets the membrane. In many studies EDTA can react as a synergistic agent with other antibacterial compounds (Lambert et al., 2004; Umerska et al., 2018). Lambert et al. (2004) demonstrated that the treatment of *P. aeruginosa* with EDTA made it more sensitive to antimicrobial agents (surfactants and antibiotics). However, in contrast, Thuptimdang et al. (2015) reported that EDTA did not make *P. putida* planktonic cells more susceptible to AgNPs after treatment for 3 h. however, in this study EDTA treatment made the biofilms more susceptible to the antibacterial effects GO. This discrepancy between results can be explained by the differences in the antibacterial mechanisms between GO and AgNPs or antimicrobial agents. For example, EDTA is able to disrupt the lipopolysaccharide in the outer membrane of *P. putida* which increase the sensitivity of surfactants and antibiotics or GO to attach the cell wall. On the other hand, AgNPs may not attach the cell wall the membrane disruption caused by EDTA may not increase cells susceptibility.

The removal of EPS led to an increase in susceptibility of *P. putida* cells to GO. Sheng and Li, (2011) studied the effect of sliver on wastewater biofilms. They removed the loosely bound EPS using NaCl. The removal of EPS caused slight loss of biofilm and cell susceptibility increased to over 80% when AgNPs were applied. Their study shows that EPS plays a major role in cells' protection. In addition, removal of the loose EPS from biofilms increased cells' resistance compared with planktonic cells. This could be related to protection of tight EPS (Xue et al., 2013), where biofilm was found to be more resistant to chlorine and monochloramine with EPS.

Since EDTA treatment destabilises the biofilm matrix and also removes EPS it would be expected that some of the cells would be removed during the washing steps, however, this is not the case as the counts between control (dH_2O) and Go at initial time 0 h were similar. Moreover, the effect of EDTA on EPS would be significantly reduced after the washing steps and prior to further treatment with GO or dH_2O and therefore the observed reduction in counts would only be explained by the synergistic effects of EDTA and GO and not due to the washing steps facilitated by EDTA.

The damage to the cell wall caused by EDTA made biofilm cells more sensitive to GO but not planktonic cells. The reason why EDTA effect biofilms and not planktonic cells, this could be due to three reasons. 1) EDTA chelates divalent cations and divalent cations are important in cell wall stability. Therefore, the data suggest that divalent cations might be more important in cell wall stability in *P. putida* biofilm cells compared to planktonic cells (Nikaido and Vaara, 1985). A less stable cell wall would be more sensitive to GO. 2) It could be that the act of removing EPS from biofilm cells using EDTA damages the cells. The destabilization and destruction of the EPS can break down cohesive (cell-cell) and adhesive (cell-surface) forces which may affect the cells negatively (Chaudhary and Payasi, 2012). However, EDTA treatment of planktonic cells does not do this. 3) it could be that EDTA trapped in EPS between the cells which increases its concentration around the cells and also the contact time with the cell wall.

5.5.2. FTIR Spectroscopy

FTIR analysis was done to study the differences between treated and untreated samples with GO. FTIR spectroscopy was used to try to identify the functional groups in organic molecules according to the vibration at different infrared frequencies. The

spectra of bacteria were well identified (Ojeda et al., 2008; Schmitt and Flemming, 1998). **Figure 5.4** show the ATR-FTIR spectra of *P. putida* planktonic and biofilm cells. The observed IR bands corresponded to the presence of different chemical compounds, such as protein, lipid and polysaccharides functional groups (Tugarova et al., 2017).

Additionally, ATR-FTIR spectra of treated and untreated biofilm confirmed molecular interactions between GO and bacterial cells. The infrared spectra of treated and untreated cells exhibit distinct bands (**figure 5.4**). Although the region between 3600 and 2500 cm^{-1} exhibits similar bands, the treated sample at the approximate region 3000-2900 cm^{-1} has only one peak instead of two peaks for untreated. This region corresponds to C-H stretching in aliphatic compounds (Filip et al., 2004). Cell wall components, such as lipids and carbohydrates, could be responsible for this feature (Filip et al., 2004).

Fatty acid spectra bands in regions 3100 and 2800 cm^{-1} and 1500-1200 cm^{-1} can determine the harshness of the impact of the nanoparticles on the bacterial cell wall (Faghihzadeh et al., 2016; Mihoubi et al., 2017). A study showed that the composition of Gram-negative bacteria was changed in terms of fatty acids, amide I and amide II of proteins, peptides and amino acid regions, compared with untreated bacteria (Pulingam et al., 2019). Another study showed the impact of fullerene on bacterial membrane using FTIR and reported that the fullerene changed the composition of phospholipid (Fang et al., 2007).

The region between 1700 and 1480 cm^{-1} represents N-H stretching of amide I and amide II which indicates the presence of protein (Sabbatini et al., 2017). The amide I is located between region 1700-1600 cm^{-1} and has a stretch vibration of C=O, while

amide II is located between 1600 and 1480 cm^{-1} and has a stretch vibration of N-H (Faghihzadeh et al., 2016; Sabbatini et al., 2017). In this study, the intensity of amide I decreased, and the bands of amide II were absent in treated biofilm. This reflects the chemical changes after the treatment with GO.

The spectra of carbohydrate occurs at 1200-900 cm^{-1} region (Humbert and Quilès, 2011) and has a stretch vibration of C-O-C and C-O-P group of the polysaccharide region (Tareb et al., 2017). The chemical composition of the carbohydrate region transformed with the presence of GO. An additional band exhibited at 1140 cm^{-1} and the intensity band at 1068.9 cm^{-1} increased. This is due to a stretch vibration of C-O-P and C-O-H of carbohydrates and nucleic acids (Tareb et al., 2017; Ojeda and Dittrich, 2012). The treated biofilm also showed a small and weak band in the region between 900-600 cm^{-1}, called the fingerprint region (Faghihzadeh et al., 2016). The band corresponded to CH_2, which could be assigned to cellulose (Szymańska-Chargot et al., 2011).

In conclusion, in this study, direct attachment of GO to *P. putida* biofilm was performed by removing EPS. The removal of EPS by EDTA reduced the viability of *P. putida* biofilm cells. The removal of EPS increased the susceptibility of *P. putida* to GO. The study of the functional groups was done by FTIR. Results showed that the biofilm cells treated with GO changed the chemical compounds in their cell wall which may play a role in their viability. Additional work is need in future with different bacteria and different carbon nanotubes.

Chapter 6. Final discussion and future work

The aim of this thesis was to study the effect of carbon-based nanomaterials on soil bacteria. Over the recent years, intense research was focusing on the toxicity of these nanomaterials on bacteria. Many of the research indicates that these nanomaterials have an antibacterial effect on the bacterial cells. One of these nanomaterials is GO which is a thin layer of carbon atoms with oxygen groups on the top of the layer and it has been used recently in many applications. As the industries expands the production of GO, it will certainly release into the environment and might affect the soil bacteria. Therefore, it was important to study the impact of GO on soil bacteria in planktonic cells and biofilms.

This chapter is a summary on the main findings of the four result chapters; synthesis of GO, toxicity of GO on bacteria, effect of environmental stresses on GO treated bacteria and bacterial cell wall, the thesis and highlights the future work.

Previous studies showed conflicting results on the antibacterial activity of GO due to variability in its purity. Therefore, it was important to synthesize pure GO and characterise it before the test. In chapter one, pure GO was successfully produced from graphite flakes by modified Hummers' method and was characterized by different techniques. Each technique presents a different characteristic such as size, thickness, oxygen groups and purity. TEM was used to identify the size of GO and the achieved size of GO sheets were 100-200 and 400-600 nm by sonication for 10 or 120 min, respectively. While the thickness of the GO sheets was measured by AFM and showed 1.6-2 nm. The presence of oxygen groups showed that the GO has a negative charge while XPS confirmed the purity of the sample.

In the second chapter, GO was tested against *P. putida* and *Acinetobacter sp*. as model bacteria in biofilm and planktonic form. Both biofilms of these bacteria were developed in CDC reactor.

The viability of the bacterial strains was measured by plate counting and colony-forming units (CFU) were determined while two tests were used to measure the antibacterial activity of GO including: flow cytometry to study the integrity of the cell membrane and confocal microscopy to investigate the morphological changes of the cells. The CFU results showed that *P. putida* biofilms were reduced at 48h while *Acinetobacter sp* were reduced at 72h. Both strains at these times showed cell membrane damage and the cells detached showed susceptibility to GO. However, the planktonic cells for both strains showed no changes to GO. The results indicated that the susceptibility of GO to biofilm depends on age of biofilm which might be due to the physiological state of the cells during biofilm's maturation.

In the third chapter, after testing the effect of GO on bacteria, it was important to study the environmental stresses on *P. putida* and GO such as temperature, pH and osmotic stresses. The pH and osmotic stresses were applied to bacteria before GO treatment. The viability was tested by plate counting and CFU was determined while the physiology of the biofilms was investigated by confocal microscopy. The tested temperature stresses were 4, 25 and 40 ^{o}C. The incubation of GO for both planktonic cells and biofilms in all temperatures showed no significant difference which means the temperature does not play a role in the susceptibility of bacteria with GO. The exposed to low pH (5 and 6) on biofilms cells showed a slight reduction in CFU, while at 7-9 pH no differences were observed between them. However, the combined exposure of the post-treated bacteria with GO showed reduction in low and high pH but the reductions were not significant between the pH ranges of 5, 6, 7, 8 and 9.

There was no impact of only osmotic pressure on biofilm cells which showed no reduction of CFU. However, the combined exposure of high osmotic pressure (NaCl 320 mM) and GO showed a reduction of CFU more than at low osmotic pressure. This reduction could be from the high osmotic pressure which cause changes to the bacterial membrane and make it more susceptible to GO. On the contrary, the reduction on the planktonic cells were high when the osmotic pressure increased. It is possible that the cell membrane gets altered from the salts and the cells shrink due to high osmotic pressure around the cells and such changes to the membrane may have caused them to become more susceptible to GO treatment.

In the last chapter, after studying the effect of GO on bacteria and their environmental stresses, it was necessary to study the role of EPS on protection of biofilm cells from GO and to study its chemical compounds to understand its interaction with GO. The EPS is known to play an important role in the protection of biofilms. Therefore, in the last chapter the susceptibility of *P. putida* biofilms after EPS removal was investigated. The method to remove the EPS was by using EDTA. The removal was shown to increase the susceptibility of *P. putida* cells to GO. The study of the chemical compounds was done by FTIR and it showed that GO changed the compounds of the cell wall which may explain the decrease in cell viability.

Future work

Graphene oxide (GO) has been reported to have strong antibacterial activity against Gram-positive and Gram-negative bacteria. However, synthesising high-quality GO is essential to study the impact of GO on bacteria. In my study, I have successfully generated high-quality GO by optimising modified Hummer's method and testing its antibacterial activity on both planktonic cells and biofilms under different environmental factors such as pH, osmosis and temperature. However, there are still questions that need to be answered in following-up studies. Therefore, the future work should include the following:

1- Testing of the antibacterial effect of GO on Gram-positive bacteria *B. subtilis* and demonstrate the difference in the interaction between GO and Gram-negative versus Gram-positive bacteria. This can be done by measuring the viability by CFU and flow cytometry to determine the degree of bacterial membrane potential and integrity. TEM and SEM can be used to observe the bacterial morphology and to understand the interaction between the cell membrane and GO. ATR-FTIR can be used to analyse the functional group in the cells.
2- Comparing the antibacterial effect of GO with different carbon nanomaterials such as graphene, rGO and carbon nanotube on *P. putida* biofilm. This comparing can be done by measuring the viability by CFU and flow. TEM and SEM to study the morphology. The functional group will be analyse by ATR-FTIR.
3- Understand the mechanism of the antibacterial effect of GO on bacteria at the molecular level. This can be done by using RNAseq analysis to analyse the changing of transcriptome after exposing cells to GO and spot the changes in

gene expression. This could be expanded to compare the genes that are activated and repressed in biofilms and planktonic cells.

References

Abbaszadegan, A., Ghahramani, Y., Gholami, A., Hemmateenejad, B., Dorostkar, S., Nabavizadeh, M. and Sharghi, H. (2015) The effect of charge at the surface of silver nanoparticles on antimicrobial activity against Gram-positive and Gram-negative bacteria: A preliminary study. *Journal of Nanomaterials*, 16(1): 1-8 doi:10.1155/2015/720654.

Abdallah, M., Benoliel, C., Ferreira-Theret, P., Drider, D., Dhulster, P. and Chihib, N.E. (2015) Effect of culture conditions on the resistance of *Pseudomonas aeruginosa* biofilms to disinfecting agents. *Biofouling*, 31 (1): 49–59. doi:10.1080/08927014.2014.993390.

Abdel-el-haleem, D. (2003) *Acinetobacter* : environmental and biotechnological applications. *African Journal of Biotechnology*, 2 (4): 71–74.

Acemel, R.D., Govantes, F. and Cuetos, A. (2018) Computer simulation study of early bacterial biofilm development. *Scientific Reports*, 8: 5340. doi:10.1038/s41598-018-23524-x.

Agarwala, M., Choudhury, B. and Yadav, R.N.S. (2014) Comparative Study of Antibiofilm Activity of Copper Oxide and Iron Oxide Nanoparticles Against Multidrug Resistant Biofilm Forming Uropathogens. *Indian Journal of Microbiology*, 54 (3): 365–368. doi:10.1007/s12088-014-0462-z.

Ahmed, F. and Rodrigues, D.F. (2013) Investigation of acute effects of graphene oxide on wastewater microbial community: a case study. *Journal of Hazardous Materials*, 256–257: 33–9. doi:10.1016/j.jhazmat.2013.03.064.

Akhavan, O. and Ghaderi, E. (2010) Toxicity of graphene and graphene oxide nanowalls against bacteria. *ACS Nano*, 4 (10): 5731–5736. doi:10.1021/nn101390x.

Akiyama, H., Yamasaki, O., Kanzaki, H. and Tada, J. (1998) Effects of sucrose and silver on *Staphylococcus aureus* biofilm. *Journal of Antimicrobial Chemotherapy*, 42: 629–634. doi:10.1093/jac/42.5.629.

Ali-Boucetta, H., Bitounis, D., Raveendran-Nair, R., Servant, A., Van den Bossche, J. and Kostarelos, K. (2013) Purified graphene oxide dispersions lack in vitro cytotoxicity and in vivo pathogenicity. *Advanced Healthcare Materials*, 2 (3): 433–41. doi:10.1002/adhm.201200248.

Allaker, R.P. and Memarzadeh, K. (2014) Nanoparticles and the control of oral infections. *International Journal of Antimicrobial Agents*, 43 (2): 95–104. doi:10.1016/j.ijantimicag.2013.11.002.

Ansari, M.A., Khan, H.M., Khan, A.A., Ahmad, M.K., Mahdi, A.A., Pal, R. and Cameotra, S.S. (2014) Interaction of silver nanoparticles with *Escherichia coli* and their cell envelope biomolecules. *Journal of Basic Microbiology*, 54 (9): 905–915. doi:10.1002/jobm.201300457.

Antoniou, K. and Frank, J.F. (2005) Removal of *Pseudomonas putida* biofilm and associated extracellular polymeric substances from stainless steel by alkali cleaning. *Journal of Food Protection*, 68 (2): 277–281.

Anwar, H., Dasgupta, M., Lam, K. and Costerton, J.W. (1989) Tobramycin resistance of mucoid *pseudomonas aeruginosa* biofilm grown under iron limitation. *Journal of Antimicrobial Chemotherapy*, 24: 4, 647–6. doi:10.1093/jac/24.5.647.

Arevalo-Ferro, C., Reil, G., Görg, A., Eberl, L. and Riedel, K. (2005) Biofilm formation of *Pseudomonas putida* IsoF: The role of quorum sensing as assessed by proteomics. *Systematic and Applied*

Microbiology, 28 (2): 87–114. doi:10.1016/j.syapm.2004.10.005.

Azam, A., Ahmed, A.S., Oves, M., Khan, M.S., Habib, S.S. and Memic, A. (2012) Antimicrobial activity of metal oxide nanoparticles against Gram-positive and Gram-negative bacteria : a comparative study. *International Journal of Nanomedicine*, 7: 6003–6009.

Balcázar, J.L., Subirats, J. and Borrego, C.M. (2015) The role of biofilms as environmental reservoirs of antibiotic resistance. *Frontiers in Microbiology*, 6 (1216). doi:10.3389/fmicb.2015.01216.

Banin, E., Brady, K.M. and Greenberg, E.P. (2006) Chelator-Induced Dispersal and Killing of *Pseudomonas aeruginosa* Cells in a Biofilm. *Applied and Environmental Microbiology*, 72 (3): 2064–2069. doi:10.1128/AEM.72.3.2064.

Barbolina, I., Woods, C.R., Lozano, N., Kostarelos, K., Novoselov, K.S. and Roberts, I.S. (2016) Purity of graphene oxide determines its antibacterial activity. *2D Materials*, 3 (2): 025025. doi:10.1088/2053-1583/3/2/025025.

Beales, N. (2004) Adaptation of microorganisms to cold temperatures, Weak Acid Preservatives, Low pH, and osmotic Stress: A Review. *Comprehensive Reviews in Food Science and Food Safety*, 3: 1–20. doi:10.1111/j.1541-4337.2004.tb00057.x.

Bester, E., Wolfaardt, G., Joubert, L., Garny, K. and Saftic, S. (2005) Planktonic-cell yield of a pseudomonad biofilm. *Applied and Environmental Microbiology*, 71 (12): 7792–7798. doi:10.1128/AEM.71.12.7792-7798.2005.

Bianco, A. (2013) Graphene: safe or toxic? The two faces of the medal. *Angewandte Chemie International Edition*, 52 (19): 4986–97. doi:10.1002/anie.201209099.

Biniak, S., Szymański, G., Siedlewski, J. and Światkoski, A. (1997) The characterization of activated carbons with oxygen and nitrogen surface groups. *Carbon*, 35 (12): 1799–1810. doi:10.1016/S0008-6223(97)00096-1.

Bitounis, D., Ali-Boucetta, H., Hong, B.H., Min, D.-H.H. and Kostarelos, K. (2013) Prospects and challenges of graphene in biomedical applications. *Advanced Materials*, 25 (16): 2258–2268. doi:10.1002/adma.201203700.

Bosch-Navarro, C., Busolo, F., Coronado, E., Duan, Y., Martí-Gastaldo, C. and Prima-Garcia, H. (2013) Influence of the covalent grafting of organic radicals to graphene on its magnetoresistance. *Journal of Materials Chemistry C*, 1 (30): 4590–4598. doi:10.1039/c3tc30799a.

Bridier, a, Briandet, R., Thomas, V. and Dubois-Brissonnet, F. (2011) Resistance of bacterial biofilms to disinfectants: a review. *Biofouling*, 27 (9): 1017–32. doi:10.1080/08927014.2011.626899.

Brodie, B.C. (1859) On the Atomic Weight of Graphite. *Philosophical Transactions of the Royal Society of London*, 149 (0): 249–259. doi:10.1098/rstl.1859.0013.

Brodie, B.C. (1860) On the combination of carbonic oxide with potassium. *Quarely Journal of the Chemical Society of London,* 12: 269–272.

Brossard, K. a and Campagnari, A.A. (2012) The *Acinetobacter baumannii* biofilm-associated protein plays a role in adherence to human epithelial cells. *Infection and Immunity*, 80 (1): 228–33. doi:10.1128/IAI.05913-11.

Bunch, J.S., Verbridge, S.S., Alden, J.S., Van Der Zande, A.M., Parpia, J.M., Craighead, H.G. and McEuen, P.L. (2008) Impermeable atomic membranes from graphene sheets. *Nano Letters*. 8

(8):2458-2462. doi:10.1021/nl801457b.

Bussy, C., Ali-Boucetta, H. and Kostarelos, K. (2013) Safety considerations for graphene: lessons learnt from carbon nanotubes. *Accounts of Chemical Research*, 46 (3): 692–701. doi:10.1021/ar300199e.

Camesano, T.A. and Abu-Lail, N.I. (2002) Heterogeneity in bacterial surface polysaccharides, probed on a single-molecule basis. *Biomacromolecules*, 3: 661–667. doi:10.1021/bm015648y.

Campos-Delgado, J., Castro, K.L.S., Munguia-Lopez, J.G., González, A.K., Mendoza, M.E., Fragneaud, B., Verdan, R., Araujo, J.R., González, F.J., Navarro-Contreras, H., Pérez-Maldonado, I.N., León-Rodríguez, A.D and Achete, C.A. (2016) Effect of graphene oxide on bacteria and peripheral blood mononuclear cells. *Journal of Applied Biomaterials & Functional Materials*, 14 (4): e423–e430. doi:10.5301/jabfm.5000325.

Cavaliere, R., Ball, J.L., Turnbull, L. and Whitchurch, C.B. (2014) The biofilm matrix destabilizers, EDTA and DNaseI, enhance the susceptibility of nontypeable *Hemophilus influenzae* biofilms to treatment with ampicillin and ciprofloxacin. *MicrobiologyOpen*, 3 (4): 557–567. doi:10.1002/mbo3.187.

Chang, L. and Craik, S. (2012) Laboratorysimulation of the effect of ozone and monochloramine on biofilms in drinking water mains. *Ozone: Science and Engineering*, 34: 243–251. doi:10.1080/01919512.2012.686864.

Chang, W.S., Van De Mortel, M., Nielsen, L., De Guzman, G.N., Li, X. and Halverson, L.J. (2007) Alginate production by *Pseudomonas putida* creates a hydrated microenvironment and contributes to biofilm architecture and stress tolerance under water-limiting conditions. *Journal of Bacteriology*, 189 (22): 8290–8299. doi:10.1128/JB.00727-07.

Chaudhary, M. and Payasi, A. (2012) Role of EDTA and CSE1034 in curli formation and biofilm eradication of Klebsiella pneumoniae: a comparison with other drugs. *The Journal of Antibiotics*, (65): 631–633.

Chauke, V.P., Maity, A. and Chetty, A. (2015) High-performance towards removal of toxic hexavalent chromium from aqueous solution using graphene oxide-alpha cyclodextrin-polypyrrole nanocomposites. *Journal of Molecular Liquids*, 11: 71–77. doi:10.1016/j.molliq.2015.06.044.

Chen, H.-Q.Q., Gao, D., Wang, B., Zhao, R.-F.F., Guan, M., Zheng, L.-N.N., Zhou, X.-Y.Y., Chai, Z.-F.F. and Feng, W.-Y.Y. (2014a) Graphene oxide as an anaerobic membrane scaffold for the enhancement of *B. adolescentis* proliferation and antagonistic effects against pathogens E. coli and S. aureus. *Nanotechnology*, 25 (16): 165101. doi:10.1088/0957-4484/25/16/165101.

Chen, J., Peng, H., Wang, X., Shao, F., Yuan, Z. and Han, H. (2014b) Graphene oxide exhibits broad-spectrum antimicrobial activity against bacterial phytopathogens and fungal conidia by intertwining and membrane perturbation. *Nanoscale*, 6 (3): 1879–89. doi:10.1039/c3nr04941h.

Cheng, W., Weng, L.T., Li, Y., Lau, A., Chan, C.K. and Chan, C.M. (2013) Surface chemical composition of size-fractionated urban walkway aerosols determined by x-ray photoelectron spectroscopy. *Aerosol Science and Technology*, 47 (10): 1118–1124. doi:10.1080/02786826.2013.824066.

Choi, A.H.K.K., Slamti, L., Avci, F.Y., Pier, G.B. and Maira-Litrán, T. (2009) The pgaABCD locus of Acinetobacter baumannii encodes the production of poly-β-1-6-N-acetylglucosamine, which is critical for biofilm formation. *Journal of Bacteriology*, 191 (19): 5953–5963. doi:10.1128/JB.00647-09.

Choy, W., Zhou, L., Syn, C.K., Zhang, L. and Swarup, S. (2004) MorA defines a new class of regulators

affecting flagellar development and biofilm formation in diverse *Pseudomonas species*. Journal of Bacteriology, 186 (21): 7221-7228. doi:10.1128/JB.186.21.7221.

Chua, C.K. and Pumera, M. (2014) Chemical reduction of graphene oxide: A synthetic chemistry viewpoint. *Chemical Society Reviews*, 43, 291-312. doi:10.1039/c3cs60303b.

Chumkhunthod, P., Schraft, H. and Griffiths, M.W. (1998) Rapid monitoring method to assess efficacy of sanitizers against *Pseudomonas putida* biofilms. *Journal of Food Protection*, 61 (8): 1043–1046. doi:10.4315/0362-028x-61.8.1043.

Coblentz, W.W. (1911) Radiometric investigation of water of crystallisation, light filters and standard absorption bands. Washington, D.C. Bulletin of the Bureau of Standards. 7: 619-663

Coenye, T. and Nelis, H.J. (2010) In vitro and in vivo model systems to study microbial biofilm formation. *Journal of Microbiological Methods*, 83 (2): 89–105. doi:10.1016/j.mimet.2010.08.018.

Combarros, R.G., Collado, S. and Díaz, M. (2016) Toxicity of graphene oxide on growth and metabolism of *Pseudomonas putida*. *Journal of Hazardous Materials*. 310, 246–252 doi:10.1016/j.jhazmat.2016.02.038.

Combrouse, T., Sadovskaya, I., Faille, C., Kol, O., Guérardel, Y. and Midelet-Bourdin, G. (2013) Quantification of the extracellular matrix of the *Listeria monocytogenes* biofilms of different phylogenic lineages with optimization of culture conditions. *Journal of Applied Microbiology*, 114: 1120–1131. doi:10.1111/jam.12127.

Csonka, L.N. and Hanson, D. (1991) Prokaryotic Osmoregulation: Genetics and physiology. *Annual Reviews Microbiology*, 45: 569–606.

Csonka, L.N. (1989) Physiological and genetic responses of bacteria to osmotic stress. *Microbiological Reviews*, 53:121-147.

D'Alvise, P.W., Sjøholm, O.R., Yankelevich, T., Jin, Y., Wuertz, S. and Smets, B.F. (2010) TOL plasmid carriage enhances biofilm formation and increases extracellular DNA content in *Pseudomonas putida* KT2440. *FEMS microbiology letters*, 312 (1): 84–92. doi:10.1111/j.1574-6968.2010.02105.x.

Dailloux, M., Albert, M., Laurain, C., Andolfatto, S., Lozniewski, A., Hartemann, P. and Mathieu, L. (2003) *Mycobacterium xenopi* and drinking water biofilms. *Applied and Environmental Microbiology*, 69 (11): 6946–6948. doi:10.1128/AEM.69.11.6946-6948.2003.

Davey, M.E. and O'toole, G.A. (2000) Microbial Biofilms: from Ecology to Molecular Genetics. *Microbiology and Molecular Biology Reviews*, 64 (4): 847–867. doi:10.1128/MMBR.64.4.847-867.2000.

Doğan, H.Ö., Ekinci, D. and Demir, Ü. (2013) Atomic scale imaging and spectroscopic characterization of electrochemically reduced graphene oxide. *Surface Science*, 611: 54–59. doi:10.1016/j.susc.2013.01.014.

Dresselhaus, M.S., Dresselhaus, G., Saito, R. and Jorio, A. (2005) Raman spectroscopy of carbon nanotubes. *Physics Reports*, 409 (2): 47–99. doi:10.1016/j.physrep.2004.10.006.

Dreyer, D.R., Park, S., Bielawski, C.W. and Ruoff, R.S. (2010) The chemistry of graphene oxide. *Chem. Soc. Rev.*, 39: 228–240. doi:10.1007/978-3-319-15500-5_3.

Du, J., Hu, X. and Zhou, Q. (2015) Graphene oxide regulates the bacterial community and exhibits property changes in soil. *RSC Adv.*, 5: 27009–27017. doi:10.1039/C5RA01045D.

Eda, G., Choowalla, M. (2010) Chemically derived graphene oxide: towards large-area thin-film electronics and optoelectronics. *Advanced Materials*, 22(22):2392-2415. doi: 10.1002/adma.200903689

Eigler, S. (2011) Transparent and Electrically Conductive Films from Chemically Derived Graphene. In *Physics and Applications of Graphene - Experiments*, Mikhailov, S (ed.) inTech, pp.109-134 doi:10.5772/14133.

Eijkelkamp, B. a, Stroeher, U.H., Hassan, K. a, Papadimitrious, M.S., Paulsen, I.T. and Brown, M.H. (2011) Adherence and motility characteristics of clinical *Acinetobacter baumannii* isolates. *FEMS microbiology letters*, 323 (1): 44–51. doi:10.1111/j.1574-6968.2011.02362.x.

Elayatt, A.K. and Romero-Gonzalez, M.E. (2016) Colorimetric characterization of extracellular polymeric substances (EPS) extracted From *Pseudomonas putida* ATCC 11172 at different growth medium. *Imperial Journal of Interdisciplinary Research*, 2 (8): 1628–1635.

Erickson, K., Erni, R., Lee, Z., Alem, N., Gannett, W. and Zettl, A. (2010) Determination of the local chemical structure of graphene oxide and reduced graphene oxide. *Advanced Materials*, 22: 4467–4472. doi:10.1002/adma.201000732.

Facklam, R.R. (1973) Comparison of several laboratory media for presumptive i dentification of Enterococci and Group D Streptococci. *Applied and Environmental Microbiology*, 26 (2): 138–145.

Faghihzadeh, F., Anaya, N.M., Schifman, L.A. and Oyanedel-Craver, V. (2016) Fourier transform infrared spectroscopy to assess molecular-level changes in microorganisms exposed to nanoparticles. *Nanotechnology for Environmental Engineering*, 1 (1): 1–16. doi:10.1007/s41204-016-0001-8.

Fang, J., Lyon, D.Y., Wiesner, M.R., Dong, J. and Alvarez, P.J.J. (2007) Effect of a fullerene water suspension on bacterial phospholipids and membrane phase behavior. *Environmental Science and Technology*, 41 (7): 2636–2642. doi:10.1021/es062181w.

Fang, W., Hu, J. and Ong, S.L. (2010) Effects of phosphorus on biofilm disinfections in model drinking water distribution systems. *Journal of Water and Health*, 8 (3): 446–454. doi:10.2166/wh.2009.303.

de Faria, A.F., Martinez, D.S.T., Meira, S.M.M., de Moraes, A.C.M., Brandelli, A., Filho, A.G.S. and Alves, O.L. (2014) Anti-adhesion and antibacterial activity of silver nanoparticles supported on graphene oxide sheets. *Colloids and surfaces. B, Biointerfaces*, 113: 115–24. doi:10.1016/j.colsurfb.2013.08.006.

Farid, M.U., Jeong, S., Seo, D.H., Ahmed, R., Lau, C., Gali, N.K., Ning, Z. and An, A.K. (2018) Mechanistic insight into the in vitro toxicity of graphene oxide against biofilm forming bacteria using laser-induced breakdown spectroscopy. *Nanoscale*, 10: 4475–4487. doi:10.1039/c8nr00189h.

Feng, L., Wu, J., Chen, G.Q., Cui, F.Z., Kim, T.N. and Kim, J.O. (2000) A mechanistic study of the antibacterial effect of silver ions on *Escherichia coli* and *Staphylococcus aureus*. *J Bio Mat Res*, 52: 662–668. doi:10.1007/s00289-005-0414-1.

Ferrari, A.C. (2007) Raman spectroscopy of graphene and graphite: Disorder, electron-phonon coupling, doping and nonadiabatic effects. *Solid State Communications*, 143 (1–2): 47–57. doi:10.1016/j.ssc.2007.03.052.

Ferrari, A.C., Meyer, J.C., Scardaci, V., Casiraghi, C., Lazzeri, M., Mauri, F., Piscanec, S., Jiang, D., Novoselov, K.S., et al. (2006) Raman spectrum of graphene and graphene layers. *Physical Review Letters*, 97 (18): 1–4. doi:10.1103/PhysRevLett.97.187401.

Filip, Z., Hermann, S. and Demnerová, K. (2008) FT-IR spectroscopic characteristics of differently cultivated Escherichia coli. *Czech Journal of Food Sciences*, 26 (6): 458–463.

Filip, Z., Herrmann, S. and Kubat, J. (2004) FT-IR spectroscopic characteristics of differently cultivated Bacillus subtilis. *Microbiological Research*, 159 (3): 257–262. doi:10.1016/j.micres.2004.05.002.

Frank, J.F. and Koffi, R.A. (1990) Surface-adherent growth of *Listeria monocytogenes* is Associated with Increased Resistance to Surfactant Sanitizers and Heat. *Journal of Food Protection*, 53 (7): 55-554.

Ganesh, E.N. (2013) Single walled and multi walled carbon nanotube structure, synthesis and applications.Internatioal Journal of Innovative Technology and Exploring Engineering, 2: 311-320.

Gao, Y., Wu, J., Ren, X., Tan, X., Hayat, T., Alsaedi, A., Cheng, C. and Chen, C. (2017) Impact of graphene oxide on the antibacterial activity of antibiotics against bacteria. *Environmental Science: Nano*, 4 (5): 1016–1024. doi:10.1039/c7en00052a.

Ge, Y., Schimel, J.P. and Holden, P. a (2011) Evidence for negative effects of TiO2 and ZnO nanoparticles on soil bacterial communities. *Environmental Science and Technology*, 45 (4): 1659–64. doi:10.1021/es103040t.

Geim, A.K. and Novoselov, K.S. (2007) The rise of graphene. *Nature Materials*, 6: 183. doi.org/10.1038/nmat1849.

Geng, X., Guo, Y., Li, D., Li, W., Zhu, C., Wei, X., Chen, M., Gao, S., Qiu, S., et al. (2013) Interlayer catalytic exfoliation realizing scalable production of large-size pristine few-layer graphene. *Scientific Reports*, 3: 1–12. doi:10.1038/srep01134.

Georgakilas, V., Tiwari, J.N., Kemp, K.C., Perman, J.A., Bourlinos, A.B., Kim, K.S. and Zboril, R. (2016) Noncovalent functionalization of graphene and graphene oxide for energy materials, biosensing, catalytic, and biomedical applications. *Chemical Reviews*. doi:10.1021/acs.chemrev.5b00620.

Gil-Sotres, F., Trasar-Cepeda, C., Leiro, M.C. and Seoane, S. (2005) Different approaches to evaluating soil quality using biochemical properties. *Soil Biol. Biochem*, 37: 877–887.

Gillooly, D.J., Robertson, A.G.S. and Fewson, C.A. (1998) Molecular characterization of benzyl alcohol dehydrogenase and benzaldehyde dehydrogenase II of *Acinetobacter calcoaceticus*. Biochem J, 330 (3):1375-1381. doi: 10.1042/bj3301375

Gjermansen, M., Ragas, P., Sternberg, C., Molin, S. and Tolker-Nielsen, T. (2005) Characterization of starvation-induced dispersion in *Pseudomonas putida* biofilms. *Environmental microbiology*, 7 (6): 894–906. doi:10.1111/j.1462-2920.2005.00775.x.

Goenka, S., Sant, V. and Sant, S. (2014) Graphene-based nanomaterials for drug delivery and tissue engineering. *Journal of Controlled Release*. doi:10.1016/j.jconrel.2013.10.017.

Goeres, D.M., Loetterle, L.R., Hamilton, M.A., Murga, R., Kirby, D.W. and Donlan, R.M. (2005) Statistical assessment of a laboratory method for growing biofilms. *Microbiology*, 151 (3): 757–762. doi:10.1099/mic.0.27709-0.

Gomes, I.B., Simões, M. and Simões, L.C. (2014) An overview on the reactors to study drinking water biofilms. *Water Research*, 62: 62–87. doi:10.1016/j.watres.2014.05.039.

Gómez-Navarro, C., Meyer, J.C., Sundaram, R.S., Chuvilin, A., Kurasch, S., Burghard, M., Kern, K. and Kaiser, U. (2010) Atomic structure of reduced graphene oxide. *Nano Letters*, 10 (4): 1144-1148

doi:10.1021/nl9031617.

Gosselin, F., Madeira, L.M., Juhna, T. and Block, J.C. (2013) Drinking water and biofilm disinfection by fenton-like reaction. *Water Research*, 47 (15): 5631-5638. doi:10.1016/j.watres.2013.06.036.

Guo, X. and Mei, N. (2014) Assessment of the toxic potential of graphene family nanomaterials. *Journal of Food and Drug Analysis*, 22 (1): 105–115. doi:10.1016/j.jfda.2014.01.009.

Guo, Z., Xie, C., Zhang, P., Zhang, J., Wang, G., He, X., Ma, Y., Zhao, B. and Zhang, Z. (2017) Toxicity and transformation of graphene oxide and reduced graphene oxide in bacteria biofilm. *Science of The Total Environment*, 580: 1300–1308. doi:10.1016/j.scitotenv.2016.12.093.

Gurunathan, S. (2015) Cytotoxicity of graphene oxide nanoparticles on plant growth promoting rhizobacteria. *Journal of Industrial and Engineering Chemistry*, 32: 282–291. doi:10.1016/j.jiec.2015.08.027.

Hajipour, M.J., Fromm, K.M., Ashkarran, A.A., Jimenez de Aberasturi, D., de Larramendi, I.R., Rojo, T., Serpooshan, V., Parak, W.J. and Mahmoudi, M. (2012) Antibacterial properties of nanoparticles. *Trends in biotechnology*, 30 (10): 499–511. doi:10.1016/j.tibtech.2012.06.004.

Hall-Stoodley, L., Costerton, J.W. and Stoodley, P. (2004) Bacterial biofilms: From the natural environment to infectious diseases. *Nature Reviews Microbiology*, 2: 95–108. doi:10.1038/nrmicro821.

Hansen, S.K., Haagensen, J.A.J.J., Gjermansen, M., Jørgensen, T.M., Tolker-Nielsen, T. and Molin, S. (2007) Characterization of a *Pseudomonas putida* rough variant evolved in a mixed-species biofilm with *Acinetobacter sp*. strain C6. *Journal of Bacteriology*, 189 (13): 4932–4943. doi:10.1128/JB.00041-07.

Hashim, N., Muda, Z., Hussein, M.Z., Isa, I.M., Mohamed, A., Kamari, A., Bakar, S.A., Mamat, M. and Jaafar, A.M. (2016) A brief review on recent graphene oxide-based material nanocomposites: Synthesis and applications. *Journal of Materials and Environmental Science*. doi:10.1124/dmd.31.7.861.

He, J.-Z., Li, C.-C., Wang, D.-J. and Zhou, D.-M. (2015a) Biofilms and extracellular polymeric substances mediate the transport of graphene oxide nanoparticles in saturated porous media. *Journal of Hazardous Materials*, 300: 467–474. doi:10.1016/j.jhazmat.2015.07.026.

He, J., Zhu, X., Qi, Z., Wang, C., Mao, X., Zhu, C., He, Z., Li, M. and Tang, Z. (2015b) Killing dental pathogens using antibacterial graphene oxide. *ACS Applied Materials and Interfaces*, 7 (9): 5605–5611. doi:10.1021/acsami.5b01069.

Herrera-Alonso, M., Abdala, A.A., McAllister, M.J, Aksay, I.A. and Prud'homme, R.K. (2007) Intercalation and stitching of graphite oxide with diaminoalkanes. *Langmuir*, 23: 10644-10649. doi:org/10.1021/la0633839

Heydorn, A., Heydorn, A., Nielsen, A.T., Nielsen, A.T., Hentzer, M. and Hentzer, M. (2000) Quantication of biofilm structures by the novel computer program. *Image Processing*, (2000): 2395–2407. doi:10.1099/00221287-146-10-2395.

Hofmann, U. and Holst, R. (1939) The acidic nature and the methylation of graphitoxide. *Berichte Der Deutschen Chemischen Gesellschaft* , 72: 754–771.

Høiby, N., Krogh Johansen, H., Moser, C., Song, Z., Ciofu, O. and Kharazmi, A. (2001) Pseudomonas aeruginosa and the in vitro and in vivo biofilm mode of growth. *Microbes and Infection*, 3: 23−35.

doi:10.1016/S1286-4579(00)01349-6.

Hossain, M.Z., Johns, J.E., Bevan, K.H., Karmel, H.J., Liang, Y.T., Yoshimoto, S., Mukai, K., Koitaya, T., Yoshinobu, J., et al. (2012) Chemically homogeneous and thermally reversible oxidation of epitaxial graphene. *Nature Chemistry*, 4: 305–309. doi:10.1038/nchem.1269.

Van Houdt, R. and Michiels, C.W. (2010) Biofilm formation and the food industry, a focus on the bacterial outer surface. *Journal of applied microbiology*, 109 (4): 1117–31. doi:10.1111/j.1365-2672.2010.04756.x.

Hu, W., Peng, C., Luo, W., Lv, M., Li, X., Li, D., Huang, Q. and Fan, C. (2010) Graphene-based antibacterial paper. *ACS nano*, 4 (7): 4317–4323. doi:10.1021/nn101097v.

Hu, X. and Zhou, Q. (2013) Health and ecosystem risks of graphene. *Chemical Reviews*, 113 (5): 3815–3835. doi:10.1021/cr300045n.

Huang, N., Lim, H., Chia, C., Yarmo, M. and Muhamad, M. (2011) Simple room-temperature preparation of high-yield large-area graphene oxide. *International Journal of Nanomedicine*, 6: 3443–3448.

Hui, L., Piao, J.G., Auletta, J., Hu, K., Zhu, Y., Meyer, T., Liu, H. and Yang, L. (2014) Availability of the basal planes of graphene oxide determines whether it is antibacterial. *ACS Applied Materials and Interfaces*, 6 (15): 13183–13190. doi:10.1021/am503070z.

Humbert, F. and Quilès, F. (2011) In-situ study of early stages of biofilm formation under different environmental stresses by ATR-FTIR spectroscopy. *Science against Microbial Pathogens: Communicating Current Research and Technological Advances, A. Mendez-Vilas (eds.)*, pp. 889–895.

Hummers, W.S. and Offeman, R.E. (1958) Preparation of Graphitic Oxide. *J. Am. Chem. Soc.*, 80: 1339.

Ikuma, K., Decho, A.W. and Lau, B.L.T. (2015) When nanoparticles meet biofilms - Interactions guiding the environmental fate and accumulation of nanoparticles. *Frontiers in Microbiology*, 6: 1–6. doi:10.3389/fmicb.2015.00591.

Jamialahmadi, N., Safari, E. and Baghdadi, M. (2018) Interaction of graphene oxide nano-sheets and landfill leachate bacterial culture. *Environmental Technology (United Kingdom)*, 39 (19): 2457–2466. doi:10.1080/09593330.2017.1356875.

Jasim, D.A., Lozano, N. and Kostarelos, K. (2016) Synthesis of few-layered, high-purity graphene oxide sheets from different graphite sources for biology. *2D Materials*. doi:10.1088/2053-1583/3/1/014006.

Jastrzębska, A.M., Kurtycz, P. and Olszyna, A.R. (2012) Recent advances in graphene family materials toxicity investigations. *Journal of nanoparticle research : an interdisciplinary forum for nanoscale science and technology*, 14 (12): 1320. doi:10.1007/s11051-012-1320-8.

Jiao, H., Chen, J., Li, W., Wang, F., Zhou, H., Li, Y. and Yu, C. (2014) Nucleic acid-regulated perylene probe-induced gold nanoparticle aggregation: A new strategy for colorimetric sensing of alkaline phosphatase activity and inhibitor screening. *ACS Applied Materials and Interfaces*, 6 (3): 1979–1985. doi:10.1021/am405020b.

Jiao, Y., Cody, G.D., Harding, A.K., Wilmes, P., Schrenk, M., Wheeler, K.E., Banfield, J.F. and Thelen, M.P. (2010) Characterization of extracellular polymeric substances from acidophilic microbial biofilms. *Applied and Environmental Microbiology*, 76 (9): 2916–2922. doi:10.1128/AEM.02289-09.

Johansen, A., Pedersen, A.L., Jensen, K.A., Karlson, U., Hansen, B.M., Scott-Fordsmand, J.J. and Winding, A. (2008) Effects of C60 fullerene nanoparticles on soil bacteria and protozoans. *Environmental Toxicology and Chemistry*, 27 (9): 1895–1903. doi:10.1897/07-375.1.

Johnsen, A.R., Wick, L.Y. and Harms, H. (2005) Principles of microbial PAH-degradation in soil. *Environmental Pollution*, 133 (1): 71–84. doi:10.1016/j.envpol.2004.04.015.

Johnson, D.W., Dobson, B.P. and Coleman, K.S. (2015) A manufacturing perspective on graphene dispersions. *Current Opinion in Colloid and Interface Science*, 20: 367–382. doi:10.1016/j.cocis.2015.11.004.

Juni, E. (1978) Genetics and physiology of *Acinetobacter*., pp. 349–371.

Kano, E., Kvashnin, D.G., Sakai, S., Chernozatonskii, L.A., Sorokin, P.B., Hashimoto, A. and Takeguchi, M. (2017) One-atom-thick 2D copper oxide clusters on graphene. *Nanoscale*, 9 (11): 3980–3985. doi:10.1039/c6nr06874j.

Karpouzas, D.G. and Walker, A. (2000) Factors influencing the ability of *Pseudomonas putida* strains epI and II to degrade the organophosphate ethoprophos. *Journal of Applied Microbiology*, 89 (1): 40–48. doi:10.1046/j.1365-2672.2000.01080.x.

Kashyap, S., Mishra, S., Behera, S.K., Kashyap, S., Mishra, S. and Behera, S.K. (2014) Aqueous Colloidal stability of graphene oxide and chemically converted graphene. *Journal of Nanoparticles*, e640281. doi:10.1155/2014/640281, 10.1155/2014/640281.

Kemp, K.C., Seema, H., Saleh, M., Le, N.H., Mahesh, K., Chandra, V. and Kim, K.S. (2013) Environmental applications using graphene composites: water remediation and gas adsorption. *Nanoscale*, 5 (8): 3149–71. doi:10.1039/c3nr33708a.

Kim, J., Kuk, E., Yu, K., Kim, J., Park, S., Lee, H., Kim, S., Park, Y., Park, Y., et al. (2007) Antimicrobial effects of silver nanoparticles. *Nanomedicine: Nanotechnology, Biology, and Medicine*, 3: 95 – 101. doi:10.1016/j.nano.2006.12.001.

Kim, K.S., Zhao, Y., Jang, H., Lee, S.Y., Kim, J.M., Kim, K.S., Ahn, J.H., Kim, P., Choi, J.Y., et al. (2009) Large-scale pattern growth of graphene films for stretchable transparent electrodes. *Nature*, 457 (7230): 706–710. doi:10.1038/nature07719.

Klausen, M., Gjermansen, M., Kreft, J.U. and Tolker-Nielsen, T. (2006) Dynamics of development and dispersal in sessile microbial communities: Examples from *Pseudomonas aeruginosa* and *Pseudomonas putida* model biofilms. *FEMS Microbiology Letters*, 261 (1): 1–11. doi:10.1111/j.1574-6968.2006.00280.x.

Krishnakumar, R., Kuzhimattam, M. and Kumar, G. (2015) Ogilvie's syndrome following posterior spinal instrumentation in thoraco lumbar trauma. *Journal of Craniovertebral Junction and Spine*. doi:10.4103/0974-8237.167866.

Kumar, S., Raj, S., Kolanthai, E., Sood, A.K., Sampath, S. and Chatterjee, K. (2015) Chemical functionalization of graphene to augment stem cell osteogenesis and inhibit biofilm formation on polymer composites for orthopedic applications. *ACS Applied Materials and Interfaces*, 7 (5): 3237–3252. doi:10.1021/am5079732.

Kurtz, J. and Huffman, D.R. (1990) Combined infrared and ultraviolet-visible spectroscopy matrix-isolated carbon vapor. *The Journal of Chemical Physics*, 92 (1): 30–35. doi:10.1063/1.458478.

Lakshminarayanan, P. V., Toghiani, H. and Pittman, C.U. (1983) Nitric acid oxidation of vapor grown

carbon nanofibers. *Carbon*, 42: 2433–2442. doi:10.1016/j.carbon.2004.04.040.

Lambert, R.J.W., Hanlon, G.W. and Denyer, S.P. (2004) The synergistic effect of EDTA/antimicrobial combinations on *Pseudomonas aeruginosa*. *Journal of Applied Microbiology*, 96 (2): 244–253. doi:10.1046/j.1365-2672.2004.02135.x.

Lee, W.S. (1972) Improved procedure for identification of group D enterococci with two new media. *Applied microbiology*, 24 (1): 1–3.

Lee, Y., Seo, H., Yeom, J. and Park, W. (2011) Molecular characterization of the extracellular matrix in a *Pseudomonas putida* dsbA mutant: Implications for acidic stress defense and plant growth promotion. *Research in Microbiology*, 162 (3): 302–310. doi:10.1016/j.resmic.2010.11.002.

Lehtola, M.J., Torvinen, E., Kusnetsov, J., Pitkänen, T., Maunula, L., Von Bonsdorff, C.H., Martikainen, P.J., Wilks, S.A., Keevil, C.W., Miettinen, I.T. (2007) Survival of *Mycobacterium avium*, *Legionella pneumophila*, *Escherichia coli*, and Caliciviruses in drinking water-associated biofilms grown under high-shear turbulent flow. *Applied and Environmental Microbiology*, 73 (9): 2854–2859. doi:10.1128/AEM.02916-06.

Lehtola, M.J., Torvinen, E., Miettinen, I.T. and Keevil, C.W. (2006) Fluorescence in situ hybridization using peptide nucleic acid probes for rapid detection of *Mycobacterium avium* subsp. *avium* and *Mycobacterium avium* subsp. *paratuberculosis* in potable-water biofilms. *Applied and Environmental Microbiology*, 72 (1): 848-853. doi:10.1128/AEM.72.1.848-853.2006.

León, A., Reuquen, P., Garín, C., Segura, R., Vargas, P., Zapata, P. and Orihuela, P.A. (2017) FTIR and Raman characterization of TiO2 nanoparticles coated with polyethylene glycol as carrier for 2-methoxyestradiol. *Applied Sciences*, 7 (1): 49. doi:10.3390/app7010049.

Lerf, A., He, H., Forster, M. and Klinowski, J. (1998) Structure of Graphite Oxide Revisited. *Journal of Physical Chemistry B*, (102): 4477–4482. doi:10.1021/jp9731821.

Leriche, V. and Carpentier, B. (1995) Viable but Nonculturable *Salmonella typhimurium* in Single- and Binary-Species Biofilms in Response to Chlorine Treatment. *Journal of Food Protection*, 58: 1186–1191. doi:10.4315/0362-028x-58.11.1186.

Li, D., Müller, M.B., Gilje, S., Kaner, R.B. and Wallace, G.G. (2008) Processable aqueous dispersions of graphene nanosheets. *Nature Nanotechnology*, 3 (2): 101–105. doi:10.1038/nnano.2007.451.

Li, J., Wang, G., Zhu, H., Zhang, M., Zheng, X., Di, Z., Liu, X. and Wang, X. (2014) Antibacterial activity of large-area monolayer graphene film manipulated by charge transfer. *Scientific Reports*, 4: 4359. doi:10.1038/srep04359.

Lin, H., Chen, G., Long, D. and Chen, X. (2014) Responses of unsaturated *Pseudomonas putida* CZ1 biofilms to environmental stresses in relation to the EPS composition and surface morphology. *World Journal of Microbiology and Biotechnology*, 30 (12): 3081–3090. doi:10.1007/s11274-014-1735-8.

Liu, J., Tang, J. and Gooding, J.J. (2012a) Strategies for chemical modification of graphene and applications of chemically modified graphene. *Journal of Materials Chemistry*, 22 (25): 12435. doi:10.1039/c2jm31218b.

Liu, S., Hu, M., Zeng, T.H., Wu, R., Jiang, R., Wei, J., Wang, L., Kong, J. and Chen, Y. (2012b) Lateral dimension-dependent antibacterial activity of graphene oxide sheets. *Langmuir : the ACS journal of surfaces and colloids*, 28 (33): 12364–72. doi:10.1021/la3023908.

Liu, S., Zeng, T.H., Hofmann, M., Burcombe, E., Wei, J., Jiang, R., Kong, J. and Chen, Y. (2011) Antibacterial activity of graphite, graphite oxide, graphene oxide, and reduced graphene oxide: Membrane and oxidative stress. *ACS Nano*, 5 (9): 6971–6980. doi:10.1021/nn202451x.

López-Díaz, D., López Holgado, M., García-Fierro, J.L. and Velázquez, M.M. (2017) Evolution of the Raman spectrum with the chemical composition of graphene oxide. *Journal of Physical Chemistry C*, 121: 20489−20497. doi:10.1021/acs.jpcc.7b06236.

Lu, L., Shen, Y., Chen, X., Qian, L. and Lu, K. (2004) Ultrahigh strength and high electrical conductivity in Copper. *Science*. doi:10.1126/science.1092905.

Lu, X., Feng, X., Werber, J.R., Chu, C., Zucker, I., Kim, J.-H., Osuji, C.O. and Elimelech, M. (2017) Enhanced antibacterial activity through the controlled alignment of graphene oxide nanosheets. *Proceedings of the National Academy of Sciences*.114 (46), E9793-E9801. doi:10.1073/pnas.1710996114.

Lui, C.H., Liu, L., Mak, K.F., Flynn, G.W. and Heinz, T.F. (2009) Ultraflat graphene. *Nature*. 462: 339-341. doi:10.1038/nature08569.

Macià, M.D., Rojo-Molinero, E. and Oliver, A. (2014) Antimicrobial susceptibility testing in biofilm-growing bacteria. *Clinical Microbiology and Infection*, 20 (10): 981–990. doi:10.1111/1469-0691.12651.

Manafi, M., Manafi, P., Agarwal, S., Bharti, A.K., Asif, M. and Gupta, V.K. (2017) Synthesis of nanocomposites from polyacrylamide and graphene oxide: Application as flocculants for water purification. *Journal of Colloid and Interface Science*, 490: 505–510. doi:10.1016/j.jcis.2016.11.096.

Mangadlao, J.D., Santos, C.M., Felipe, M.J.L., de Leon, A.C.C., Rodrigues, D.F. and Advincula, R.C. (2015) On the antibacterial mechanism of graphene oxide (GO) Langmuir–Blodgett films. *Chem. Commun.*, 51 (14): 2886–2889. doi:10.1039/C4CC07836E.

Marcano, D.C., Kosynkin, D. V., Berlin, J.M., Sinitskii, A., Sun, Z., Slesarev, A., Alemany, L.B., Lu, W. and Tour, J.M. (2010) Improved synthesis of graphene oxide. *ACS Nano*. doi:10.1021/nn1006368.

Marsden, A.E., Grudzinski, K., Ondrey, J.M., DeLoney-Marino, C.R. and Visick, K.L. (2017) Impact of salt and nutrient content on biofilm formation by *Vibrio fischeri*. *PLoS ONE*, 12 (1): 1–19. doi:10.1371/journal.pone.0169521.

Mascio, C.T.M., Alder, J.D. and Silverman, J.A. (2007) Bactericidal action of daptomycin against stationary-phase and nondividing *Staphylococcus aureus* cells. *Antimicrobial Agents and Chemotherapy*, 51 (12): 4255–4260. doi:10.1128/AAC.00824-07.

Mejías Carpio, I.E., Santos, C.M., Wei, X. and Rodrigues, D.F. (2012) Toxicity of a polymer–graphene oxide composite against bacterial planktonic cells, biofilms, and mammalian cells. *Nanoscale*, 4 (15): 4746. doi:10.1039/c2nr30774j.

Mendonca, A.F., Amoroso, T.L. and Knabel, S.J. (1994) Destruction of gram-negative food-borne pathogens by high pH involves disruption of the cytoplasmic membrane. *Applied and Environmental Microbiology*, 60 (11): 4009–4014.

Mihoubi, W., Sahli, E., Gargouri, A. and Amiel, C. (2017) FTIR spectroscopy of whole cells for the monitoring of yeast apoptosis mediated by p53 over-expression and its suppression by *Nigella sativa* extracts. *PLoS ONE*, 12 (7): 1–16. doi:10.1371/journal.pone.0180680.

Miller, J.K., Neubig, R., Clemons, C.B., Kreider, K.L., Wilber, J.P., Young, G.W., Ditto, A.J., Yun, Y.H.,

Milsted, A., et al. (2013) Nanoparticle deposition onto biofilms. *Annals of Biomedical Engineering*, 41 (1): 53–67. doi:10.1007/s10439-012-0626-0.

Mkhoyan, K.A., Contryman, A.W., Silcox, J., Stewart, D.A., Eda, G., Mattevi, C., Miller, S. and Chhowalla, M. (2009) Atomic and electronic structure of graphene-oxide. *Nano Letters*, 9 (3): 1058–1063. doi:10.1021/nl8034256.

Yusoff, A.R.M., Dai, L., Cheng, H.-M. and Liu, J. (2015) Graphene Based Energy Devices. *Nanoscale*, 7: 6881–6882. doi:10.1002/9783527690312.ch3.

Mokkapati, V.R.S.S., Pandit, S., Kim, J., Martensson, A., Lovmar, M., Westerlund, F. and Mijakovic, I. (2018) Bacterial response to graphene oxide and reduced graphene oxide integrated in agar plates. *Royal Society Open Science*, 5: 181083. doi:10.1098/rsos.181083.

Molina-Höppner, A., Doster, W., Vogel, R.F. and Gänzle, M.G. (2004) Protective effect of sucrose and sodium chloride for lactococcus lactis during sublethal and lethal high-pressure treatments. *Applied and Environmental Microbiology*. doi:10.1128/AEM.70.4.2013-2020.2004.

Møller, S., Sternberg, C., Andersen, J.B.O., Bak, B., Ramos, J.L., Givskov, M., Andersen, J.B.O., Christensen, B.B.A.K. and Molin, S. (1998) *In situ gene expression in mixed-culture biofilms: evidence of metabolic interactions between community members. Applied Environmental Microbiology, 64 (2): 721-732*

Monds, R.D. and O'Toole, G.A. (2009) The developmental model of microbial biofilms: ten years of a paradigm up for review. *Trends in Microbiology*, 17 (2): 73–87. doi:10.1016/j.tim.2008.11.001.

Morimatsu, K., Eguchi, K., Hamanaka, D., Tanaka, F. and Uchino, T. (2012) Effects of temperature and nutrient conditions on biofilm formation of *Pseudomonas putida*. *Food Science and Technology Research*, 18 (6): 879–883. doi:10.3136/fstr.18.879.

Mukherjee, R., Bhunia, P. and De, S. (2016) Impact of graphene oxide on removal of heavy metals using mixed matrix membrane. *Chemical Engineering Journal*, 292: 284–297. doi:10.1016/j.cej.2016.02.015.

Munna, M.S., Zeba, Z. and Noor, R. (2015) Influence of temperature on the growth of *Pseudomonas putida. Stamford Journal of Microbiology*, 5 (1): 9–12. doi:10.1111/j.1758-2229.2010.00229.x.

Nanda, S.S., Yi, D.K. and Kim, K. (2016) Study of antibacterial mechanism of graphene oxide using Raman spectroscopy. *Scientific Reports*, 6: 28443. doi:10.1038/srep28443.

Ndiongue, S., Huck, P.M. and Slawson, R.M. (2005) Effects of temperature and biodegradable organic matter on control of biofilms by free chlorine in a model drinking water distribution system. *Water Research*, 39 (6): 953–964. doi:10.1016/j.watres.2004.12.019.

Nelson, K.E., Weinel, C., Paulsen, I.T., Dodson, R.J., Hilbert, H., Santos, V.A.P.M., Fouts, D.E., Gill, S.R., Pop, M., et al. (2002) *Complete genome sequence and comparative analysis of the metabolically versatile Pseudomonas putida KT2440.*, 4: 799–808.

Nethravathi, C. and Rajamathi, M. (2008) Chemically modified graphene sheets produced by the solvothermal reduction of colloidal dispersions of graphite oxide. *Carbon*, 46: 1994–1998. doi:10.1016/j.carbon.2008.08.013.

Nikaido, H. and Vaara, M. (1985) Molecular basis of bacterial outer membrane permeability. *Microbiological Reviews*, 49 (1):1-32.

Niu, C. and Gilbert, E.S. (2004) Colorimetric Method for Identifying Plant Essential Oil Components That Affect Biofilm Formation and Structure. *Applied and Environmental Microbiology*, 70 (12): 6951–6956. doi:10.1128/AEM.70.12.6951.

Niyogi, S., Boukhalfa, S., Chikkannanavar, S.B., McDonald, T.J., Heben, M.J. and Doorn, S.K. (2007) Selective aggregation of single-walled carbon nanotubes via salt addition. *Journal of the American Chemical Society*, 129 (7): 1898–1899. doi:10.1021/ja068321j.

Novoselov, K.S., Geim, a K., Morozov, S. V, Jiang, D., Zhang, Y., Dubonos, S. V, Grigorieva, I. V and Firsov, a a (2004) Electric field effect in atomically thin carbon films. *Science (New York, N.Y.)*, 306 (5696): 666–9. doi:10.1126/science.1102896.

Oh, W.C. and Zhang, F.J. (2011) Preparation and characterization of graphene oxide reduced from a mild chemical method. *Asian Journal of Chemistry*, 23(2):875-879.

Ojeda, J.J. and Dittrich, M. (2012) Fourier transform infrared spectroscopy for molecular analysis of microbial cells. *Methods and Protocols*, 881: 187-211.. doi:10.1007/978-1-61779-827-6_8.

Ojeda, J.J., Romero-Gonzalez, M.E., Pouran, H.M. and Banwart, S.A. (2008) In situ monitoring of the biofilm formation of Pseudomonas putida on hematite using flow-cell ATR-FTIR spectroscopy to investigate the formation of inner-sphere bonds between the bacteria and the mineral. *Mineralogical Magazine*, 72 (1): 101–106. doi:10.1180/minmag.2008.072.1.101.

Omoike, A. and Chorover, J. (2004) Spectroscopic study of extracellular polymeric substances from Bacillus subtilis: aqueous chemistry and adsorption effects. *Biomacromolecules*, 5 (4): 1219–30. doi:10.1021/bm034461z.

Palmieri, V., Bugli, F., Lauriola, M.C., Cacaci, M., Torelli, R., Ciasca, G., Conti, C., Sanguinetti, M., Papi, M., et al. (2017) Bacteria meet graphene: modulation of graphene oxide nanosheet interaction with human pathogens for effective antimicrobial therapy. *ACS Biomaterials Science and Engineering*. doi:10.1021/acsbiomaterials.6b00812.

Pandit, S., Cai, J.N., Jung, J.E., Lee, Y.S. and Jeon, J.G. (2015) Effect of brief cetylpyridinium chloride treatments during early and mature cariogenic biofilm formation. *Oral Diseases*, 21: 565–571. doi:10.1111/odi.12312.

Paredes, J.I., Villar-Rodil, S., Solís-Fernández, P., Martínez-Alonso, A. and Tascón, J.M.D. (2009) Atomic force and scanning tunneling microscopy imaging of graphene nanosheets derived from graphite oxide. *Langmuir*, 25 (10): 5957–5968. doi:10.1021/la804216z.

Parikh, S.J. and Chorover, J. (2005) FTIR spectroscopic study of biogenic Mn-oxide formation by *Pseudomonas putida* GB-1. *Geomicrobiology Journal*, 22 (5): 207–218. doi:10.1080/01490450590947724.

Parikh, S.J., Goyne, K.W., Margenot, A.J., Mukome, F.N.D. and Calderón, F.J. (2014) Soil chemical insights provided through vibrational spectroscopy. *Advances in Agronomy*, 126: 1-148. doi:10.1016/B978-0-12-800132-5.00001-8.

Park, S. and Ruoff, R.S. (2009) Chemical methods for the production of graphenes. *Nature Nanotechnology*, 4 (4): 217–224. doi:10.1038/nnano.2009.58.

Pearson, J., Southam, G.G. and Holley, R.A. (1987) Survival and transport of bacteria in egg washwater. *Applied and environmental microbiology*, 53 (9): 2060–2065.

Pendolino, F. and Armata, N. (2017) “Synthesis, characterization and models of graphene oxide.”

Graphene Oxide in Environmental Remediation Process. pp. 5–21. doi:10.1007/978-3-319-60429-9_2.

Perreault, F., Faria, A.F. de, Nejati, S. and Elimelech, M. (2015) *Antimicrobial Properties of Graphene Oxide Nanosheets: Why Size Matters*., (7): 7226–7236. doi:10.1021/acsnano.5b02067.

Peulen, T.O. and Wilkinson, K.J. (2011) Diffusion of nanoparticles in a biofilm. *Environmental Science and Technology*, 45 (8): 3367–3373. doi:10.1021/es103450g.

Pintar, K.D.M. and Slawson, R.M. (2003) Effect of temperature and disinfection strategies on ammonia-oxidizing bacteria in a bench-scale drinking water distribution system. *Water Research*, 37 (8): 1805–1817. doi:10.1016/S0043-1354(02)00538-9.

Poh, H.L., Šaněk, F., Ambrosi, A., Zhao, G., Sofer, Z. and Pumera, M. (2012) Graphenes prepared by Staudenmaier, Hofmann and Hummers methods with consequent thermal exfoliation exhibit very different electrochemical properties. *Nanoscale*, 4: 3515–3522. doi:10.1039/c2nr30490b.

Pulingam, T., Thong, K.L., Ali, M.E., Appaturi, J.N., Dinshaw, I.J., Ong, Z.Y. and Leo, B.F. (2019) Graphene oxide exhibits differential mechanistic action towards Gram-positive and Gram-negative bacteria. *Colloids and Surfaces B: Biointerfaces*, 181: 6–15. doi:10.1016/j.colsurfb.2019.05.023.

Rathnayake, R.M.N.M., Wijayasinghe, H.W.M.A.C., Pitawala, H.M.T.G.A., Yoshimura, M. and Huang, H.H. (2017) Synthesis of graphene oxide and reduced graphene oxide by needle platy natural vein graphite. *Applied Surface Science*, 393: 309–315. doi:10.1016/j.apsusc.2016.10.008.

Reva, O.N., Weinel, C., Weinel, M., Böhm, K., Stjepandic, D., Hoheisel, J.D. and Tümmler, B. (2006) Functional genomics of stress response in *Pseudomonas putida* KT2440. *Journal of Bacteriology*, 188 (11): 4079–4092. doi:10.1128/JB.00101-06.

Rickard, A.H., McBain, A.J., Stead, A.T. and Gilbert, P. (2004) Shear rate moderates community diversity in freshwater biofilms. *Applied and Environmental Microbiology*, 70 (12): 7426–7435. doi:10.1128/AEM.70.12.7426-7435.2004.

Ricker, E.B. and Nuxoll, E. (2017) Synergistic effects of heat and antibiotics on *Pseudomonas aeruginosa* biofilms. *Biofouling*, 33 (10): 855–866. doi:10.1080/08927014.2017.1381688.

Riding, M.J., Martin, F.L., Trevisan, J., Llabjani, V., Patel, I.I., Jones, K.C. and Semple, K.T. (2012) Concentration-dependent effects of carbon nanoparticles in gram-negative bacteria determined by infrared spectroscopy with multivariate analysis. *Environmental Pollution*, 163: 226–234. doi:10.1016/j.envpol.2011.12.027.

Rizzello, L., Cingolani, R. and Pompa, P.P. (2013) Nanotechnology tools for antibacterial materials. *Future Medicine*, 8: 807–821.

Rodrigues, D.F. and Elimelech, M. (2010) Toxic effects of single-walled carbon nanotubes in the development of E. coli biofilm. *Environmental Science & Technology*, 44 (12): 4583–4589. doi:10.1021/es1005785.

Rodríguez-González, C., Martínez-Hernández, A.L., Castaño, V.M., Kharissova, O. V., Ruoff, R.S. and Velasco-Santos, C. (2012) Polysaccharide nanocomposites reinforced with graphene oxide and keratin-grafted graphene oxide. *Industrial & Engineering Chemistry Research*, 51: 3619–3629. doi:10.1021/ie200742x.

Rodriguez-Pastor, I., Ramos-Fernandez, G., Varela-Rizo, H., Terrones, M. and Martin-Gullon, I. (2015) Towards the understanding of the graphene oxide structure: How to control the formation of humic-

and fulvic-like oxidized debris. *Carbon*, 84 (1): 299–309. doi:10.1016/j.carbon.2014.12.027.

Romeo, T. (2008) *Bacterial Biofilms*: Springer, Berlin Heidelberg Springer. doi:10.1007/978-3-540-75418-3.

Ruess, G. (1947) Uber das Graphitoxyhydroxyd (Graphitoxyd). *Monatshefte Chem*, 76: 381–417. doi:10.1007/BF00898987.

Ruiz, O.N., Fernando, K. a S., Wang, B., Brown, N. a, Luo, P.G., McNamara, N.D., Vangsness, M., Sun, Y.-P. and Bunker, C.E. (2011a) Graphene oxide: A Nonspecific Enhancer of Cellular Growth. *ACS nano*, 5 (10): 8100–8107. doi:10.1021/nn202699t.

Ruiz, O.N., Fernando, K.A.S., Wang, B., Brown, N.A., Luo, P.G., Mcnamara, N.D., Vangsness, M., Sun, Y. and Bunker, C.E. (2011b) Graphene oxide : A nonspecific enhancer of cellular growth. *ACS Nano*, 5 (10): 8100–8107.

Sabbatini, S., Conti, C., Orilisi, G. and Giorgini, E. (2017) Infrared spectroscopy as a new tool for studying single living cells: Is there a niche? *Biomedical Spectroscopy and Imaging*, 6 (3–4): 85–99. doi:10.3233/BSI-170171.

Sambhy, V., MacBride, M.M., Peterson, B.R. and Sen, A. (2006) Silver bromide nanoparticle/polymer composites: Dual action tunable antimicrobial materials. *Journal of the American Chemical Society*, 128: 9798–9808. doi:10.1021/ja061442z.

Sarawutanukul, S., Phattharasupakun, Nutthaphon Wutthiprom, J. and Sawangphruk, M. (2018) 3D CVD graphene oxide on Ni foam towards hydrogen evolution reaction in acid electrolytes at different concentrations. *Electrochemical Society Transaction*, 85 (11): 49–63.

Schmitt, J. and Flemming, H.-C. (1998) FTIR-spectroscopy in microbial and material analysis. *International Biodeterioration & Biodegradation*, 41 (1): 1–11. doi:10.1016/S0964-8305(98)80002-4.

Scholz, W. and Boehm, H.P. (1969) Betrachtungen zur Struktur des Graphitoxids. *Zeitschrift Fur Anorganische Und Allgemeine Chemie*, (369(3–6)): 327–340.

Seabra, A.B., Paula, A.J., de Lima, R., Alves, O.L. and Durán, N. (2014) Nanotoxicity of graphene and graphene oxide. *Chemical research in toxicology*, 27 (2): 159–68. doi:10.1021/tx400385x.

Seil, J.T. and Webster, T.J. (2012) Antimicrobial applications of nanotechnology: methods and literature. *International journal of nanomedicine*, 7: 2767–81. doi:10.2147/IJN.S24805.

Shamaila, S., Sajjad, A.K.L. and Iqbal, A. (2016) Modifications in development of graphene oxide synthetic routes. *Chemical Engineering Journal*, 294: 458-477. doi:10.1016/j.cej.2016.02.109.

Shao, G., Lu, Y., Wu, F., Yang, C., Zeng, F. and Wu, Q. (2012) Graphene oxide: The mechanisms of oxidation and exfoliation. *Journal of Materials Science*, 47: 4400–4409. doi:10.1007/s10853-012-6294-5.

Shao, W., Liu, H., Liu, X., Wang, S. and Zhang, R. (2015) Anti-bacterial performances and biocompatibility of bacterial cellulose/graphene oxide composites. *RSC Advances*, 5 (7): 4795–4803. doi:10.1039/C4RA13057J.

Shen, Y., Stojicic, S. and Haapasalo, M. (2011) Antimicrobial efficacy of chlorhexidine against bacteria in biofilms at different stages of development. *Journal of Endodontics*, 37 (5): 667-661. doi:10.1016/j.joen.2011.02.007.

Sheng, Z. and Liu, Y. (2011) Effects of silver nanoparticles on wastewater biofilms. *Water Research*,

45 (18): 6039–6050. doi:10.1016/j.watres.2011.08.065.

Shih, C.J., Lin, S., Sharma, R., Strano, M.S. and Blankschtein, D. (2012) Understanding the pH-dependent behavior of graphene oxide aqueous solutions: A comparative experimental and molecular dynamics simulation study. *Langmuir*, 28: 235–241. doi:10.1021/la203607w.

Shim, S.E., Yashin, V. V. and Isayev, A.I. (2002) The EPS matix: The House of biofilms cells. Journal of Bacteriology, 189 (22): 7945-7947. doi:10.1128/JB.00858-07.

Smith, S.C. and Rodrigues, D.F. (2015) Carbon-based nanomaterials for removal of chemical and biological contaminants from water: A review of mechanisms and applications. *Carbon*, 91 (4): 122 – 143. doi:10.1016/j.carbon.2015.04.043.

Sondi, I. and Salopek-Sondi, B. (2004) Silver nanoparticles as antimicrobial agent: A case study on *E. coli* as a model for Gram-negative bacteria. *Journal of Colloid and Interface Science*, 275 (1): 177–182. doi:10.1016/j.jcis.2004.02.012.

Song, C., Yang, C.M., Sun, X.F., Xia, P.F., Qin, J., Guo, B.B. and Wang, S.G. (2018) Influences of graphene oxide on biofilm formation of Gram-negative and Gram-positive bacteria. *Environmental Science and Pollution Research*, 25: 2853–2860. doi:10.1007/s11356-017-0616-8.

Song, N.J., Chen, C.M., Lu, C., Liu, Z., Kong, Q.Q. and Cai, R. (2014) Thermally reduced graphene oxide films as flexible lateral heat spreaders. *Journal of Materials Chemistry A*, 2 (39): 16563–16568. doi:10.1039/c4ta02693d.

Srivastava, S., Yadav, A., Seem, K., Mishra, S., Chaudhary, V. and Nautiyal, C.S. (2008) Effect of high temperature on *Pseudomonas putida* NBRI0987 biofilm formation and expression of stress sigma factor RpoS. *Current Microbiology*, 56 (5): 453–457. doi:10.1007/s00284-008-9105-0.

Stankovich, S., Dikin, D.A., Piner, R.D., Kohlhaas, K.A., Kleinhammes, A., Jia, Y., Wu, Y., Nguyen, S.B.T. and Ruoff, R.S. (2007) Synthesis of graphene-based nanosheets via chemical reduction of exfoliated graphite oxide. *Carbon*, 45 (7): 1558–1565. doi:10.1016/j.carbon.2007.02.034.

Starkey, M., Parsek, M.R., Gray, K.A. and Chang, S. (2004) *A Sticky Business the Extracellular Polymeric Substance Matrix of Bacterial Biofilms*. M., O'Toole, G.A. (ed.). Washington, DC: In Microbial Biofilms.

Starkey, M., Parsek, M., Gray, K. and Chang, S. (2004) A Sticky Business: the Extracellular Polymeric Substance Matrix of Bacterial Biofilms, p 174-191. In Ghannoum M, O'Toole G (ed), Microbial Biofilms. ASM Press, Washington, DC. doi: 10.1128/9781555817718.ch10

Staudenmaier, L. (1898) Verfahren zur darstellung der graphitsäure. *Berichte der deutschen chemischen Gesellschaft banner*, 31: 1481–1487.

Steinberger, R.E. and Holden, P.A. (2005) Extracellular DNA in single- and multiple-species unsaturated biofilms. *Applied and environmental microbiology*, 71 (9): 5404–5410. doi:10.1128/AEM.71.9.5404-5410.2005.

Stepanović, S., Ćirković, I., Mijač, V. and Švabić-Vlahović, M. (2003) Influence of the incubation temperature, atmosphere and dynamic conditions on biofilm formation by Salmonella spp. *Food Microbiology*, 20 (3): 339–343. doi:10.1016/S0740-0020(02)00123-5.

Strankowski, M., W?odarczyk, D., Piszczyk, ?ukasz and Strankowska, J. (2016) Thermal and Mechanical Properties of Microporous Polyurethanes Modified with Reduced Graphene Oxide. *International Journal of Polymer Science*. doi:10.1155/2016/8070327.

Su, C.Y., Xu, Y., Zhang, W., Zhao, J., Liu, A., Tang, X., Tsai, C.H., Huang, Y. and Li, L.J. (2010) Highly efficient restoration of graphitic structure in graphene oxide using alcohol vapors. *ACS Nano*. doi:10.1021/nn101691m.

Sur, U.K., Saha, A., Datta, A., Ankamwar, B., Surti, F., Dutta Roy, S. and Roy, D. (2016) Synthesis and characterization of stable aqueous dispersions of graphene. *Bull. Mater. Sci. Indian Academy of Sciences*, 39 (1): 159–165. Available at: http://www.ias.ac.in/article/fulltext/boms/039/01/0159-0165.

Sutherland, I.W. (2001) Biofilm exopolysaccharides: a strong and sticky framework. *Microbiology*, 147: 3–9. doi:10.1099/00221287-147-1-3.

Szabó, T., Berkesi, O., Forgó, P., Josepovits, K., Sanakis, Y., Petridis, D. and Dékány, I. (2006) Evolution of Surface Functional Groups in a Series of Progressively Oxidized Graphite Oxides. *Chem. Mater.*, (18): 2740– 2749. doi:10.1021/cm060258.

Szymańska-Chargot, M., Cybulska, J. and Zdunek, A. (2011) Sensing the structural differences in cellulose from apple and bacterial cell wall materials by Raman and FT-IR Spectroscopy. *Sensors*, 11 (6): 5543–5560. doi:10.3390/s110605543.

Tareb, R., Bernardeau, M., Amiel, C. and Vernoux, J.P. (2017) Usefulness of FTIR spectroscopy to distinguish rough and smooth variants of *Lactobacillus farciminis* CNCM-I-3699. *FEMS Microbiology Letters*. 364 (3) p. fnw298. doi:10.1093/femsle/fnw298.

Tegou, E., Magana, M., Katsogridaki, A.E., Ioannidis, A., Raptis, V., Jordan, S., Chatzipanagiotou, S., Chatzandroulis, S., Ornelas, C., et al. (2016) Terms of endearment: Bacteria meet graphene nanosurfaces. *Biomaterials*, 89 (2): 38–55. doi:10.1016/j.biomaterials.2016.02.030.

Thuptimdang, P., Limpiyakorn, T., McEvoy, J., Prüß, B.M. and Khan, E. (2015) Effect of silver nanoparticles on *Pseudomonas putida* biofilms at different stages of maturity. *Journal of Hazardous Materials*, 290: 127–133. doi:10.1016/j.jhazmat.2015.02.073.

Toh, S.Y., Loh, K.S., Kamarudin, S.K. and Daud, W.R.W. (2014) Graphene production via electrochemical reduction of graphene oxide: Synthesis and characterisation. *Chemical Engineering Journal*, 251: 422–434. doi:10.1016/j.cej.2014.04.004.

Tolker-Nielsen, T., Brinch, U.C., Ragas, P.C., Andersen, J.B., Jacobsen, C.S. and Molin, S. (2000) Development and dynamics of Pseudomonas sp. biofilms. *Journal of bacteriology*, 182 (22): 6482–6489.

Tré-Hardy, M., Macé, C., El Manssouri, N., Vanderbist, F., Traore, H. and Devleeschouwer, M.J. (2009) Effect of antibiotic co-administration on young and mature biofilms of cystic fibrosis clinical isolates: the importance of the biofilm model. *International Journal of Antimicrobial Agents*, 33: 40–45. doi:10.1016/j.ijantimicag.2008.07.012.

Tu, Y., Lv, M., Xiu, P., Huynh, T., Zhang, M., Castelli, M., Liu, Z., Huang, Q., Fan, C., et al. (2013) Destructive extraction of phospholipids from *Escherichia coli* membranes by graphene nanosheets. *Nature Nanotechnology*, 8 (8): 594–601. doi:10.1038/nnano.2013.125.

Tuantranont, A. (2013) Nanomaterials for sensing applications: Introduction and perspective. *Springer Series on Chemical Sensors and Biosensors*, 14: 1–16.

Ţucureanu, V., Matei, A., and Avram, A.M. (2016) FTIR Spectroscopy for Carbon Family Study. *Critical Reviews in Analytical Chemistry*. 46 (6): 502–520. dio: 10.1080/10408347.2016.1157013

Tugarova, A. V., Scheludko, A. V., Dyatlova, Y.A., Filip'echeva, Y.A. and Kamnev, A.A. (2017) FTIR spectroscopic study of biofilms formed by the rhizobacterium Azospirillum brasilense Sp245 and its mutant Azospirillum brasilense Sp245.1610. *Journal of Molecular Structure*, 1140: 142–147. doi:10.1016/j.molstruc.2016.12.063.

Tuinstra, F. and Koenig, J.L. (1970) Raman Spectrum of Graphite. *The Journal of Chemical Physics*, 53 (3): 1126–1130. doi:10.1063/1.1674108.

Umerska, A., Strandh, M., Cassisa, V., Matougui, N., Eveillard, M. and Saulnier, P. (2018) Synergistic Effect of Combinations Containing EDTA and the Antimicrobial Peptide AA230, an Arenicin-3 Derivative, on Gram-Negative Bacteria. *Biomolecules*, 8 (4): 122. doi:10.3390/biom8040122.

Verma, G. and Mishra, M. (2018) Development and Optimization of UV-Vis Spectroscopy. *World Journal of Pharmaceutical Research*, 7 (11): 1170–1180. doi:10.20959/wjpr201811-12333.

Vorregaard, M. (2008) Comstat2-a modern 3D image analysis environment for biofilms*, Informatics and Mathematical Modelling*. Technical University of Denmark.

van der Waal, S. V., van der Sluis, L.W.M., Özok, A.R., Exterkate, R.A.M., van Marle, J., Wesselink, P.R. and de Soet, J.J. (2011) The effects of hyperosmosis or high pH on a dual-species biofilm of *Enterococcus faecalis* and *Pseudomonas aeruginosa*: An in vitro study. *International Endodontic Journal*, 44 (12): 1110–1117. doi:10.1111/j.1365-2591.2011.01929.x.

Wang, G., Qian, F., Saltikov, C.W., Jiao, Y. and Li, Y. (2011) Microbial reduction of graphene oxide by *Shewanella*. *Nano Research*, 4 (6): 563–570. doi:10.1007/s12274-011-0112-2.

Wang, H., Yuan, X., Wu, Y., Huang, H., Peng, X., Zeng, G., Zhong, H., Liang, J. and Ren, M. (2013) Graphene-based materials: fabrication, characterization and application for the decontamination of wastewater and wastegas and hydrogen storage/generation. *Advances in colloid and interface science*, 195–196: 19–40. doi:10.1016/j.cis.2013.03.009.

Wang, M., Niu, Y., Zhou, J., Wen, H., Zhang, Z., Luo, D., Gao, D., Yang, J., Liang, D., et al. (2016) The dispersion and aggregation of graphene oxide in aqueous media. *Nanoscale*. doi:10.1039/c6nr03503e.

Wang, Y.-W., Cao, A., Jiang, Y., Zhang, X., Liu, J.-H., Liu, Y. and Wang, H. (2014) Superior antibacterial activity of zinc oxide/graphene oxide composites originating from high zinc concentration localized around bacteria. *ACS applied materials & interfaces*, 6 (4): 2791–8. doi:10.1021/am4053317.

Willcock, L., Gilbert, P., Holah, J., Wirtanen, G. and Allison, D.G. (2000) A new technique for the performance evaluation of clean-in-place disinfection of biofilms. *Journal of Industrial Microbiology and Biotechnology*, 25 (5): 235e241. doi:10.1038/sj.jim.7000063.

Winding, A., Hund-Rinke, K. and Rutgers, M. (2005) The use of microorganisms in ecological soil classification and assessment concepts. *Ecotoxicology and Environmental Safety*, 62 (2): 230–248. doi:10.1016/j.ecoenv.2005.03.026.

Wu, G., Xu, X., He, X. and Yan, Y. (2018) Preparation and characterization of graphene oxide-modified Sapium sebiferum oil-based polyurethane composites with improved thermal and mechanical properties. *Polymers*, 10 (133): 1-13. doi:10.3390/polym10020133.

Xu, S.X., Zhang, L.L., Zhang, H.C., Zeng, Y., Shi, Z.M. and Ni, S.J. (2016) A salt-assisted graphene oxide aggregation method for the determination of dimethylamine and trimethylamine by ion chromatography with conductivity detection. *Analytical Methods*, 8 (8): 1828–1835. doi:10.1039/c5ay03242c.

Xue, Z., Hessler, C.M., Panmanee, W., Hassett, D.J. and Seo, Y. (2013) Pseudomonas aeruginosa inactivation mechanism is affected by capsular extracellular polymeric substances reactivity with chlorine and monochloramine. *FEMS Microbiology Ecology*, 83 (1): 101–111. doi:10.1111/j.1574-6941.2012.01453.x.

Yadav, N., Dubey, A., Shukla, S., Saini, C.P., Gupta, G., Priyadarshini, R. and Lochab, B. (2017) Graphene oxide-coated surface: inhibition of bacterial biofilm formation due to specific surface-interface interactions. *ACS Omega*, 2: 3070−3082. doi:10.1021/acsomega.7b00371.

Yan, Q.L., Gozin, M., Zhao, F.Q., Cohen, A. and Pang, S.P. (2016) Highly energetic compositions based on functionalized carbon nanomaterials. *Nanoscale*. 8: 4799-4851. doi:10.1039/c5nr07855e.

Yang, L., Liu, Y., Wu, H., Høiby, N., Molin, S. and Song, Z. (2011) Current understanding of multi-species biofilms. *International Journal of Oral Science*, 3 (2): 74–81. doi:10.4248/IJOS11027.

Yeo, M.K. and Nam, D.H. (2013) Influence of different types of nanomaterials on their bioaccumulation in a paddy microcosm: A comparison of TiO2 nanoparticles and nanotubes. *Environmental Pollution*, 178: 166–172. doi:10.1016/j.envpol.2013.03.040.

Yu, H., Zhang, B., Bulin, C., Li, R. and Xing, R. (2016) High-efficient Synthesis of Graphene Oxide Based on Improved Hummers Method. *Scientific Reports*, 6: 36143. doi:10.1038/srep36143.

Zeng, F., Sun, Z., Sang, X., Diamond, D., Lau, K.T., Liu, X. and Su, D.S. (2011) In Situ One-Step Electrochemical Preparation of Graphene Oxide Nanosheet-Modified Electrodes for Biosensors. *ChemSusChem*, 4 (11): 1587–1591. doi:10.1002/cssc.201100319.

Zhang, C., Ren, L., Wang, X. and Liu, T. (2010) Graphene oxide-assisted dispersion of pristine multiwalled carbon nanotubes in aqueous media. *Journal of Physical Chemistry C*, 114 (26): 11435-11440. doi:10.1021/jp103745g.

Zhang, Q., Jie, Y.W., Loong, W.L.C., Zhang, J., Fane, A.G., Kjelleberg, S., Rice, S.A. and McDougald, D. (2014) Characterization of biofouling in a lab-scale forward osmosis membrane bioreactor (FOMBR). *Water Research*, 58: 141–151. doi:10.1016/j.watres.2014.03.052.

Zhao, J., Deng, B., Lv, M., Li, J.J., Zhang, Y., Jiang, H., Peng, C., Li, J.J., Shi, J., et al. (2013) Graphene oxide-based antibacterial cotton fabrics. *Advanced healthcare materials*, 2 (9): 1259–66. doi:10.1002/adhm.201200437.

Zhao, J., Pei, S., Ren, W., Gao, L. and Cheng, H.M. (2010) Efficient Preparation of Large-Area Graphene Oxide Sheets for Transparent Conductive Films. *Acs Nano*, 4 (9): 5245–5252. doi:Doi 10.1021/Nn1015506.

Zheng, H., Ma, R., Gao, M., Tian, X., Li, Y.-Q., Zeng, L. and Li, R. (2018) Antibacterial applications of graphene oxides: structure-activity relationships, molecular initiating events and biosafety. *Science Bulletin*, 63: 133–142 Contents. doi:10.1016/j.scib.2017.12.012.

Zhou, L., Zhang, Y. and Li, G. (2009) Effect of pipe material and low level disinfectants on biofilm development in a simulated drinking water distribution system. *Journal of Zhejiang University-SCIENCE A*, 10 (5): 725–731. doi:10.1631/jzus.A0820486.

Zou, X., Zhang, L., Wang, Z. and Luo, Y. (2016) Mechanisms of the Antimicrobial Activities of Graphene Materials. *Journal of the American Chemical Society*, 138: 2064−2077. doi:10.1021/jacs.5b11411.